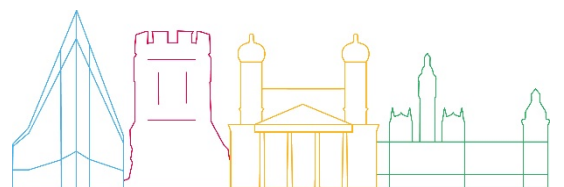




ARCH D4.3

Threats and Hazard Information System



Deliverable No.	D4.3
Work Package	WP4
Dissemination Level	PU
Author(s)	Antonio Costanzo and Sergio Falcone (INGV)
Co-Author(s)	Artur Krukowski (RFSAT), Nieves Peña Cerezo (TECNALIA), Ludovica Giordano, Maurizio Sciortino (ENEA)
Contributor(s)	Fabrizia Buongiorno (INGV), Saioa Zorita Castresana (TECNALIA), Sonia Giovinazzi (ENEA), Pavlos Krukowski (RFSAT)
Due date	2021-09-30
Actual submission date	2021-10-04
Status	Final
Revision	1.0
Reviewed by	Maurizio Pollino (ENEA), Intza Balenciaga (ICLEI)

This document has been prepared in the framework of the European project ARCH – Advancing Resilience of historic areas against Climate-related and other Hazards. This project has received funding from the European Union’s Horizon 2020 research and innovation programme under grant agreement no. 820999.

The sole responsibility for the content of this publication lies with the authors. It does not necessarily represent the opinion of the European Union. Neither the REA nor the European Commission are responsible for any use that may be made of the information contained therein.

Contact

arch@iais.fraunhofer.de

www.savingculturalheritage.eu



This project has received funding from the European Union’s Horizon 2020 research and innovation programme under Grant Agreement no. 820999.

Executive Summary

This deliverable has been prepared for the European Commission-funded research project ARCH: Advancing Resilience of historic areas against Climate-related and other Hazards. It is the key output of Task 4.3 “Information Management about Environmental Hazards” within work package 4 “Hazard & Object Information Management System”. The aim of Task 4.3 was the development of systems, tools and data-processing to provide measurable indicators, which characterise threats and hazards potentially affecting the historic areas.

The match-making online meetings and co-creation processes (led by ICLEI) involving cities, stakeholders and technical partners, allowed to identify the main environmental threats and hazards, as well as to select measurable indicators for their characterisation. However, considering that the historic areas in ARCH are exposed to different threats, specific analyses and tools were required for each case study, and only some datasets were collected in the same way for all cities. To this end, ad-hoc services and database were developed to manage historical datasets, real-time measures from monitoring systems and projections for the future. The indicators obtained from the data-processing are provided to support the subsequent risk analysis and impact scenarios, as well as to inform cities and their stakeholders.

The work described in this deliverable focused on:

- the implementation of an earthquake monitoring service to notify as soon as a new earthquake occurs in the European area, by querying the official catalogues, and to process the recordings coming from the Real-Time Urban Seismic Network deployed in (and around) the historic centre of Camerino (Italy);
- the development of the database to structure: (1) environmental measurements from crowd-sensing and official monitoring system, in order to inform about the climatic conditions and air quality in near real-time, and (2) available time-series relating to different categories of indicators, which were calculated on the base of local measures, to characterise the weather and climate extremes in the past;
- the development of a sub-system for mapping environmental contaminations considering their potential spatial and temporal evolution;
- the development of ad-hoc climate services, by processing of datasets available from existing services, to elaborate specific projections of the most relevant indicators characterising the threats and the potential effects related to the climate-change.

Finally, the main information are made accessible through the GIS dashboards of the Threats and Hazard Information System (THIS), which together with the tools of the Historic Area Information System (HARIS), are implemented in the web-platform of the ARCH information systems reachable through the ARCH-Hub.

Table of contents

Executive Summary	3
Table of contents	4
List of abbreviations	6
List of indicators	7
1. Introduction	10
1.1. Purpose of this report and relation to other deliverables.....	10
1.2. Gender statement	12
1.3. Structure of this report.....	12
2. Background on the information systems and hazard\threat indicators	13
2.1. Hazard\Threat indicators	16
2.2. Structure of the THIS database	21
3. Earthquake monitoring service	22
3.1. Real-time earthquake monitoring.....	22
3.2. System implementation due to a local low-energy earthquake	25
4. Weather/climatic and air quality monitoring	28
4.1. Near Real-time Monitoring service for environmental parameters and air quality.....	28
4.2. Modelling spatial-temporal distribution of weather and pollutants	31
4.3. Historical Copernicus Atmosphere Monitoring Service Maps.....	38
4.3.1. Time-lapse data repository	41
4.3.2. Time-lapse KML file format.....	42
4.4. Air quality provided by the MINNI modelling system in Italy.....	44
5. Historical climate.....	45
6. Climate services	50
6.1. CDS data and temporal coverage selected.....	50
6.2. Delta scaling methodology	51
6.3. Approach for EURO-CORDEX Models selection ensemble	54
6.4. CDS Toolbox.....	55
6.5. Climate Services for Bratislava.....	56
6.5.1. Thermal Oscillations application in the Toolbox.....	57
6.5.2. Precipitation indexes application in the Toolbox	60
6.5.3. Georeferenced datasets	61
6.6. Climate Services for Valencia.....	62
6.6.1. Bioindicators for Valencia	64

6.6.2. Agro-indicators for Valencia.....	66
6.6.3. Heatwaves characterization in Valencia.....	68
6.6.4. Typical Summer Days Characterization in Valencia	76
6.7. Sea Level Rise and Floods in Hamburg.....	78
6.7.1. Elbe river- Hamburg Water level changes application in the Toolbox.....	86
6.8. Climate services for Camerino.....	88
6.8.1. Multi-model ensemble building	89
6.8.2. Indices of climate change	89
7. Web-dashboards and operational guide in THIS	96
7.1. How to access information systems.....	96
7.2. Earthquake monitoring service	99
7.3. Satellite products.....	100
7.4. Air quality	102
7.5. Real-Time Environment parameters	103
7.6. Historical climate	104
7.7. Climate Services	105
8. Conclusions.....	107
9. References.....	108

List of abbreviations

Abbreviation	Meaning
CAMS	Copernicus Atmosphere Monitoring Service
CAV10	Standard Cumulative Absolute Velocity
CDS	Climate Data Store
CH	Cultural Heritage
CORDEX	Coordinated Regional Climate Downscaling Experiment
CSV	Comma-separated values
DB	Database
DSS	Decision Support System
Dx.y	Deliverable of the ARCH project related to the WPx and numbered y
ECA&D	European Climate Assessment & Dataset
EEA	European Environment Agency
FTP	File Transfer Protocol
FTPS	File Transfer Protocol Secure
GCM	Global Climate Models
GeoJSON	Geographical JavaScript Object Notation
GHG	Greenhouse gas
GIS	Geographical Information System
HAris	Historic Areas Information System
HTTP	Hypertext Transfer Protocol
HTTPS	Hypertext Transfer Protocol Secure
InSAR	Interferometric Synthetic Aperture Radar
JSON	JavaScript Object Notation
KML	Keyhole Markup Language
KMZ	Keyhole Markup Language Zipped
MARS	Copernicus Emergency Management Service
MME	Multi-model ensemble
NetCDF	Network Common Data Form
RCM	Regional Climate Model
RCP	Representative Concentration Pathways

Abbreviation	Meaning
RUSN	Real-Time Urban Seismic Network
SAR	Synthetic Aperture Radar
THIS	Threats and Hazard Information System
WP	Work package
WSDI	Warm Spell Duration Index

List of indicators

Abbreviation	Meaning
BIO1	Annual Mean Temperature
BIO2	Mean Diurnal Range (Mean of monthly (max temp - min temp))
BIO3	Isothermality (BIO2/BIO7) ($\times 100$)
BIO4	Temperature Seasonality (standard deviation $\times 100$)
BIO5	Max Temperature of Warmest Month
BIO6	Min Temperature of Coldest Month
BIO7	Temperature Annual Range (BIO5-BIO6)
BIO8	Mean Temperature of Wettest Quarter
BIO9	Mean Temperature of Driest Quarter
BIO10	Mean Temperature of Warmest Quarter
BIO11	Mean Temperature of Coldest Quarter
BIO12	Annual Precipitation
BIO13	Precipitation of Wettest Month
BIO14	Precipitation of Driest Month
BIO15	Precipitation Seasonality (Coefficient of Variation)
BIO16	Precipitation of Wettest Quarter
BIO17	Precipitation of Driest Quarter
BIO18	Precipitation of Warmest Quarter
BIO19	Precipitation of Coldest Quarter
CDD	Maximum number of consecutive dry days (RR<1mm)
CFD	Maximum number of consecutive frost days (TN<0°C)
CSU	Consecutive Summer Days

Abbreviation	Meaning
CWD	Consecutive Wet Days
FD	Frost Days
HNO ₃	Nitric acid
O ₃	Ozone
NO ₂	Nitrogen Dioxide
PM _{2.5}	Particulate matter with a diameter of 2.5 µm or less
PM ₁₀	Particulate matter with a diameter of 10 µm or less
PGA	Peak Ground Acceleration
PSA	Pseudo-Spectral Acceleration
RR	Precipitation sum
RR1	Number of wet days, with precipitation higher than 1mm
RR2	Number of wet days, with precipitation higher than 2mm
RR10	Number of wet days, with precipitation higher than 10mm
RR20	Number of wet days, with precipitation higher than 20mm
RX1DAY	Maximum amount of precipitation in 1 day
RX2DAY	Maximum amount of precipitation in 2 days
RX5DAY	Maximum amount of precipitation in 5 days
R75p	Days with precipitation > 75 th percentile of daily amounts
R75pTOT	Precipitation fraction due to R75p
R95p	Days with precipitation > 95 th percentile of daily amounts
R95pTOT	Precipitation fraction due to R95p
R99p	Days with precipitation > 99 th percentile of daily amounts
R99pTOT	Precipitation fraction due to R99p
SPI3	3-months Standardised Precipitation index
SPI6	6-months Standardised Precipitation index
SPEI	Standardised Precipitation-Evapotranspiration Index
SO ₂	Sulphur dioxide
SU	Summer Days
TG	Mean of daily mean temperature
TGx	Maximum value of daily mean temperature
TG10p	Days with TG < 10 th percentile of daily mean temperature

Abbreviation	Meaning
TG90p	Days with TG>90 th percentile of daily mean temperature
TN	Mean of daily minimum temperature
TNx	Maximum value of daily minimum temperature
TN10p	Days with TN<10 th percentile of daily mean temperature
TN90p	Days with TN>90 th percentile of daily mean temperature
TR	Tropical Nights
TX	Mean of daily maximum temperature
TXx	Maximum value of daily maximum temperature
TG10p	Days with TN<10 th percentile of daily mean temperature
TX90p	Days with TX>90 th percentile of daily mean temperature
WSDI	Warm Spell Duration Index

1. Introduction

This deliverable has been prepared for the European Commission-funded research project ARCH: Advancing Resilience of historic areas against Climate-related and other Hazards. ARCH will develop decision support tools and methodologies to improve the resilience of historic areas to climate change-related and other hazards. These tools and methodologies are developed with and for the pilot cities of Bratislava (Slovakia), Camerino (Italy), Hamburg (Germany), and Valencia (Spain), ensuring the ARCH co-creation approach for cooperation between local stakeholders (policy makers, practitioners, community members) scientific and city partners. The resulting solutions will be combined into a collaborative disaster risk management platform for guided resilience building and will include:

- Information Management System for relevant geo-referenced properties of historic areas
- **Information Management System for geo-referenced data regarding hazards and risks relevant for historic areas**
- Decision Support System (DSS) for risk and impact analysis of historic areas
- Inventory of resilience building measures and appropriate financing sources
- Visual planning tool for resilience pathways
- Resilience assessment framework to identify resilience weak points and formulate resilience action plans

1.1. Purpose of this report and relation to other deliverables

The objectives of Work Package 4 (WP4) "Hazard and Object Information Management System" are the development and implementation of two information systems:

- Historic Areas Information System (HARIS): for archiving the properties of the heritage and the characteristics of the historic area as a whole interacting with the surrounding urban and natural systems;
- Threats and Hazard Information System (THIS) to "combine" data from different sources to obtain measurable indicators to characterize the hazards that potentially affect the historic area and to collect historical and real-time data performed by climate services and / or through specific monitoring.

In the framework of WP4, datasets are structured and tools developed to support:

- Decision Support System (DSS) in the production of hazard models and vulnerability analyses, with the main purpose of evaluating impact scenarios and quantifying potential effects on the historic area and heritage assets, and consequently to support resilient options;
- ARCH Hub to give end-users direct access to the datasets and information relevant to their historic area.

This report (D4.3) is the accompanying document to the demonstrator for the Task 4.3 "Information Management about Environmental Hazards" and describes the activities related to these main objectives:

1. **the definition of measurable indicators** for the most relevant hazards affecting historic areas;
2. **the development of systems and procedures for the processing of historical and real-time data** obtained from climate services and via monitoring;
3. **the development of services and tools to make available the datasets** to other partners and end-users.

Accordingly, the contents of this document and the developments described therein are mainly linked to:

- technological solutions provided by WP4,
- needs arising from the co-creation process with the cities and the technical partners,
- consequent analyses performed by the other work packages.

Therefore, this deliverable is directly related to the following deliverables:

- **D3.4** Report on co-creating the information system
- **D4.1** Sensing and Repositories
- **D4.2** Historic Area Information Management System (HARIS)
- **D4.4** Knowledge information management system for decision support
- **D5.1** Hazard models for impact assessment
- **D7.3** ARCH disaster risk management framework
- **D7.4** Requirements description
- **D7.5** Interface specification and system architecture
- **D7.6** System design, realisation, and integration

The chart in Figure 1 is a graphical representation of the interaction between D4.3 and the aforementioned deliverables with their related tasks:

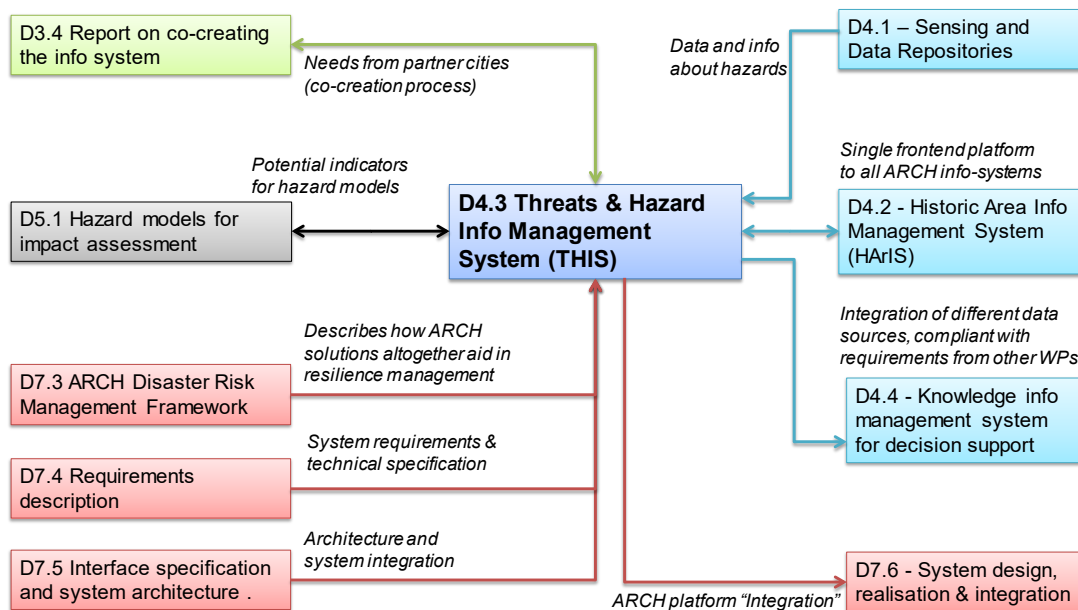


Figure 1. Representation of the main interactions between D4.3 and the other ARCH deliverables.

Please note that THIS is a dynamic information system supported by web tools, therefore the different components can be improved/updated after their submission. Likewise, any further datasets and information - as well as updates of those already included - collected within the ARCH project will feed this information system, even if they are obtained after the drafting of this document.

1.2. Gender statement

This document has been developed taking into consideration the guidance on gender in research provided in the Project Handbook (D1.2) as well as State-of-the-Art Report 5: *Gender mainstreaming in building cultural heritage resilience* D7.1 [1] on “*Gender aspects in conservation and regulation of historic areas, disaster risk management, emergency protocols, post-disaster response techniques, and techniques for building back better*”.

1.3. Structure of this report

The report is divided in nine sections.

Following this introduction, **Section 2**: provides the **background on the information systems**; lists the **reference hazard/threats indicators**, which have been identified after the co-creation process among partner cities, their stakeholders and the technical partners; outlines the **structure of the relational database** for gathering data from existing services or via monitoring.

Section 3 describes the earthquake monitoring **service developed by INGV**, in order to **continuously update both the list of earthquakes** with their characteristics, when a new one occurs in the European zone, **and the ground motion parameters** recorded in the Camerino historic area, if a given threshold of acceleration is reached.

Section 4 illustrates the **modelling spatiotemporal distribution of weather and pollutants developed by RFSAT and how the measurements**, which are provided by the near real-time services described in Section 2 of D4.1 [2], **are structured in THIS DB**.

Section 5 reports the available **indicators selected to characterise the climate in past years**, and how they are structured in THIS DB in order to allow observing trends (or differences).

Section 6 describes the **methodologies and data-processing to produce climate services based on available datasets**, these services have been performed by TECNALIA for the pilot areas of Bratislava, Hamburg and Valencia and by ENEA for Camerino.

Section 7 is an **operational guide for the THIS web-tools**, which have been developed by INGV and integrated in the same platform of HARIS (cf. Section 5 in D4.2 [3]) in order to access information of the previous sections and the surveys on satellite data (cf. Section 2 of D4.1 [2]).

Section 8 summarises the **main findings** related to Task 4.3.

Bibliographic references (Section 9) are reported at the end of the document.

2. Background on the information systems and hazard/threat indicators

In this introductory paragraph, a description of the background on the information systems is provided, as indeed already reported in D4.2 [3], instead, in the next ones the hazard indicators are listed and the structure of the THIS DB is presented.

The historic areas Information System (HARIS) and the Threats and Hazards Information System (THIS) are the two information systems provided by the ARCH project: the first is developed to capture the characteristics of the historic areas; whereas, the second one is oriented to the collection of information and data to quantify indicators related to the hazards affecting the same areas. The two information systems have the same concept and are integrated between them. However, the databases are specifically designed to allow the storage and management of the different types of information.

The mission of THIS was described in the D7.4 [4]; it enables end-users to access geo-referenced information about historic and real-time environmental threat indicators for historic areas. The strategy chosen to implement the information systems and integrate these in ARCH platform is also described in D7.5 [5]. The information systems are based on the Service Oriented Architecture (SOA), which defines a way to make software components reusable via service interfaces. The interfaces are based on common protocols and methods in such a way that they can be easily incorporated into new applications without having to perform deep integration.

To this end, the key elements of the service-oriented approach are:

- integration of existing services and the reusability of those developed, that are useful to meet needs, constraints, configurations and objectives;
- flexibility in adapting the configuration of the services, also to improve the existing ones in order to improve performance, functionalities, way to access it, etc.;
- composition of (distributed) services to create new value-added services, providing high-quality, and better performance capabilities.

In this framework, the integration of the THIS components, as already made for those of HARIS, have been designed with the main objective of implementing a flexible and interoperable information system. It has also been considered the reuse of the components and the integration of simple services to obtain more complex ones, without requiring changes in the general logic of the system. This methodology is also necessary with a view to creating information systems that make it possible to meet the different needs of the ARCH partner cities. The services use protocols that describe how it can send and parse data and messages. All THIS components were properly tested prior to release. However, further evaluations, including possible corrections, will be carried out during the next project months as part of ARCH Task 7.7 “Continuous system integration and validation”, following the validation of use cases by ICLEI, technical partners, and city partners together with their local stakeholders.

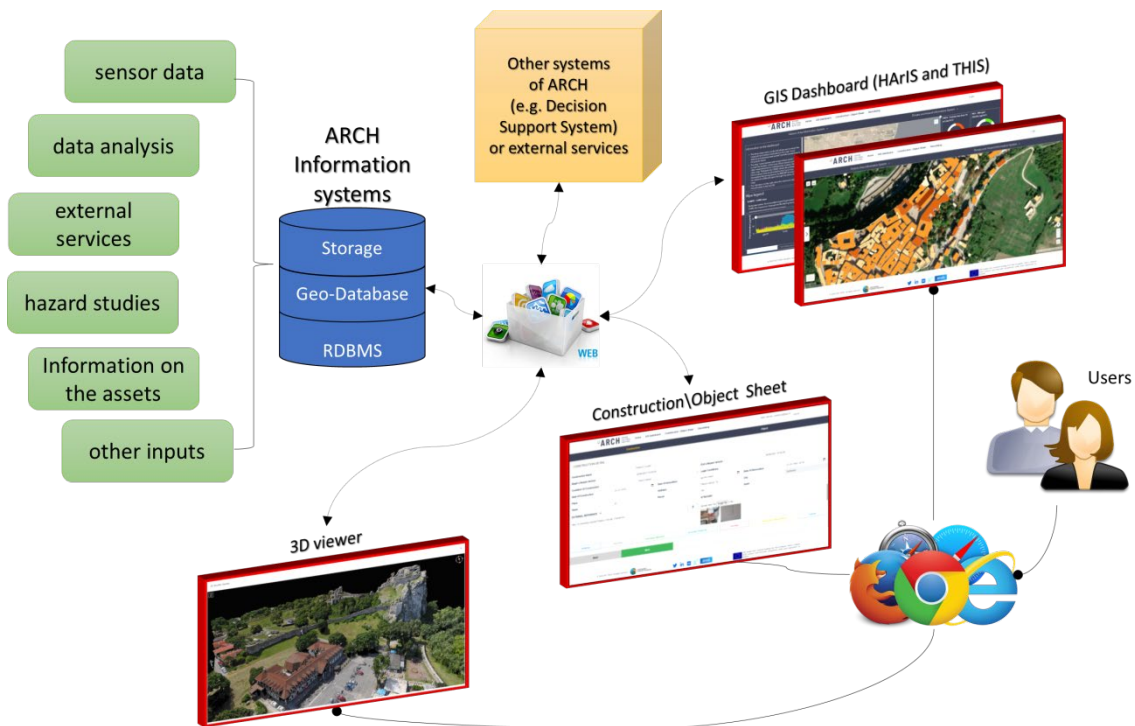


Figure 2. Functional schema of the ARCH information systems: data sources (green boxes), relational databases, repositories and management services (blue cylinders), data consumers (yellow cube), tools to access data via web (red panels). This figure is already included in D4.2 [3] to describe the information systems.

As shown in Figure 2, the information systems can be fed by several different sources (especially for the THIS systems):

- sensors for recording physical parameters;
- data analyses to produce processed information;
- external services to include data already available in other systems.

Specific service connectors have been developed for external data-providers, taking into account different transmission protocols and update intervals (e. g. 24/7 for earthquakes, one or more times per day for environmental parameters and air pollutants, occasionally for existing hazard maps), to receive and pre-process (automatically or manually) data before storing it. With this purpose, the storage repository and relational geodatabase were designed and built to structure the data.

A Relational Database Management System (RDBMS) is responsible for storing and reading data from the databases as requested by other software components. The physical storage makes use of several proprietary components such as Microsoft SQL Server, ArcGIS for Desktop and ArcGIS Server. Simple tables and well-defined attribute types are the key elements to store the schema, rule, base, and spatial attribute data for each geographic dataset. This approach provides a formal model for storing and working with the acquired data. Following this approach, structured query language (SQL) has been used to create, modify, and query tables and their data elements. The schema includes the definitions, integrity rules, and behaviour for each geographic dataset, including properties for feature classes, topologies, networks, raster catalogues, relationships and domains. In particular, the integrity and behaviour of the geographic information are defined in a collection of meta-tables in RDBMS.

The software logic adopted for the information systems allows to access and work with a variety of geographic data in different file formats, including shapefiles, computer-aided drafting files, irregular triangulated networks, grids, images, geographic language mark-up files, and numerous other GIS data sources. Furthermore, the ArcGIS applications are used to have a transaction model for managing GIS data workflows.

The core of the system is composed of middleware, applications, and processing tools. Essentially functioning as a hidden translation layer, middleware enables communication and data management for distributed applications. The database middleware and application server middleware permit the communication among the applications using messaging frameworks such as simple object access protocol (SOAP), web services, representational state transfer (REST) and JavaScript object notation (JSON). In particular, the system can manage different information that needs to be communicated, which include security authentication, transaction management, message queues, applications servers, web servers and directories.

The hardware and software components of the information systems are implemented and hosted on servers at the Laboratory of Cultural Heritage at the INGV headquarters in Rende (CS), Italy. The portal of the information system is currently reachable at the web address shown in the blue box and some examples of the current webpages are in section 7.

Web site to reach web-tools of HARIS:

<http://www.cs.ingv.it/archportal>

More details about the structure of the information systems and relationships with the other technological systems of the ARCH project can be found in D7.5 [5].

2.1. Hazard\Threat indicators

Table 1 summarizes the main threats and hazards affecting the HAs of the ARCH cities under the ARCH framework. The hazards\threats and the potential indicators have been identified following the match-making meetings, led by ICLEI, involving partner cities, local stakeholders and technical partners. The measurable indicators, metrics, data-sources and outcomes are reported in the table below for each city and threat\hazard.

Table 1. Threats and Hazards, indicators (cf. List of Indicators for the acronyms), metrics and outcomes.

Threat /Hazard	Bratislava	Camerino	Hamburg	Valencia	Measurable Indicators	Metrics	Source	Reference period	Outcomes
Earthquakes		European Zone			Magnitude	-	Earthquake monitoring service	Near Real time	Georeferenced information about earthquakes in near real-time (cf. section 3.1) structured and available in THIS platform (cf. section 7.2)
					Epicentre (longitude, latitude)	degrees WGS84			
					Hypocentral depth	km			
		Historic Area			PGA	g, cm/s ²			
					PSA	g, cm/s ²			
Ground deformation (Subsidence)			City	La Albufera	Deformation velocity	mm/y, cm/y	Survey by SAR Satellite data	Observations on the last years	Deformation velocities and LOS displacements structured and available in THIS platform (cf. section 7.3)
						Total displacement on the observation period			
Rock displacement	Devin Castle				Daily Climatology (Tmax, Tmin)	°C	C3S-CDS	(1981-2010); (2011-2040); (2041-2070); (2071-2100)	Bratislava Thermal Oscillations application (cf. section 6.5.1)
					Monthly Climatology (Tmax/Tmin)				
					Temperature range (Tmax-Tmin) Oscillations				
					<ul style="list-style-type: none"> RR1 RR2 RR10 RR20 	days			Bratislava Precipitation Extreme Indices application (cf. section 6.5.2), with georeferenced datasets integrated and available in THIS platform (cf. section 7.7)
			<ul style="list-style-type: none"> RX1DAY RX2DAY RX5DAY 	mm					

Threat /Hazard	Bratislava	Camerino	Hamburg	Valencia	Measurable Indicators	Metrics	Source	Reference period	Outcomes
Pluvial flooding	Extended area around the City				<ul style="list-style-type: none"> RR1 RR2 RR10 RR20 	days	C3S-CDSC3s	(1981-2010); (2011-2040); (2041-2070); (2071-2100)	Bratislava Precipitation Extreme Indexes application (cf. section 6.5.2), with georeferenced dataset structured and available in THIS platform (cf. section 7.7)
					<ul style="list-style-type: none"> RX1DAY RX2DAY RX5DAY 	mm			
	Historic Area (in and around)	Historic Area (in and around)			<ul style="list-style-type: none"> RR RX1DAY RX2DAY RX5DAY 	mm	Historical climate dataset from ECA&D	Annual/Monthly values on the past (up to 50 years depending on the site)	Indices of extreme precipitation (cf. section 5) from historic datasets for all cities structured and available in THIS platform (cf. section 7.6)
	Historic Area (in and around)				<ul style="list-style-type: none"> RR1 RR10 RR20 R75p R95p R99p 	days			
	Historic Area (in and around)				<ul style="list-style-type: none"> R75pTOT R95pTOT R99pTOT 	%			
	Historic Area (in and around)								

Threat/Hazard	Bratislava	Camerino	Hamburg	Valencia	Measurable Indicators	Metrics	Source	Reference period	Outcomes		
Extreme events (Drought/Floods, Extreme Temperatures, Heatwaves)	Historic Area (in and around)	Temperature	°C	Weather / climatic monitoring	Near real time	Weather parameters obtained from crowd-sensing services in and around the HAs (cf. section 4.1). The measure are structured and available in THIS platform (cf. section 7.5)					
					Humidity	%					
					Rainfall	mm					
					Pressure	hPa					
						Wind strength	kps				
						<ul style="list-style-type: none"> • TG • TN • TX • TGx • TNx • TXx 	°C	Historical climate dataset from ECA&D	Annual/Monthly values on the past (up to 50 years depending on the site)	Indices of extreme events from historic datasets (cf. section 5) for all cities structured and available in THIS platform (cf. section 7.7)	
					<ul style="list-style-type: none"> • CDD • CFD • CSU • CWD • FD • SD • TR • WSDI • TG10p • TN10p • TX10p • TG90p • TN90p • TX90p 	days					
					<ul style="list-style-type: none"> • SPI3 • SPI6 	°C					
					Pressure	hPa					
					Humidity	%					
City			City	Temperature	°C	Survey by Satellite data	images available in the last 15 years				Temperature maps and UHI based on satellite data available in THIS platform (cf. section 7.3)

Threat / Hazard	Bratislava	Camerino	Hamburg	Valencia	Measurable Indicators	Metrics	Source	Reference period	Outcomes
				City	Heatwave index (Intensity, duration, frequency)	°C, days, number	C3S	(1981-2010); (2011-2040); (2041-2070); (2071-2100)	Georeferenced datasets containing information for the heatwaves characterization in Valencia (cf. section 6.6.3)
		City			Freeze-Thaw cycles	-	CORDEX	annual values between 2030 and 2100	Annual values of the indicators for Camerino related to the negative effects (e.g. stone materials) on the built cultural heritage (cf. section 6.8.2)
					TX-TN	°C			
					RR	mm			
					RR99pTOT	%			
					RR20	days			
					SPEI	-			
				TXx	°C				
Biodiversity loss / Crop yield loss				Extended area around the City	<u>Bio-Indicators</u>	°C	C3S-CDS	(1981-2010); (2011-2040); (2041-2070); (2071-2100)	Valencia Bioclimatic Indicators application (cf. section 0), with georeferenced datasets containing the bioclimatic information (for the historical bioindicators and the average and standard deviation for each of the selected future periods). The above datasets have been structured and available in the THIS platform (section 7.7)
					• BIO1	-			
					• BIO2	°C			
					• BIO3	-			
				• BIO4	mm				
			• BIO5						
			• BIO6						
			• BIO7						
			• BIO8						
			• BIO9						
			• BIO10						
			• BIO11						
				• BIO12					
				• BIO13					
				• BIO14					
				• BIO15					
				• BIO16					
				• BIO17					
				• BIO18					
				• BIO19					

Threat /Hazard	Bratislava	Camerino	Hamburg	Valencia	Measurable Indicators	Metrics	Source	Reference period	Outcomes
					<u>Agro-Indicators</u> <ul style="list-style-type: none"> • CSU • CWD • FD • SD • TR • WSDI 	days			
Air quality	City	City	City	City	Different pollutants (cf. list in Table 13)	cf. metrics in Table 13	CAMS	every 12 hours	Maps of environmental contaminations (cf. section 4.3)
	Historic Area (in and around)	Near Real-Time Concentrations: <ul style="list-style-type: none"> • PM₁₀ • PM_{2.5} • NO₂ • SO₂ • O₃ 	µg/m ³	Air quality monitoring	Near real time	Pollutants measured by official monitoring systems and crowdsensing in and around the HAs (see section 4.1) structured and available in THIS platform (see section 7.4)			
		Central Italy			Mean Annual Concentrations <ul style="list-style-type: none"> • SO₂ • HNO₃ • PM₁₀ • O₃ 	µg/m ³	Air quality projections	2015, 2020, 2030	Annual concentrations of the pollutants for historic data and future projections (see section 4.4).
Sea Level Rise			City		total water level and surge level for different return periods	cm	C3S-CDS	(1981-2010); (2041-2070); (2071-2100)	Total water level and Tidal indicators for Hamburg pilot area for different return periods (cf. section 6.7) and prototype application on the water level changes of the Elbe river (cf. section 6.7.1)

The indicators have been collected (and updated) to learn about historical trends/events, as well as to characterize the current situation and produce future projections relating to the main threats and hazards. The public information and datasets will be made available to cities and stakeholders, as well as being used to characterise the hazard models and impact scenario in WP5.

2.2. Structure of the THIS database

To structure the different datasets related to measures and indicators (cf. Table 1) the THIS DB has been designed and developed by INGV in accordance with the structure sketched in Figure 3 below. The tables are constituted to host both the measures\indicators and the related information to characterise them (e.g. type, status, site or sensor of measurement). In particular, the “dynamic” tables to collect continuously data from the monitoring systems (e.g. earthquake, weather and air quality services in sections 3-4) or those periodically updated (historical climate in section 5) are detailed considering the relationships between them; whereas, the “static” tables for the climate services (section 6) have been developed based on the specific information of each product. Moreover, the information is accessible through the THIS web-tools (section 7).

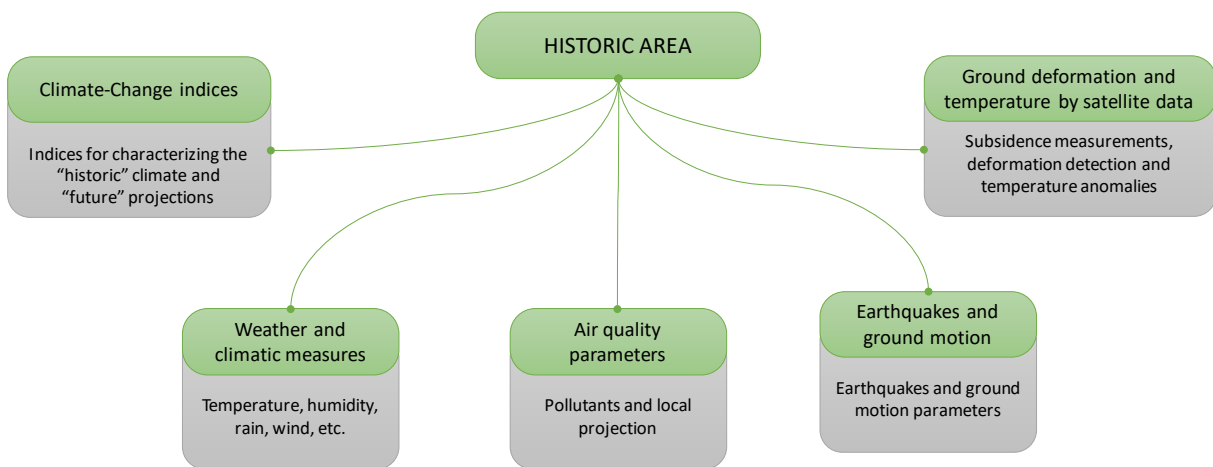


Figure 3. Structure of the database implemented in THIS.

3. Earthquake monitoring service

The earthquake monitoring service combines several data sources available in the technical and scientific literature, considering those that provide information on the Euro-Mediterranean Region, and others with more details on the Italian territory - given that the seismic risk has a strong impact on the ARCH city of Camerino (D3.3 “City baseline report – Camerino” and D3.2 “Local partnership and work plan for Camerino). As such, different typologies of information are included in THIS and the ARCH web-GIS tools:

- historic earthquakes provided by the SHARE European Earthquake Catalogue (SHEEC)¹ [6][7] and the INGV Catalogue of Strong Earthquake in Italy (CFTI5-Med)² [8][9];
- seismogenic sources provided by the European Database of Seismogenic Faults³ (EDSF)⁴ [10] and INGV Database of the Individual Seismogenic Sources⁵ (DISS) [11];
- seismic hazard maps provided by European map of seismic hazard in EU SHARE Project⁶ [12] and Italian seismic hazard map⁷ [13].
- real-time earthquake monitoring provided by web-service that polls the seismic catalogues, also providing a trigger to process recordings by the Real-Time Urban Seismic Network (cf. section 4 in D4.1 [2]) as soon as a new earthquake occurs.

3.1. Real-time earthquake monitoring

The workflow and functionalities developed by INGV and related to the earthquake monitoring service are described in this section. Figure 4 below shows the workflow to process recordings obtained by the urban seismic network and it can be summarised with the following steps:

Step 1. THIS continuously queries the earthquake catalogues managed by the European Mediterranean Seismological Centre (EMSC) [14] collecting data from 70 seismological networks of the Euro-Mediterranean region to retrieve information according to the International Federation of Digital Seismograph Networks (FDSN) standard protocols⁸. A web-service developed through ObsPy toolbox [15][16] in near real-time (every 5' minute) receives and structure the characteristics of new earthquakes (magnitude, location, date, etc.), which have a magnitude greater than three and an epicentre in the European region, storing them into a specific table of the geodatabase (Table 2). This allows providing updated information about the seismic events, directly, via the ARCH web-GIS platform.

¹ <https://www.emidius.eu/SHEEC/>

² <http://storing.ingv.it/cfti/cfti5/>

³ <http://diss.rm.ingv.it/share-edsf/>

⁴ <http://www.share-eu.org/>

⁵ <http://diss.rm.ingv.it/diss/>

⁶ <http://www.efehr.org/en/Documentation/web-services/>

⁷ <http://esse1.mi.ingv.it/>

⁸ <http://fdsn.org/services>

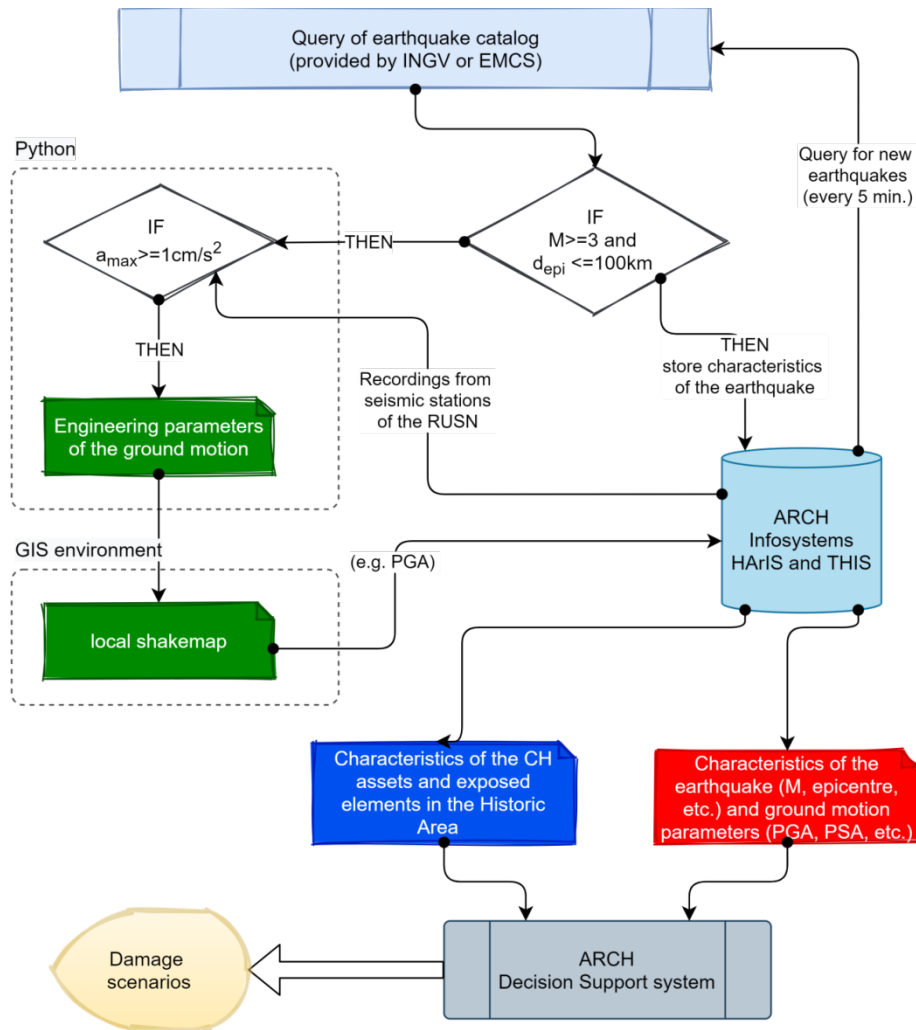


Figure 4. Workflow of systems and components for the detection of a new earthquake, the process of the recordings obtained by the RUSN and the transfer of the ARCH DSS.

- Step 2. Once a new earthquake is detected, the web service retrieves the acceleration time-histories recorded by the seismic stations of the RUSN – the characteristics of which are structured in the DB (Table 3) - and, then, also verifies if the maximum absolute value is greater than 1 cm/s^2 .
- Step 3. If the acceleration threshold has passed, another script calculates the rotation-invariant parameters of the ground-motion [17], in terms of PGA, PSA or Arias Intensity [18], Standard Cumulative Absolute Velocity [19], to take into account frequency, duration, and energy content [20]. These parameters are structured in the DB linked to the earthquake and measurement station.
- Step 4. By interpolating the measured ground-motion parameters using the inverse distance weighted (IDW) technique [21] through the ArcPy module for Python [22], a map covering the whole monitored area is obtained. The power coefficient that regulates the interpolation function has been set to 4, and, however, for each unmeasured point only the measures closer than 1000m are used in the calculation.

Table 2. “EARTHQUAKE” Table into THIS DB to structure characteristics of the earthquakes.

Attribute	Value Type	Definition
OBJECTID	integer	ID to identify object in the table
Location	text	location of the earthquake
JDay	integer	Jiulian day
Date	date	Date and time
Lat	numeric	latitude of the epicentre
Lon	numeric	longitude of the epicentre
Depth	numeric	hypocentral depth
Mag	numeric	magnitude
StationAct	Integer	activation of the RUSN (yes/no)
MagType	text	magnitude type
SHAPE	geography	Point in vector layer representing the epicentre
ResId	text	Id of earthquake in the reference catalogue
ExtLink	text	external link for detailed information

Table 3. “EARTH_STATION” Table into THIS DB to structure information about the stations of the RUSN

Attribute	Value Type	Definition
OBJECTID	integer	ID to identify object in the table
Name	text	Name of the station
Netw	text	Network od the station
Chan	text	Type of channel (e.g. HN for accelerometer)
Lat	numeric	Latitude of the station
Lon	numeric	Longitude of the station
Alt	numeric	Altitude of the station
Datalog	text	Type of data-logger
Sens	text	Type of sensor
PathTraces	text	Path of the traces in the DB
PathResp	text	Path of the instrumental response in the DB
Enable	integer	Current working (yes/no)
DateStart	date	Start date
DateEnd	date	End date
SHAPE	geography	Point in vector layer representing the station

Table 4. “EARTH_PARAMETERS” Table into THIS DB to structure ground-motion parameters

Attribute	Value Type	Definition
OBJECTID	integer	ID to identify object in the table
EarthquakeRef	Integer	Reference to table EARTHQUAKE
StationRef	Integer	Reference to table EARTH_STATION
PGA	numeric	Peak Ground Acceleration
PSA0_1s	numeric	Pseudo Spectral Acceleration at period 0.1s
PSA0_3s	numeric	Pseudo Spectral Acceleration at period 0.3s
PSA1_0s	numeric	Pseudo Spectral Acceleration at period 1s
PSA3_0s	numeric	Pseudo Spectral Acceleration at period 3s
AI	numeric	Arias Intensity
CAV10	numeric	Standard Cumulative Absolute Velocity
EpiDis	numeric	Epicentral Distance
Azim	numeric	Azimuth of the direction epicentre-station clockwise from north

3.2. System implementation due to a local low-energy earthquake

A low-energy earthquake (ML=3.3) was recorded by the urban seismic network on 18th April 2021, after about two months from the deployment of the accelerometric stations of the RUSN. This earthquake, which occurred at the epicentral distance of about 13 km south of Camerino, was recorded by the stations of the RUSN (Figure 5), allowing to verify the processing chain of the system.

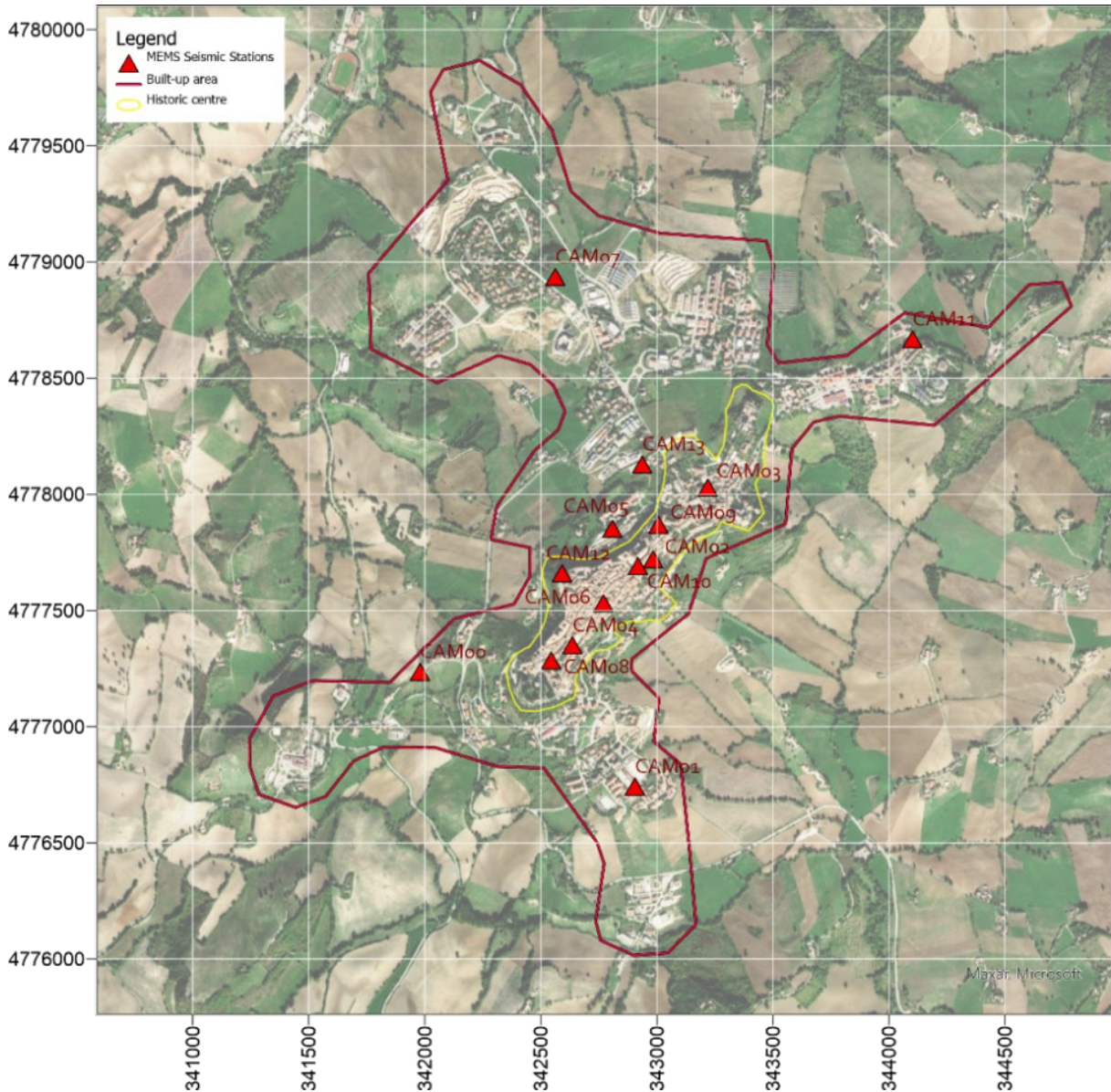


Figure 5. Seismic station of the Real-Time Urban Seismic Network (RUSN) in Camerino [2].

Figure 6 shows the PGAs calculated from the acceleration time-histories recorded by the sensors of the RUSN in the different locations of the historic area.

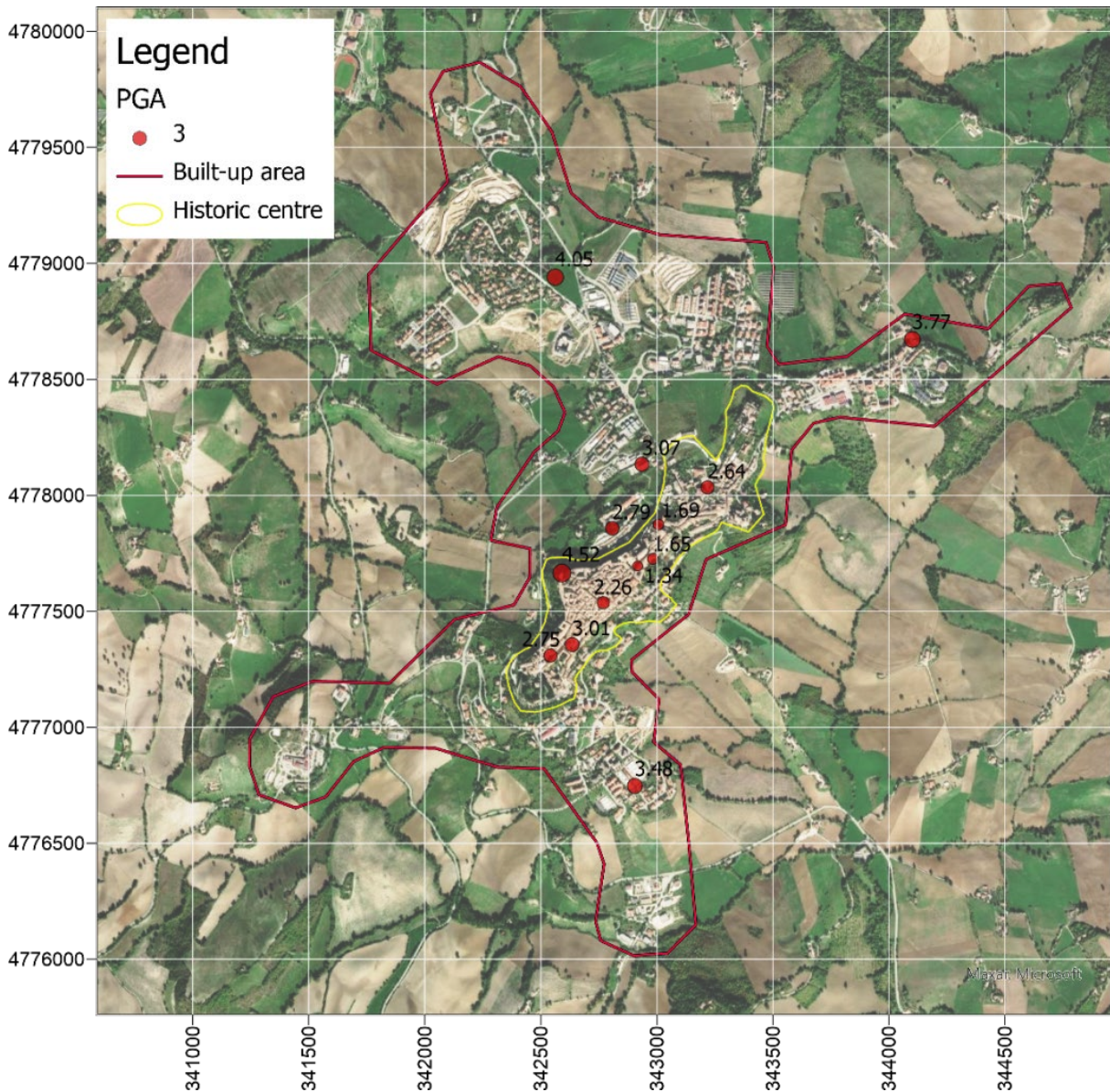


Figure 6. Peak Ground Accelerations in cm/s^2 recorded by the RUSN during the ML 3.3 earthquake occurred on 18th April 2021 at about 13km south of Camerino (<http://cnt.rm.ingv.it/en/event/26473301>).

The local shaking map in Figure 7 is obtained by interpolating the PGA values in the built-up area around the historic centre. The Inverse Distance Weighted (IDW) algorithm was used in the computation, setting the power coefficient to four and taking into consideration only measurements at a distance less than (or equal to) a thousand metres from the calculation point. In fact, in the southwestern zone of the built-up area of Camerino no value is assigned as soon as the distance from the nearest station (i.e. CAM08 in Figure 5) becomes greater than the limit because the data from CAM00 station was not available for the earthquake.

The local shake maps are available for the ARCH DSS in order to characterise the seismic actions when an earthquake occurs, taking also into account the site effects on the ground

motion due to the geometry of the deposits, the geotechnical properties of the soils and the topographic peculiarities ([23],[24],[25]).

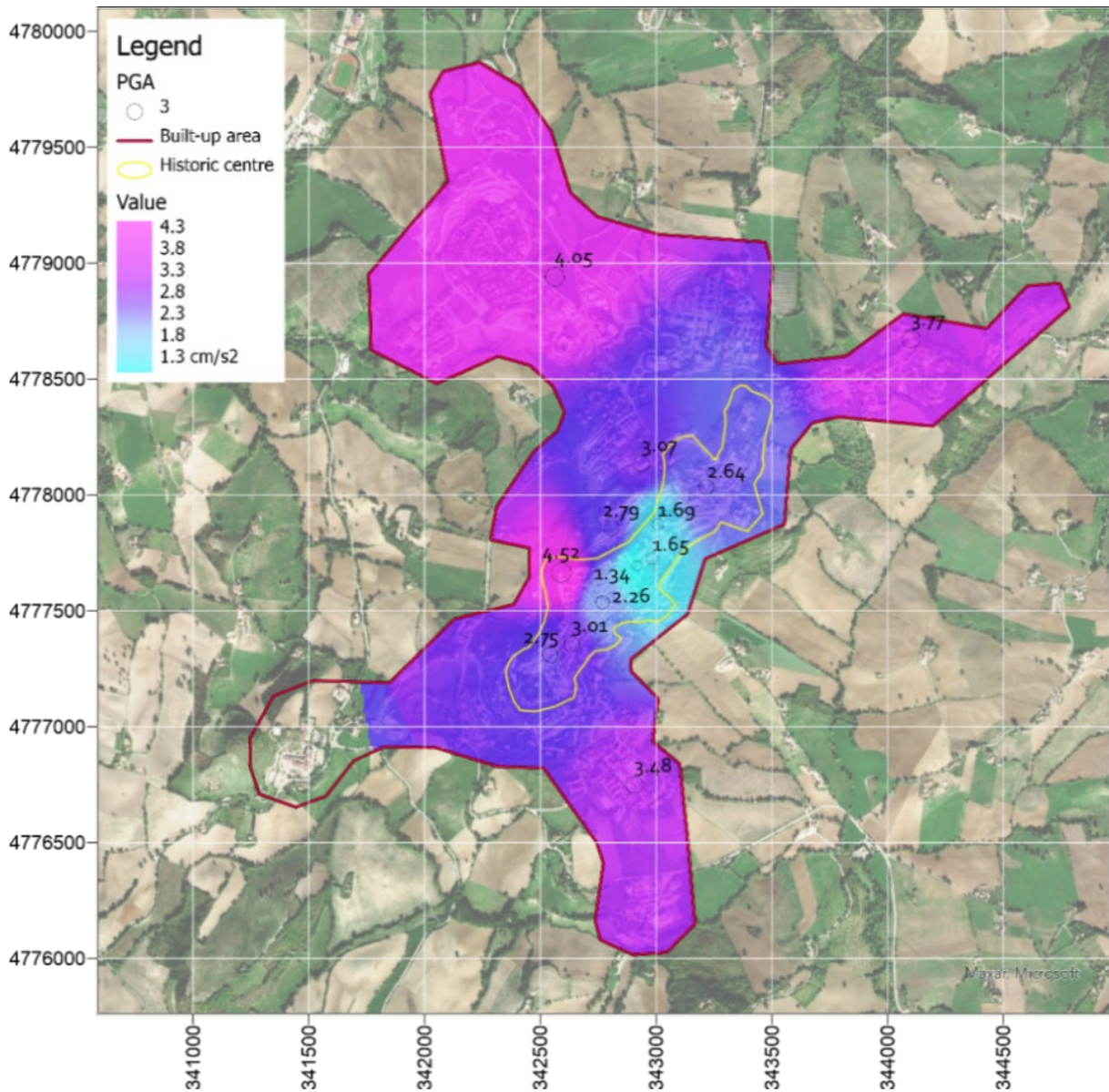


Figure 7. Local PGA-shakemap in cm/s² obtained by Inverse Distance Weighted (IDW) interpolation with power coefficient set to 4.

4. Weather/climatic and air quality monitoring

4.1. Near Real-time Monitoring service for environmental parameters and air quality

The near real-time weather conditions and air quality are provided by means of web-services developed by RFSAT and INGV to obtain observations from open data platforms and structure them in THIS. These platforms collect data from terrestrial sensors that are managed by citizens and the web-services permits to transfer the measures in near real-time to the THIS DB (cf. Section 2 of the D4.1 [2]). The environmental parameters and pollutants are structured in Table 5 and Table 6, respectively. Moreover, vocabularies to define pollutants and data-sources are provided in Table 7 and Table 8.

Table 5. “ENV_DATA” Table into THIS DB to structure environmental parameters provided by RFSAT via web-service described in D4.1

Attribute	Value Type	Definition
OBJECTID	integer	ID to identify object in the table
MeasureRef	integer	Reference to data source service
MeasurementDate	date	Date of the measurement
Latitude	numeric	Latitude of the measurement
Longitude	numeric	Longitude of the measurement
Altitude	numeric	Altitude of the measurement
Temperature	numeric	Temperature value
Humidity	numeric	Relative humidity value
Pressure	numeric	Pressure value
Rain60min	numeric	Rain value on 1 hour
WindStrength	numeric	Wind strength value
WindAngle	numeric	Wind angle value
GustStrength	Numeric	Gust strength value
GustAngle	numeric	Gust angle value
SHAPE	geography	Point in vector layer representing the measurement

Table 6. “POLLUTION_DATA_RFSAT” Table into THIS DB to structure air quality parameters provided by RFSAT via web-service described in D4.1

Attribute	Value Type	Definition
OBJECTID	integer	ID to identify object in the table
VocPollutantsRef	integer	Reference to the table VOC_POLLUTANTS (cf. next table)
Country	text	Code country
City	text	City
DateVal	date	Date of the measurement
Concentration	numeric	Value of the pollutant concentration
MinVal	numeric	Minimum concentration on the observation time (if available)
MaxVal	numeric	Maximum concentration on the observation time (if available)
Median	numeric	Median concentration on the observation time (if available)
Variance	numeric	Variance of the concentration (if available)
UnitOfMeasurement	text	Measurement unit
DataSourceRef	integer	Reference to table VOC_POLLUTION_DATASOURCES
SHAPE	geography	Point in vector layer representing the measurement

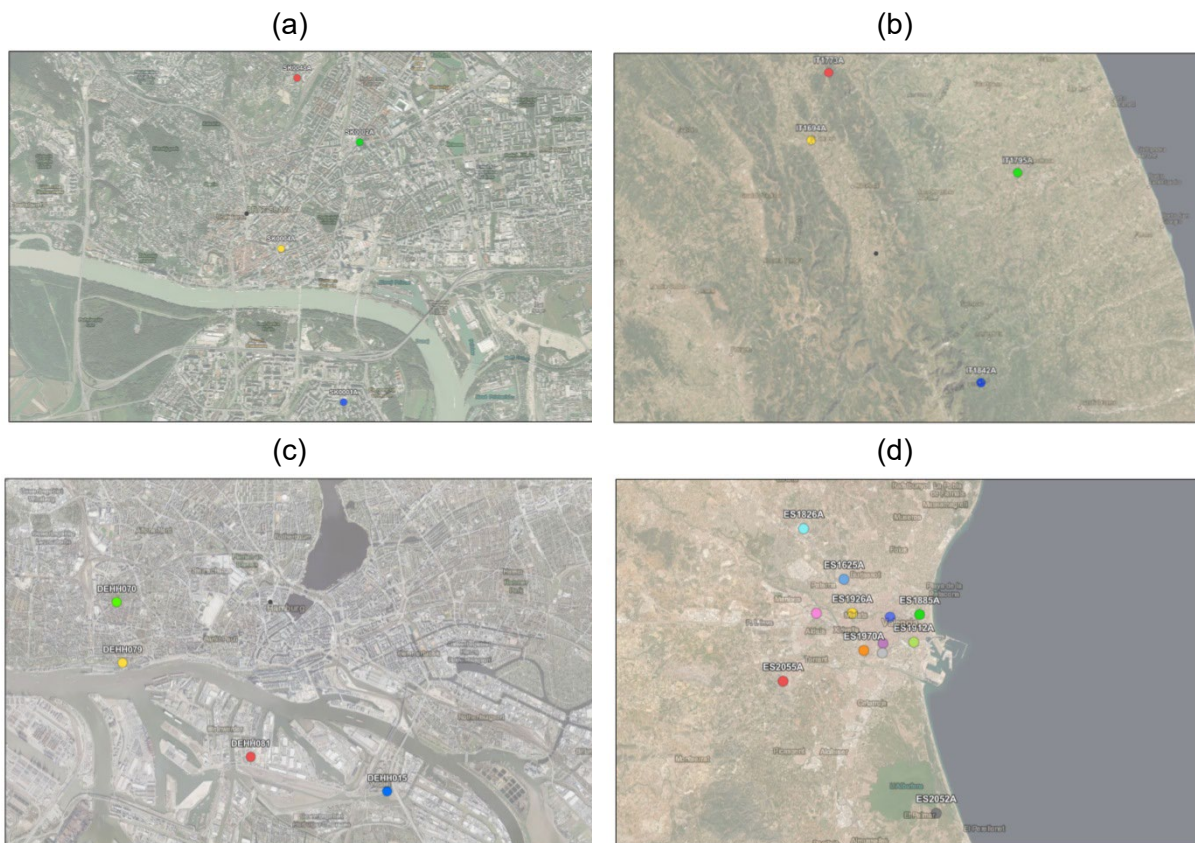
Table 7. “VOC_POLLUTANTS” Table into THIS DB for vocabulary of the air quality parameters

Attribute	Value Type	Definition
OBJECTID	integer	ID to identify object in the table
Label	text	Type of pollutant
Notation	text	Code of the pollutant

Table 8. “VOC_DATASOURCES” Table into THIS DB for vocabulary of data provider

Attribute	Value Type	Definition
OBJECTID	integer	ID to identify object in the table
Code	text	Code of the data source
Source	text	Name of the data source
WebUrl	text	Link to website
Comment	text	Any notes

Furthermore, INGV has developed a web-service to recovery the current situation of the air quality as provided by the official EEA⁹ monitoring, with updates every six hours. Monitoring stations within (and around) the pilot cities (Figure 8) were selected to obtain available information on key pollutants: particulate matter (PM₁₀); ozone (O₃); nitrogen dioxide (NO₂); sulphur dioxide (SO₂); carbon monoxide (CO).



⁹ <https://airindex.eea.europa.eu/Map/AQI/Viewer/>

Figure 8. Locations of the EEA monitoring stations between those available for the European Air Quality Index and selected in and around: Bratislava (a), Camerino (b), Hamburg (c) and Valencia (d).

Table 9. "POLLUTION_STATION" Table into THIS DB to structure air quality station of EEA

Attribute	Value Type	Definition
OBJECTID	integer	ID to identify object in the table
Country	text	Country code
AirQualityStation	text	Station code
StationType	text	Station type (background, traffic, etc.)
StationArea	text	Station area (urban, suburban, rural, etc.)
Latitude	numeric	Latitude of the station
Longitude	numeric	Longitude of the station
Altitude	numeric	Altitude of the station
SHAPE	geography	Point in vector layer representing the station

Table 10. "POLLUTION_DATA" Table into THIS DB to structure air quality parameters provided by EEA

Attribute	Value Type	Definition
OBJECTID	integer	ID to identify object in the table
StationRef	integer	Reference to table POLLUTION_STATION
SamplingProcessRef	integer	Reference to table POLLUTION_SAMPLING_PROCESS
AirPollutantRef	integer	Reference to table VOC_POLLUTANTS
AveragingTime	text	Averaging time of the measurement
Concentration	numeric	Concentration of the pollutant
UnitOfMeasurement	text	Measurement unit
DatetimeBegin	date	Start of the measurement
DatetimeEnd	date	End of the measurement
ValidityRef	integer	Reference to table VOC_VALIDITY
VerificationRef	integer	Reference to table VOC_VERIFICATION

Table 11. "VOC_VALIDITY" Table into THIS DB for the validity of the measures in Table 10

Attribute	Value Type	Definition
OBJECTID	integer	ID to identify object in the table
Label	text	Label
Status	text	Status of validity (Not valid, Valid, etc.)

Table 12. "VOC_VERIFICATION" Table in THIS DB for the verification of the measures in Table 10

Attribute	Value Type	Definition
OBJECTID	integer	ID to identify object in the table
Label	text	Label
Status	text	Status of validity (Verified, Not verified, etc.)

4.2. Modelling spatial-temporal distribution of weather and pollutants

This section described the models being developed by RFSAT to provide spatiotemporal distribution of weather conditions and contaminants (e.g. gasses) from sparse sensor networks over geographical areas of interest, such as pilot city areas.

Models are developed to take into consideration the following main contributing factors:

1. Ground\Surface elevation, including both natural ground elevation (e.g. mountains) and man-made obstacles (e.g. urban building footprints), a serious factor to accumulation of pollutants in bounded areas.
2. Weather conditions, such as wind speed and direction, as main contributing factors in directional spread of gas contaminations. Considering that sensors only provide such information at sparse locations, geographical distribution of weather conditions has to be made at every new iteration (observation time) prior to any distribution analysis of polluting gasses can be done.
3. Temperature and humidity as main factors contributing to vertical convection propagation of gases away from the ground, mainly during summer periods, while causing stronger accumulation during cold and humid winter periods.

Models assume that regular observations are made such that to be able to provide continuous analysis of changes to both weather conditions and gas distributions. Large irregularities are likely to negatively affect the accuracy of modelled distribution maps. Therefore, in case of longer “uncertainty” periods, linear approximation of intermediate values is made over the unknown time periods to allow models to operate in a more continuous manner.

Since there is no data available yet regarding actual pollution sources, such as road traffic or factory emissions, the developed models are based on sensor data only and attempt to perform analysis of distribution of pollutants between such monitoring stations. In this respect, such sensor monitoring stations are treated as “pollution injectors”, with detected levels of pollutions treated as constant (at any given time) gas injections.

A distribution model for air pollution assumes movement of particles from higher density areas to a lower density one, while keeping a constant amount of overall volume of pollution. The following equation defines a simple distribution model. It comprises parametrized impacts from additional effects such as wind speed and direction (W_S) and ground elevation (G_E):

$$V_{new} = V_{old} + \sqrt{\sum_{i \in neighbours}^{all} (V_{old} - V_i * W_S * G_E)} \quad (1)$$

The wind parameter W_S is a distribution matrix of size N, defined and applied to each location that correlates the influence of the distributions from neighbouring cells on the amount of pollutant at the current location that can be defined for any range of neighbouring cells.

$$W_S = \begin{bmatrix} W_{1,1} & \dots & W_{1,N} \\ \vdots & \ddots & \vdots \\ W_{N,1} & \dots & W_{N,N} \end{bmatrix} \quad (2)$$

In cases when there is no wind or change of elevation, the W_S reduces to unity matrix. In the simplest case when we consider only the closest cells, it can be a 3x3 size, although in such a case a larger number of iterations are required per unit time since modelled propagation is much slower. On the other hand larger matrix permits more realistic calculation of distributions, especially when accommodating for other effects like wind speed and direction, ground elevation or urban building footprint. On the other hand this also implies larger size of the borderline undefined areas and so simulation needs to extend by N on every side of the area. Hence larger N implies larger simulation area as well as significantly longer processing times, at a benefit of more accurate simulation and less iterations per unit time.

The assumption is that W_S reduces distribution by increasing impact of neighbouring cells that are against the wind and increasing spread with the wind. On the contrary, the difference of elevation from a neighbouring cell increases its influence, while lower elevation contributes to the easier distribution of the pollution distribution. Parameters W_S and G_E have a meaning of the probability and hence the total of those parameters corresponding to all neighbouring cells that are expected to contribute to the new value at a given location must be equal one. Otherwise, unpredictable effects can be expected. The black background corresponds to low density while white areas indicate highly polluted areas. Certainly, colour coding can be adjusted to comply with common colour code in THIS platform.

As can be noticed in Figure 9, with a lack of external environmental influences like wind or ground elevation, the density of pollution spreads equally in all directions. In case of sources in close vicinity, a mutual impact of distribution clouds can be observed. This clearly shows a need for dense location of sensors in order to be able to reliably model distribution of various aerial pollutants. On the other hand, as the simulation progresses (note that images comes from short simulations of only 10 minutes, corresponding to more than 3600 iteration steps), the results can be expected to become smoother while areas centred around each real sensor acquisition location become more interconnected with one another.

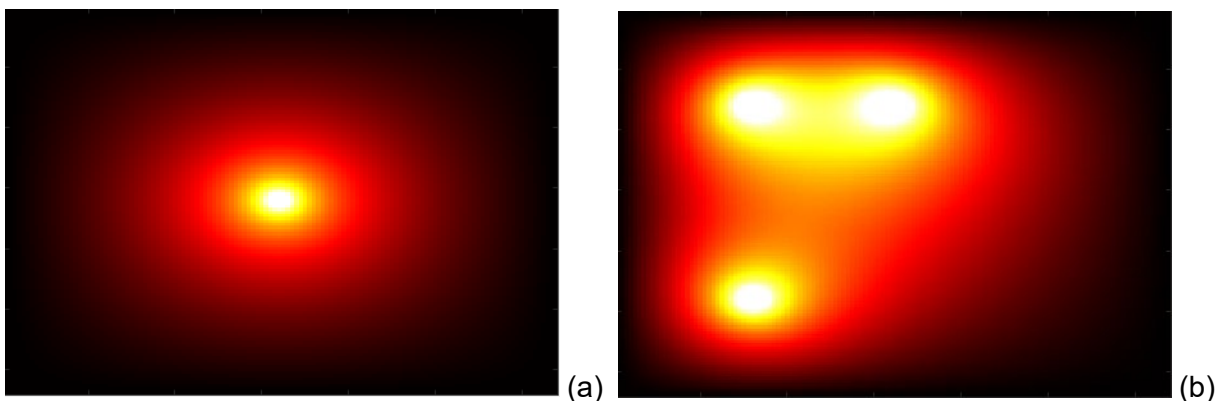


Figure 9. Hypothetical distribution of the density of pollution for (a) a single source, and (b) multiple sources.

With increased wind speed distribution of pollution causes extending higher densities for a longer distance, while faster reduction shows in the direction against the wind (Figure 10). Certainly different wind parameters can be defined for each location. Note that images in the figure correspond to constant wind and same direction over a 10 minute observation period.

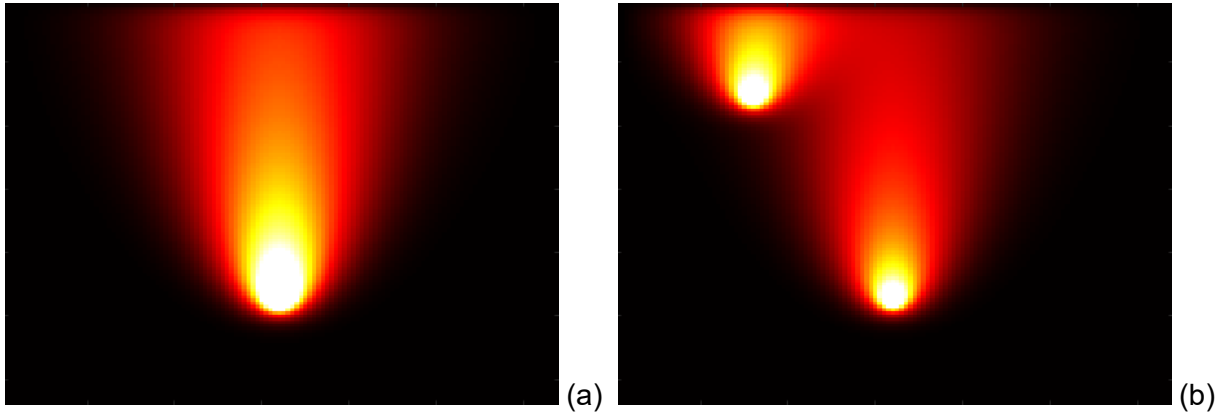


Figure 10. Hypothetical distribution of the density of pollution for (a) a single source, and (b) multiple sources, with account for wind speed and direction. In the example a strong wind comes from the South.

In order to cater for wind, the distribution matrix is no longer a unity matrix and needs to cater for reduction of the pollutions coming from cells where the wind goes to (both speed and direction) and increase from those where the wind comes from. In the simplest case a neighbourhood of $N=3$ (one cell) can be used that implies a 3×3 matrix:

$$\overrightarrow{D_{i+1}} = \overrightarrow{D_i} * \begin{bmatrix} X & 1 & 1/X \\ X & 1 & 1/X \\ X & 1 & 1/X \end{bmatrix} * \overline{R}, \quad \text{where } X = C^{W_{Speed}/W_o * T_o} \quad (3)$$

Where:

- W_{Speed} wind speed
- W_E wind factor in the matrix (2)
- W_o experimental coefficient associating wind speed with its impact
- T_s number of simulation steps per unit of time
- \overline{R} is a rotation matrix defined as:

$$\overline{R} = \begin{bmatrix} \cos \alpha & 0 & \sin \alpha \\ 0 & 1 & 0 \\ -\sin \alpha & 0 & \cos \alpha \end{bmatrix} \quad (4)$$

- α wind angle with respect to longitude axis

A similar analysis of the distribution of air pollutions (in our case determined by the location of sensor nodes that act as reference of accurate amounts of pollution) can be done to analyse effects of changing ground elevations. In the first example shown in Figure 11 a large scale simulation for an area around Dublin was made. Areas with brighter colour mark highest densities, while darker areas indicate low density. Model considers two injection data, one in central of Dublin and another one over Navan. In here a wind coming from the South causes spread of pollutant towards the North.

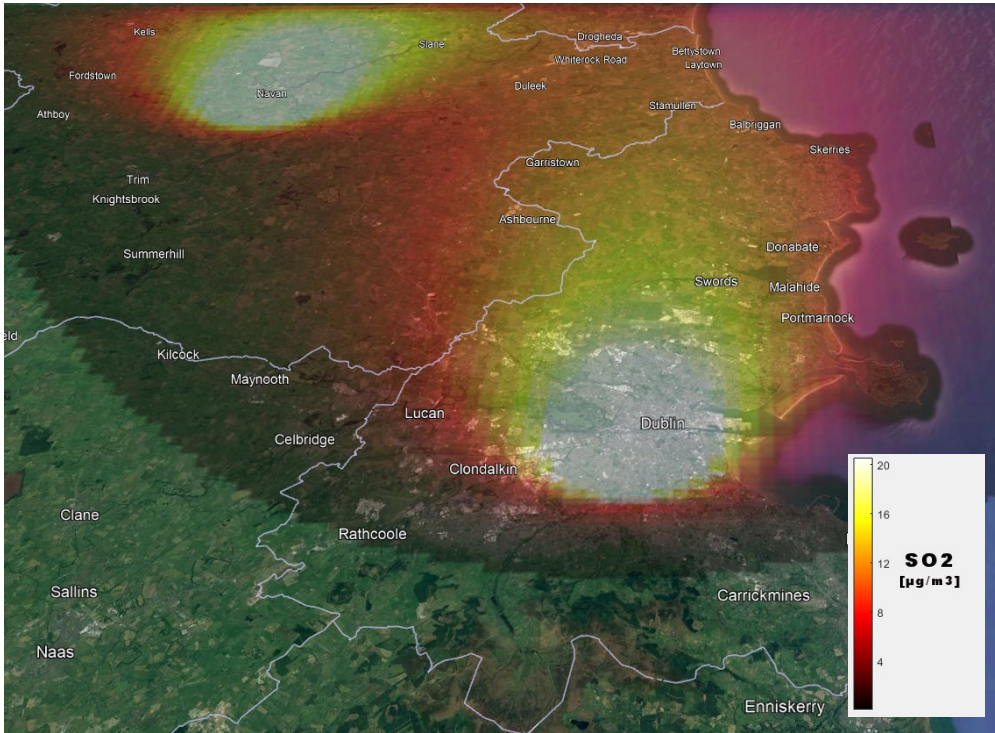


Figure 11. Example of NO₂ emission distribution in the areas surrounding Dublin.

Similar distribution of NO₂ pollutants in the centre of Rome, captured from over 8000 individual measurements taken over the period of more than two months from five (5) distinct air quality sensors with variable wind condition over the observation period is shown in Figure 12.

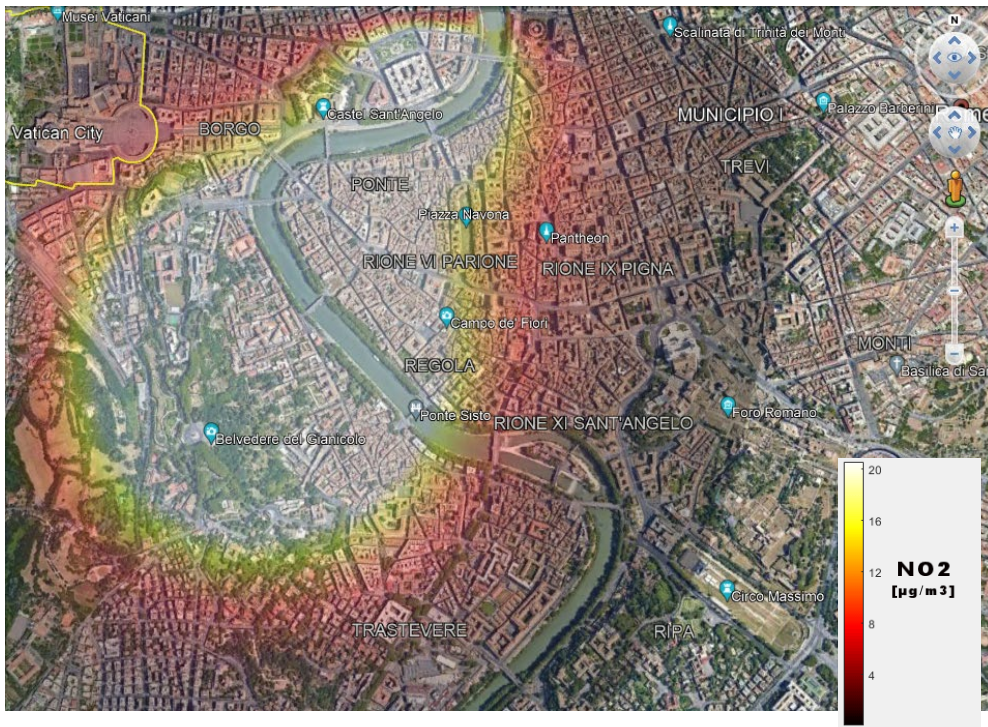


Figure 12. Example of NO₂ emission distribution in the centre of Rome.

In another real-time example in Figure 13, a distribution of SO₂ for Bratislava is shown. As in a previous the example, data was captured from Air Quality Open Data platform over the same observation period with last one dated 15th of September 2021. To make it more interesting, a hypothetical Northern wind has been also added to nearly 1500 sensor measurements.

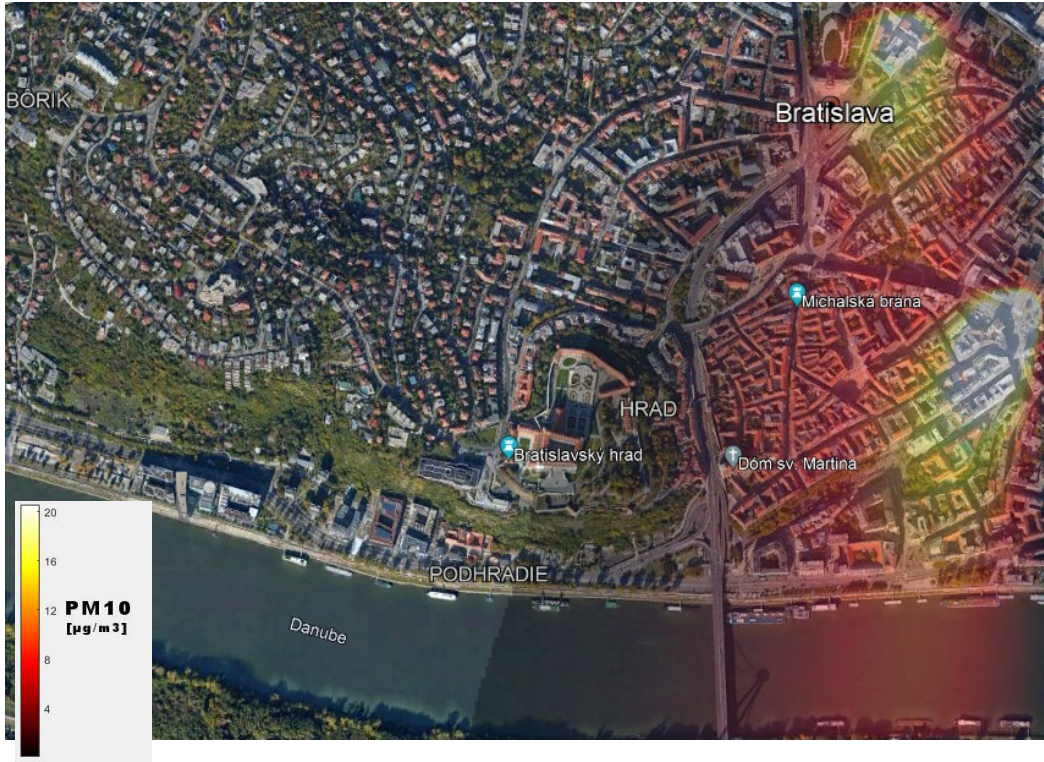


Figure 13. Real-life distribution of SO₂ air pollutant in the centre of Bratislava.

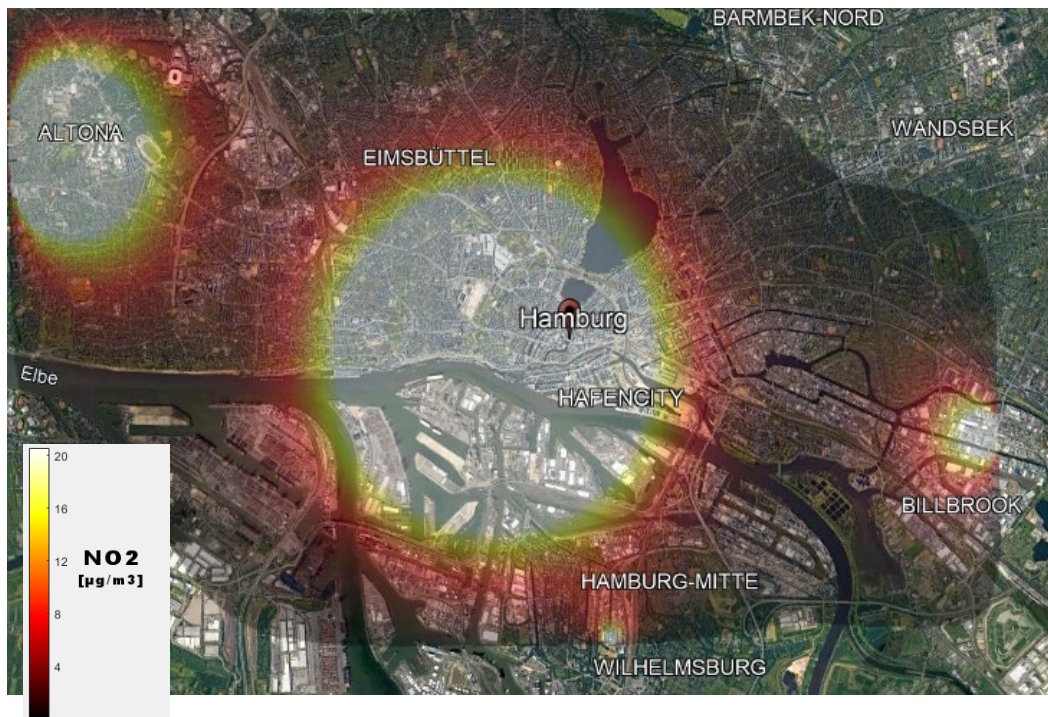


Figure 14. Real-life distribution of particulate matter PM₁₀ in the city of Hamburg.

In the next example focused on pilot cities from ARCH project, the analysis of the distribution of an important urban pollutant, the Particulate Matter and PM_{10} in particular has been performed, results of which are presented in Figure 14. As in previous simulations data was captured from Air Quality Open Data platform with last data from the 15th of September 2021. Over 8000 measurements have been used to produce the presented results. Note that higher density of the pollutant is marked in bright white, while lower concentrations in dark grey.

Another representative example is for the area of Valencia, which is one of those with highest density of available sensor nodes, i.e. 207 in total. Hence a simulation of distribution of the humidity has been performed for the whole municipal area of Valencia (Figure 15). It uses Netatmo weather sensors captured on the 15th of September 2021.

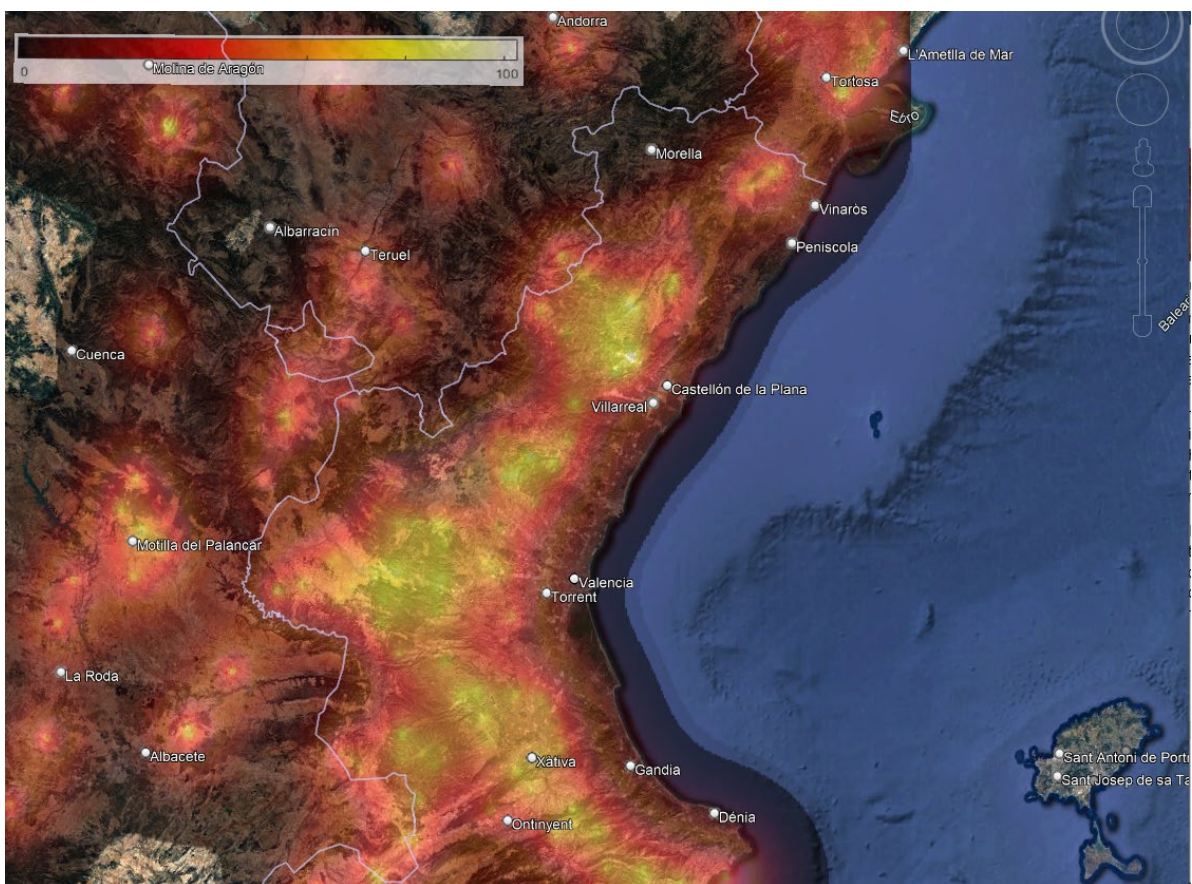


Figure 15. Real-life distribution of humidity in the municipal area of Valencia using Netatmo sensor data.

In this example humidity ranges between 30% (marked as darker areas) to 100% shown in bright white shading. With high variance of the sensor values in the whole analysed area, the model attempted to smooth those changes and provide more equivalued distribution of measurement. Note that on that day there was a very light breeze from the North that has not contributed much to the distribution of the humidity.

The ground elevation as well as high obstacles, such as buildings seriously impact convective movement and hence also the distribution of gases and other air pollutions. To model such effects additional GE i.e. Ground Elevation function has been added to equation (1) above. It is defined as the weighted slope between the point at coordinates (i, j) for which the distribution is calculated in a given iteration and its neighbouring cells. It is inverse proportional to the

change between the cell at coordinates (i, j) and its adjacent ones. In the simplest approximation this can be defined as in the following equation (4), where W is a weight linking slope with real dispersion of a particular pollutant/gas in the environment. The weight values for each type of a pollutant are expected to improve as more data becomes available in THIS.

$$\overline{GE}_{i,j} = W * \frac{\begin{bmatrix} E_{i-1,j-1} & E_{i,j-1} & E_{i+1,j-1} \\ E_{i-1,j} & 1 & E_{i+1,j} \\ E_{i-1,j+1} & E_{i,j+1} & E_{i+1,j+1} \end{bmatrix}}{E_{i,j}} \text{ for } E_{i,j} \neq 0 \quad (4)$$

In order to illustrate the concept, a hypothetical “building” has been placed in the middle of the Valencia pilot area of an over-exaggerated size (50km across) and average height of ~50 meters, for which the same simulation as in Figure 15 above has been performed.

As it can be seen in the Figure 16 below, this has resulted in two effects: (1) accumulation of the pollutants at the side of the “building” facing higher pollutant density and lower on the opposite side, and (2) significant lower density of the pollutant at the area where the obstacle was.

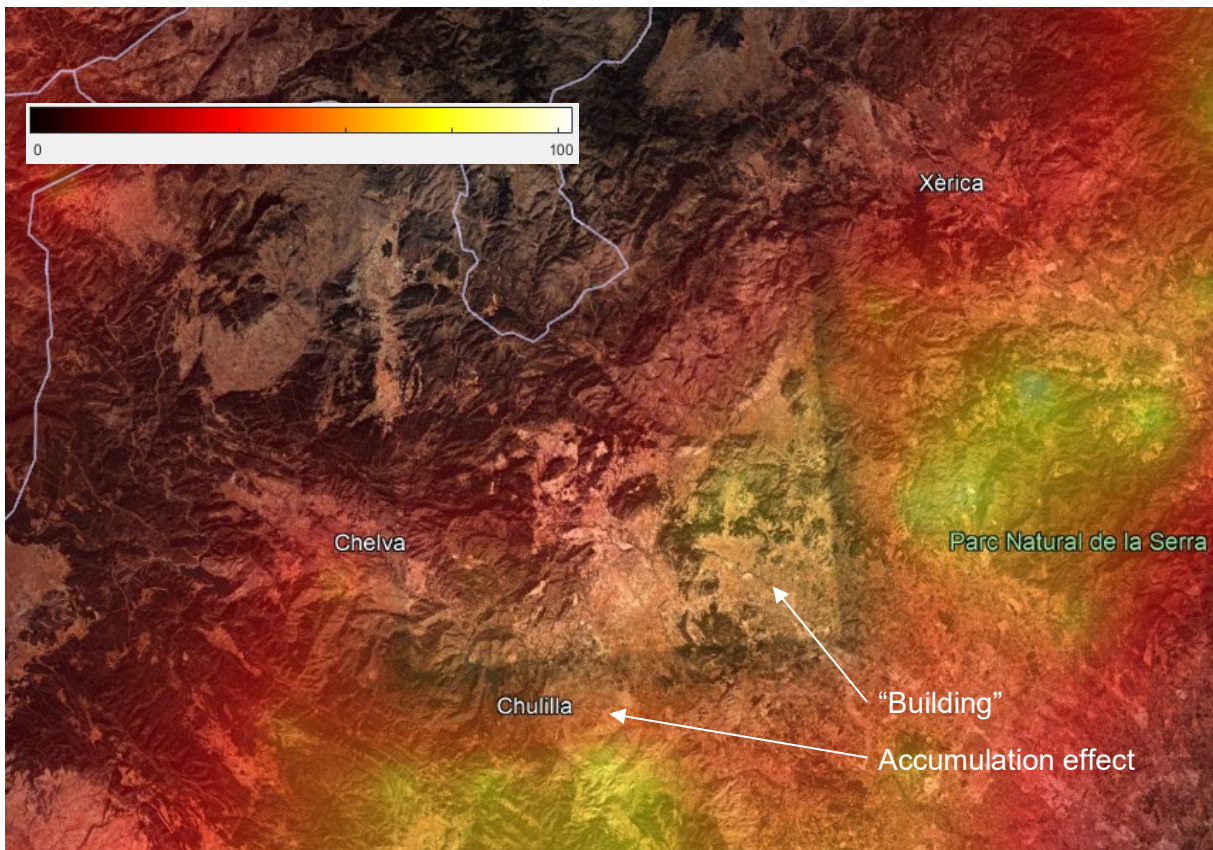


Figure 16. Real-life distribution of humidity in the municipal area of Valencia using Netatmo sensor data with a presence of a hypothetical “building” of an over-exaggerated size and height of ~50 meters.

In another example shown in Figure 17, a relaxed-slope “hill” with height extruding similarly as much from the surrounding environment as the previous obstacle has replaced the “building” from the previous example to simulate smoother changes in the ground elevation. The result shows that larger amount of pollution has been “leaking” into the “hill” area causing dilution of

a clear border between the hill and its base, while it still exhibits some level of resistance for air pollution to propagate over its area, visible as a slight red area at its base.

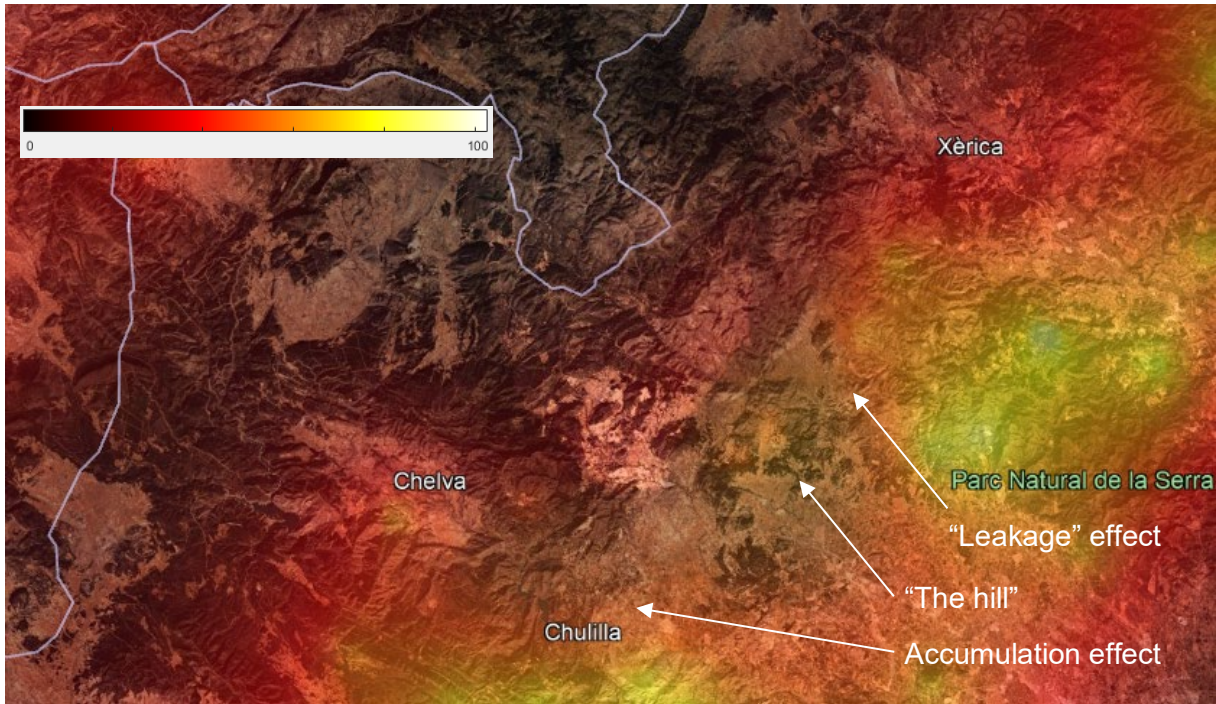


Figure 17. Real-life distribution of humidity in the municipal area of Valencia using Netatmo sensor data with a presence of a hypothetical large “hill” (50km across) of and a relaxed slope.

Similarly more complicated ground elevation contours can be incorporated into the pollution distribution model alongside actual building footprints. However, at the time of writing this deliverables, real-life evaluations of such effects were not possible due to the lack of required ground elevation and building footprint data in a format required for inclusion into the simulation alongside all sensing data captured over the past several months. Those simulations for ARCH pilot sites shall be demonstrated as part of the THIS and HARIS platforms at a later time, i.e. during consolidated pilot evaluations. Since a large number of air pollution parameters have been acquired in ARCH from a variety of sources, only few representative examples have been produced for the purpose of illustrating research results for this deliverable.

4.3. Historical Copernicus Atmosphere Monitoring Service Maps

As described in section 5.5 of the deliverable D4.1 [2], both historical and real-time data related to environmental threats were acquired from satellite observation services such as CAMS and MARS, complementing real-time sensor networks, cloud based environmental monitoring systems described in earlier sections of the same deliverable D4.1. As described therein, maps of environmental contaminations were produced as KML/KMZ overlays for displaying in THIS platform over the areas of historical nature and around important heritage assets.

Considering a global perspective of satellite based monitoring services, the mapping from CAMS has been built not only for all ARCH pilot sites, but at global scale and thus covering the whole land of the Earth. With Earth observations from Copernicus offering 12hrs regular periodicity, an add-on has been developed by RFSAT to offer not only the most recent

snapshot of the supported pollutants (refer to Table 10 on page 116 in D4.1 for the full list of supported gasses), but also full historical access to all data captured to date. Shortcuts allowing faster switching between pilot site areas have also been provided, compliant with similar approach adopted in THIS platform. Please note that such an approach offers equally easy integration into THIS platform as well as use standalone, e.g. using Google Earth for Desktop, as in an example for NO₂ gas distribution¹⁰ presented in Figure 18.

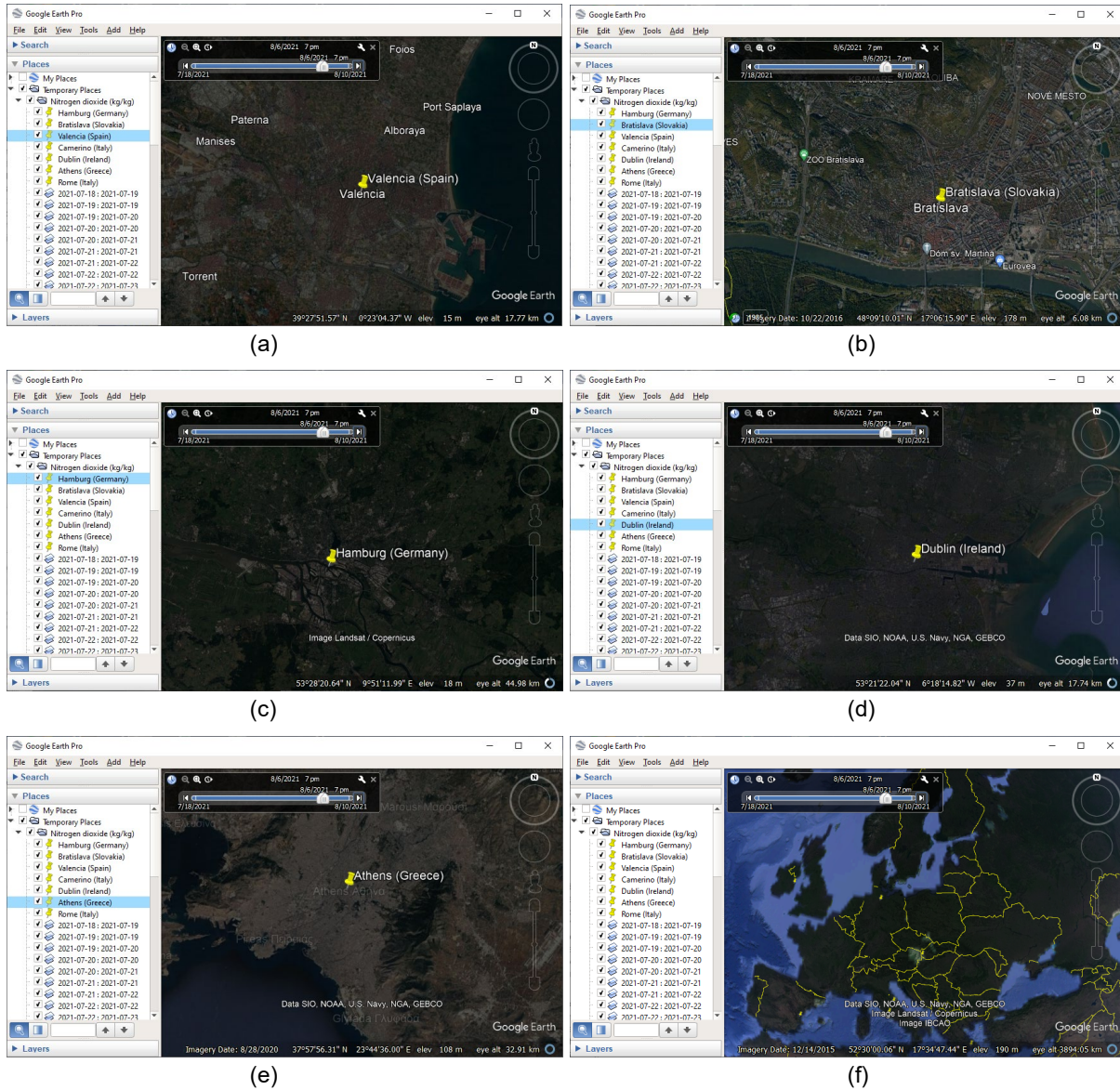


Figure 18. Examples of time-lapse access to historical data about e.g. NO₂ gas pollution at ARCH pilot sites at (a) Valencia, (b) Bratislava, (c) Hamburg, (d) Dublin, (e) Athens and (g) Earth, viewed using Google Earth.

For easier integration into THIS visualisation component from INGV, a KML based time-lapse support has been built, allowing easy scanning through past data, both manually and automatically playing back frames over time. To achieve this, a KML wrapper file has been

¹⁰ Time-lapse for NO₂: <https://www.rfsat.com/projects/H2020-ARCH/CAMSmaps/CAMS-timelaps-Earth-no2.kml>

generated, which is updated at every new data capture with information about new frame. A list of KML time-lapse overlays is given in Table 13.

The time controls are shown at the top of the map that allow users to either play the whole historical data sequence, either one time or in a loop, as well as scroll through all available data to the interesting point in time. Snapshots have been setup back-to-back, i.e. displaying a map frame from the time of acquisition of respective data until the next data is acquired. A menu shown in the left permits quick switching between pilot sites. The list of all map frames is shown below quick access place-marks showing time of observation in as their titles. Note that gas distribution uses a grey scales from black (no pollution) to white (maximum recorded value Earth-wide), while other colour codes can be also offered once a clear decision is made about acceptable (green-shaded) versus harmful (red-shaded) gas pollution levels.

Table 13. List of time-lapsed pollution overlays built out of historical data from the CAMS service

Parameter	Description	URL to time-lapse overlay
<i>lnsp</i>	Logarithm of surface pressure	CAMS-timelaps--aermr01.kml
<i>aermr01</i>	Sea Salt Aerosol (0.03 - 0.5 um) Mixing Ratio [kg/kg]	CAMS-timelaps--aermr02.kml
<i>aermr02</i>	Sea Salt Aerosol (0.5 - 5 um) Mixing Ratio [kg/kg]	CAMS-timelaps--aermr03.kml
<i>aermr03</i>	Sea Salt Aerosol (5 - 20 um) Mixing Ratio [kg/kg]	CAMS-timelaps--aermr04.kml
<i>aermr04</i>	Dust Aerosol (0.03 - 0.55 um) Mixing Ratio [kg/kg]	CAMS-timelaps--aermr05.kml
<i>aermr05</i>	Dust Aerosol (0.55 - 0.9 um) Mixing Ratio [kg/kg]	CAMS-timelaps--aermr06.kml
<i>aermr06</i>	Dust Aerosol (0.9 - 20 um) Mixing Ratio [kg/kg]	CAMS-timelaps--aermr07.kml
<i>aermr07</i>	Hydrophilic Organic Matter Aerosol Mixing Ratio [kg/kg]	CAMS-timelaps--aermr08.kml
<i>aermr08</i>	Hydrophobic Organic Matter Aerosol Mixing Ratio [kg/kg]	CAMS-timelaps--aermr09.kml
<i>aermr09</i>	Hydrophilic Black Carbon Aerosol Mixing Ratio [kg/kg]	CAMS-timelaps--aermr10.kml
<i>aermr10</i>	Hydrophobic Black Carbon Aerosol Mixing Ratio [kg/kg]	CAMS-timelaps--aermr11.kml
<i>aermr11</i>	Sulphate Aerosol Mixing Ratio [kg/kg]	CAMS-timelaps--aermr16.kml
<i>aermr16</i>	Nitrate fine mode aerosol mass mixing ratio [kg/kg]	CAMS-timelaps--aermr17.kml
<i>aermr17</i>	Nitrate coarse mode aerosol mass mixing ratio [kg/kg]	CAMS-timelaps--aermr18.kml
<i>aermr18</i>	Ammonium aerosol mass mixing ratio [kg/kg]	CAMS-timelaps--amaod550.kml
<i>c2h6</i>	Ethane [kg/kg]	CAMS-timelaps--aod1240.kml
<i>c3h8</i>	Propane [kg/kg]	CAMS-timelaps--aod469.kml
<i>c5h8</i>	Isoprene [kg/kg]	CAMS-timelaps--aod550.kml
<i>ch4_c</i>	Methane (chemistry) [kg/kg]	CAMS-timelaps--aod670.kml
<i>co</i>	Carbon monoxide	CAMS-timelaps--aod865.kml
<i>den</i>	Density [kg/m ³]	CAMS-timelaps--bcaod550.kml
<i>h2o2</i>	Hydrogen peroxide [kg/kg]	CAMS-timelaps--c2h6.kml
<i>hcho</i>	Formaldehyde [kg/kg]	CAMS-timelaps--c3h8.kml
<i>hno3</i>	Nitric acid [kg/kg]	CAMS-timelaps--c5h8.kml
<i>no</i>	Nitric oxide [kg/kg]	CAMS-timelaps--ch4_c.kml
<i>no2</i>	Nitric dioxide [kg/kg]	CAMS-timelaps--co.kml
<i>oh</i>	Hydroxyl radical [kg/kg]	CAMS-timelaps--den.kml
<i>pan</i>	Peroxyacetyl nitrate [kg/kg]	CAMS-timelaps--duaod550.kml
<i>so2</i>	Sulphur dioxide	CAMS-timelaps--gtco3.kml

Parameter	Description	URL to time-lapse overlay
amaod550	Ammonium aerosol optical depth at 550 nm [-]	CAMS-timelaps--h2o2.kml
aod1240	Total Aerosol Optical Depth at 1240nm [-]	CAMS-timelaps--hcho.kml
aod469	Total Aerosol Optical Depth at 469nm	CAMS-timelaps--hno3.kml
aod550	Total Aerosol Optical Depth at 550nm	CAMS-timelaps--lnsp.kml
aod670	Total Aerosol Optical Depth at 670nm	CAMS-timelaps--lsm.kml
aod865	Total Aerosol Optical Depth at 865nm	CAMS-timelaps--niaod550.kml
bcaod550	Black Carbon Aerosol Optical Depth at 550nm	CAMS-timelaps--no.kml
duaod55	Dust Aerosol Optical Depth at 550nm	CAMS-timelaps--no2.kml
gtco3	GEMS Total column ozone [kg/m ²]	CAMS-timelaps--oh.kml
lsm	Land-sea mask (0 to 1)	CAMS-timelaps--omaod550.kml
niaod550	Nitrate aerosol optical depth at 550 nm	CAMS-timelaps--pan.kml
omaod550	Organic Matter Aerosol Optical Depth at 550nm	CAMS-timelaps--pm1.kml
ssaod550	Sea Salt Aerosol Optical Depth at 550nm	CAMS-timelaps--pm10.kml
tchcho	Total column Formaldehyde [kg/m ²]	CAMS-timelaps--pm2p5.kml
tcno2	Total column Nitrogen dioxide [kg/m ²]	CAMS-timelaps--so2.kml
tcso2	Total column Sulphur dioxide [kg/m ²]	CAMS-timelaps--ssaod550.kml
tc_c2h6	Total column ethane [kg/m ²]	CAMS-timelaps--tchcho.kml
tc_c3h8	Total column propane [kg/m ²]	CAMS-timelaps--tcno2.kml
tc_c5h8	Total column isoprene [kg/m ²]	CAMS-timelaps--tcso2.kml
tc_ch4	Total column methane [kg/m ²]	CAMS-timelaps--tc_c2h6.kml
tc_h2o2	Total column hydrogen peroxide [kg/m ²]	CAMS-timelaps--tc_c3h8.kml
tc_hno3	Total column nitric acid [kg/m ²]	CAMS-timelaps--tc_c5h8.kml
tc_no	Total column nitrogen monoxide [kg/m ²]	CAMS-timelaps--tc_ch4.kml
tc_oh	Total column hydroxyl radical [kg/m ²]	CAMS-timelaps--tc_h2o2.kml
tc_pan	Total column peroxyacetyl nitrate [kg/m ²]	CAMS-timelaps--tc_hno3.kml
z	Geopotential [m ² /s ²]	CAMS-timelaps--tc_no.kml
pm1	Particulate matter d < 1 um [kg/m ³]	CAMS-timelaps--tc_oh.kml
pm10	Particulate matter d < 10 um [kg/m ³]	CAMS-timelaps--tc_pan.kml
pm2p5	Particulate matter d < 2.5 um [kg/m ³]	CAMS-timelaps--uvbed.kml
uvbed	UV biologically effective dose	CAMS-timelaps--uvbedcs.kml
uvbedcs	UV biologically effective dose clear-sky	CAMS-timelaps--z.kml

4.3.1. Time-lapse data repository

The data repository of time-lapse overlays is hosted on RFSAT server at:

Server URL: <https://www.rfsat.com/projects/H2020-ARCH/CAMSmaps/CAMS-timelapse-maps.html>

FTP server: ftp.rfsat.com

Username: arch

Password: available on request

For security reasons, direct listing of files stored at the RFSAT repository is not permitted via public HTTP/HTTPS links. It can only be done when connecting via FTP/FTPS. The list of overlays can still be obtained from “*CAMS-timelapse-maps.html*” file.

The content of the repository is updated every 12 hours, in sync with data made available from CAMS service. At such times (1) a new image is uploaded for each of the gas distribution, and (2) KML files for all gases are updated to include a reference to such a new image. Therefore, for any client device to integrate the time-lapse service, it is sufficient to make a note of the links to KML files referring to gas distributions of interest, which will provide always up to date info about all time slices captured and available to date.

4.3.2. Time-lapse KML file format

Since some clients might wish to amend the content of the original KML files produced by RFSAT, we provide below a brief explanation of its content and functionalities.

The file starts with a header, defining format compliance, file encoding and data file title:

```
<?xml version="1.0" encoding="UTF-8"?>
<kml xmlns="http://earth.google.com/kml/2.2">
<!-- TimeSpan is recommended for GroundOverlays -->
<Folder>
  <name>Nitrogen dioxide (kg/kg)</name>
```

It follows with a definition of the default geo-located viewpoint using “*LookAt*” tag. Since gas distribution is provided at ground level, images are wrapped on the ground elevation.

```
<LookAt>
  <longitude>15.59848919022441</longitude>
  <latitude>51.95021076768184</latitude>
  <altitude>0</altitude>
  <heading>-6.414032506134286</heading>
  <tilt>0</tilt>
  <range>4726162.712125629</range>
  <gx:altitudeMode>relativeToSeaFloor</gx:altitudeMode>
</LookAt>
```

Next placemarks are defined to allow quick switching between places of interest. The placemarks specify both the centre of the map using “*Point*” and its range using “*LookAt*”. An example below refers to the Hamburg pilot area. Similarly, placemarks can be defined for other pilot sites.

```

<Placemark>
  <name>Hamburg (Germany)</name>
  <LookAt>
    <longitude>10.05687907784399</longitude>
    <latitude>53.5605499775493</latitude>
    <altitude>0</altitude>
    <heading>0.03160851574592017</heading>
    <tilt>0</tilt>
    <range>44954.59649947804</range>
    <gx:altitudeMode>relativeToSeaFloor</gx:altitudeMode>
  </LookAt>
  <Point>
    <gx:drawOrder>1</gx:drawOrder>
    <coordinates>9.992275961137015,53.53725839229069,0</coordinates>
  </Point>
</Placemark>

```

Each of the time frames are then provided using “*GroundOverlay*” tag. The “*TimeSpan*” defines the observation time, i.e. when the image is expected to be displayed. By default, all time slices are aligned back-to-back, i.e. end of the previous one is the same with the beginning of the next one. The “*Icon*” specifies the network location of an image to be displayed, which can be either in a local folder or accessible from a remote repository over the Internet. The “*LatLonBox*” defines a geographical extent of the image, which covers the whole Earth.

```

<GroundOverlay>
  <name>2021-07-18 : 2021-07-19</name>
  <TimeSpan>
    <begin>2021-07-18T12:00Z</begin>
    <end>2021-07-19T00:00Z</end>
  </TimeSpan>
  <color>b3ffffff</color>
  <Icon>
    <href>https://www.rfsat.com/projects/H2020-ARCH/CAMSmaps/1626652800-CAMS-Earth-
no2.png</href>
  </Icon>
  <LatLonBox>
    <north>90</north>
    <south>-90</south>
    <east>180</east>
    <west>-180</west>
  </LatLonBox>
</GroundOverlay>

```

The file finishes with closing the “*Folder*” and “*kml*” tags:

```

</Folder>
</kml>

```

4.4. Air quality provided by the MINNI modelling system in Italy

In order to calculate the material degradation caused by air pollution for the main materials utilised in the construction of the monumental buildings of the Camerino historic area, the dose-response functions provided by the UN ECE ICP Materials [26] were selected. Such dose-response functions, which will be fully described within the WP5-related deliverables together with the whole impact analysis, need as input the annual mean concentrations of different pollutants and climatic parameters.

Therefore, for the Camerino case-study the annual mean of the main input parameters, such as PM₁₀, SO₂, HNO₃, O₃ concentrations, as well as temperature, relative humidity and the total annual amount of Precipitation were provided, in NetCDF format, by the Atmospheric Modelling System of the Italian National Integrated Assessment Model MINNI¹¹, developed by ENEA and funded by the Italian Ministry for the Environment, Land and Sea. In particular, three years were considered: 2015, 2020 and 2030 to analyse the changes over time.

It is worth stressing the advantages of using the MINNI-FORAIR modelled data with respect to the available one from the CAMS. Indeed, on one hand the MINNI-FORAIR models allow to obtain higher spatial resolution data (4x4 km, instead of 12 x 12 km) and on the other hand the possibility to have a least one projection in the near future, for the year 2030.

¹¹ <https://impatti.sostenibilita.enea.it/en/research/activity/8962>

5. Historical climate

As for the characterisation of the historical climate, indices related to weather and climate extremes are extracted by the datasets provided from the ECA&D project¹² [27]. These indices are calculated on the measures recorded by stations within or closer to the historic areas identified by the city partners (Figure 19).

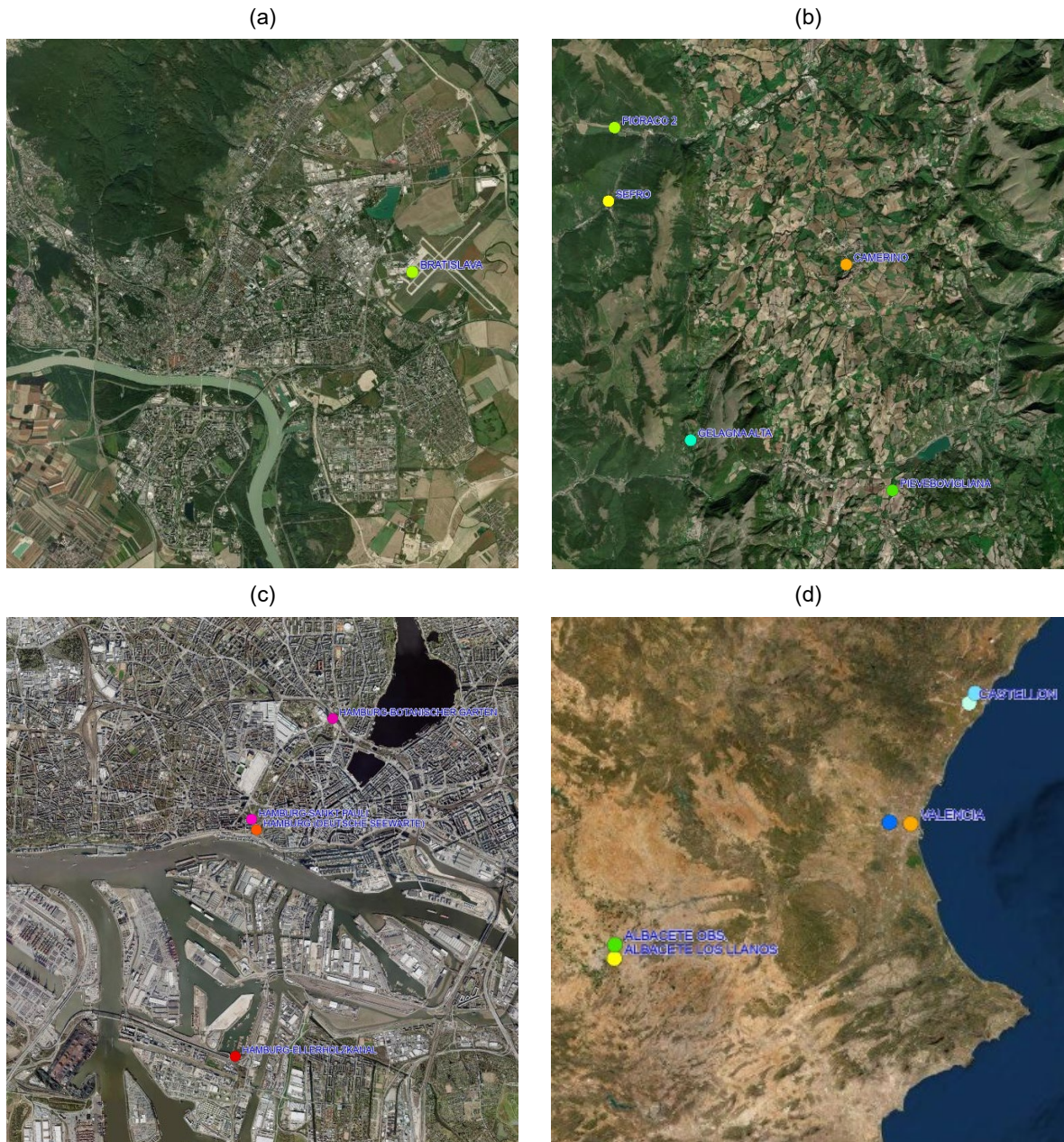


Figure 19. Locations of the ECA&D monitoring stations selected close to the historic area of the ARCH cities: Bratislava (a), Camerino (b), Hamburg (c) and Valencia (d).

¹² <https://www.ecad.eu>

Different stations were selected, if available. However, the blended series are downloaded from the ECA&D dataset, so the gaps in a station can be infilled with observations from nearby stations (those at distance less than 12.5km and height differences less than 25m)¹³.

The time-series of the indices can be used both to characterise the anomalies for a given year (or season), by comparing the single values respect to a reference period, and to evaluate the trend over time. The indices chosen to characterise the historical climate change are divided by categories in Table 14.

Table 14. List of indices to describe the characteristic of the historic climate change divided by category

Category	Index
Cold	GD4 - Growing degree days GSL - Growing season length CFD - No. consecutive frost days FD - No. frost days CSDI - Cold spell duration index TG10p - No. of cold days TN10p - No. of cold nights TX10p - No. of cold day-times
Compound	CD - No. of cold/dry days CW - No. of cold/wet days WD - No. of warm/dry days WW - No. of warm/wet days TCI - Tourism Climate Index (only for Valencia) UTCI - Universal Thermal Climate Index (only for Valencia) HI - Heliothermal or Huglin Index (only for Valencia) BEDD - Biologically Effective Degree Days (only for Valencia) TCI60 - Good tourism days (TCI \geq 60) (only for Valencia) TCI80 - Excellent tourism days (TCI \geq 80) (only for Valencia)
Drought	CDD - Maximum no. of consecutive dry days SPI6 - 6-month Standardized Precipitation Index SPI3 - 3-month Standardized Precipitation Index
Heat	No. of summer days TR - No. tropical nights WSDI - Warm spell duration index TG90p - No. of warm days TN90p - No. of warm nights TX90p - No. of warm day-times TXx - Maximum of daily maximum temperature TNx - Maximum of daily minimum temperature CSU - Consecutive summer days CSU - Consecutive summer days
Humidity	RH - Mean of daily mean relative humidity

¹³ <https://www.ecad.eu/FAQ/index.php#3>

Category	Index
Pressure	PP - Mean of daily surface air pressure- an of daily surface air pressure
Rain	RR - Precipitation sum RR1 - No. of wet days CWD - Maximum no. of consecutive wet days R10mm - Heavy precipitation days (> 10mm) R20mm - Very heavy precipitation days (> 20mm) RX1day - Highest 1-day precipitation amount RX5day - Highest 5-day precipitation amount R75p - No. of moderate wet days R75pTOT - Precipitation fraction due to moderate wet days R95p - No. of very wet days R95pTOT - Precipitation fraction due to very wet days R99p - No. of extremely wet days R99pTOT - Precipitation fraction due to extremely wet days PRCPTOT - Precipitation amount due to wet days
Temperature	TG - Mean of daily mean temperature TN - Mean of daily minimum temperature TX - Mean of daily maximum temperature DTR - Mean of diurnal temperature range ETR - Intra-period extreme temperature range vDTR - Mean absolute day-to-day difference in DTR

As an example only, the precipitation in Hamburg for annual measures between 1950 and 2020 and for monthly values from 2010 to 2020 is reported in Figure 20 and Figure 21, respectively.

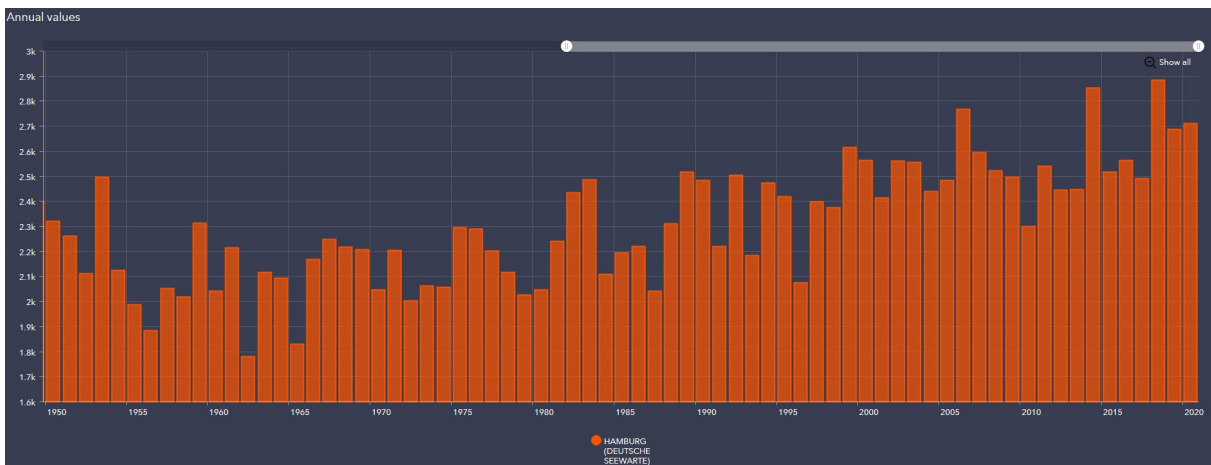


Figure 20. Example of historic climate change index: Precipitation sum on annual period in Hamburg.

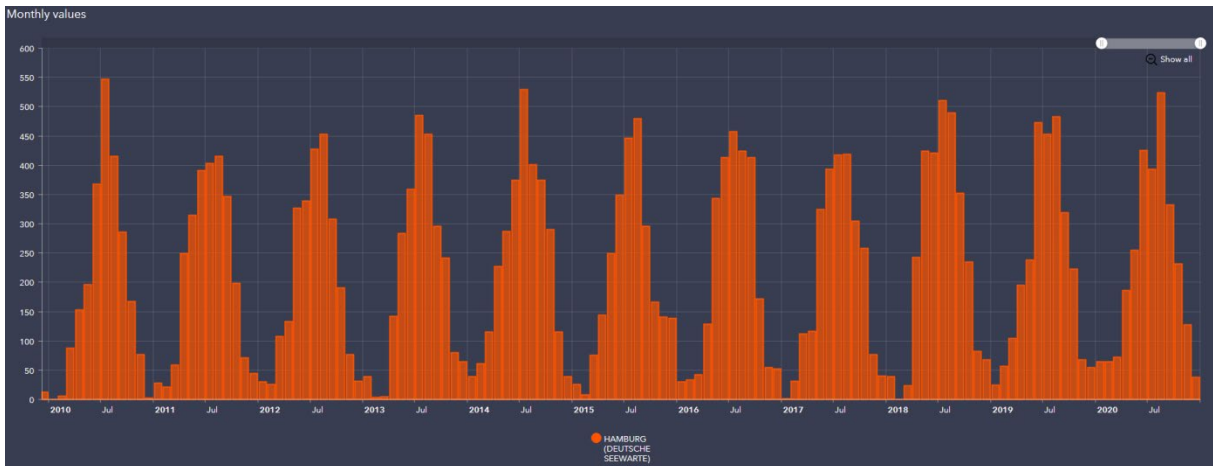


Figure 21. Example of historic climate change index: Precipitation sum on monthly period in Hamburg.

The datasets are structured (and updated) in THIS DB by means of specific tables linked between them. In fact, each measure is referred both to the type of index (cf. Table 15) and the monitoring station (Table 16). Moreover, the measures calculated over different reference periods (e.g. annual, monthly, seasons, etc.) are available in the ARCH information system (Table 17).

Table 15. “HCC_ VOC_INDEX” Table into THIS DB for the vocabulary of the indices

Attribute	Value Type	Definition
OBJECTID	integer	ID to identify object in the table
Code	text	Code of the index (cf. Table 14)
Description	text	Description of the index (cf. Table 14)
Category	text	Category of the index (cf. Table 14)
Link	text	Link to the ECA&D vocabulary

Table 16. “HCC_ VOC_STATION” Table into THIS DB to define the monitoring stations

Attribute	Value Type	Definition
OBJECTID	integer	ID to identify object in the table
StationIdentifier	integer	Identifier of the station in the ECA&D dataset
StationName	text	Name of the station
CountryCode	text	Code of the country
Latitude	double	Latitude
Longitude	double	Longitude
Altitude	integer	Altitude
SHAPE	geography	Point in vector layer representing the station

Table 17. “Hist_CC_Ind” Table in THIS DB to structure historic indices about CC extreme events

Attribute	Value Type	Definition
OBJECTID	integer	ID to identify object in the table
StationRef	integer	Reference to table HCC_VOC_STATION
IndexRef	integer	Reference to table HCC_VOC_INDEX
Year	integer	Reference year
CalculatedIndex	double	Value over the year
WinterHalfYear	double	Value over the winter half year
SummerHalfYear	double	Value over the summer half year
Winter	double	Value over period between December and February
Spring	double	Value over period between March and May
Summer	double	Value over period between June and August
Autumn	double	Value over period between September and November
January	double	Value over the monthly period
February	double	Value over the monthly period
March	double	Value over the monthly period
April	double	Value over the monthly period
May	double	Value over the monthly period
June	double	Value over the monthly period
July	double	Value over the monthly period
August	double	Value over the monthly period
September	double	Value over the monthly period
October	double	Value over the monthly period
November	double	Value over the monthly period
December	double	Value over the monthly period

6. Climate services

As defined in the European Roadmap for Climate Services¹⁴, climate services concept covers the transformation of climate-related data into customized products or services that include data, information and/or knowledge to support decision making in adaptation, mitigation or disaster risk management (DRM). Therefore, the co-development and co-production is key for producing climate services that are really tailored to user needs. Additionally, there is a massive amount of climate data from past, present and future at European level available through the Copernicus Climate Change Service¹⁵ but not easily accessible for the ARCH city partners as it requires specific treatment and advanced knowledge to be digested and adapted into knowledge ready to be used.

Thus, one of Task 4.3's objectives is to capture, exploit and adapt model data on future climate change hazards for the ARCH's areas of interest to assist in their resilience building. In this sense, a co-creation work aligned with T3.4.2 has been done with each of partner cities to understand their needs, climate information gaps that may be relevant for decision-making and transform already available information from the Copernicus Climate Change Service to allow its exploitation and use to support decision making.

6.1. CDS data and temporal coverage selected

Based on discussions held with the ARCH partner cities and the identification of their needs, three different sources of data have been used from Copernicus Climate Change Service for the development of climate services:

- **E-OBS [1950 to present]**: This dataset provides daily gridded land-only observational data over Europe. The blended time series from the station network of the ECA&D. For more detail information¹⁶.
- **EURO-CORDEX [2011-2100]**: This dataset provides Regional Climate Model (RCM) data on single levels from a number of experiments, models, domains, resolutions, ensemble members, time frequencies and periods computed over several regional domains all over the World in the framework of the CORDEX. For this case study the finer resolution of 0.11 degree (EUR-11, ~12.5km) has been selected. For more detail information¹⁷
- **WATER LEVEL CHANGE INDICATORS [1977 to 2100]**: This dataset presents extreme-value, return period, and percentile indicators for coastal sea levels in a European-wide domain. The indicators are computed from tidal dynamics, storm surge and sea level rise data based upon past observational data and future climate projections. To compute these indicators, the Deltares Global Tide and Surge Model

¹⁴ISBN 978-92-79-44341-1. DOI: 10.2777/702151

¹⁵ <https://climate.copernicus.eu/>

¹⁶ <https://cds.climate.copernicus.eu/cdsapp#!/dataset/insitu-gridded-observations-europe>

¹⁷ <https://cds.climate.copernicus.eu/cdsapp#!/dataset/projections-cordex-domains-single-levels>

(GTSM) version 3.0 is used together with regional climate forcing and sea level rise initial conditions. For more detail information¹⁸

Based on the available temporal coverage of the previous datasets, a fixed set of predefined periods were selected for the different case studies (cf. Table 18-Table 19).

Table 18. Predefined periods for Valencia and Bratislava

Periods	Historical	Future (RCP8.5)
1981-2010	X	
2011-2041	-	X
2041-2070	-	X
2071-2100	-	X

Table 19. Predefined periods for Hamburg

Periods	Historical	Future (RCP4.5)	Future (RCP8.5)
1977-2005	X		
2011-2041	-		
2041-2070	-		X
2071-2100	-	X	

As it can be observe in the above tables, the projections for Valencia and Bratislava are calculated considering the worst case scenario (RCP8.5)for all the future periods, while for Hamburg the projections are calculated for 2041-2070, considering the worst-case scenario (RCP8.5) and for 2071-2100 considering the best case-scenario.

6.2. Delta scaling methodology

Climate projections are portions of a simulation that represent the future. These simulations are based on global and/or regional climate models that are used for the estimation of future climate conditions. Nevertheless, each of these models present some biases relative to the observed values, especially when the estimations refer to extremes (e.g. maximum or minimum values). This is the reason why several researchers have studied several statistical methods to minimize the biases between climate models and observed values. The report “A guidebook on climate scenarios” [28] describes in detail the delta-scaling method selected in this project.

Figure 22 summarizes in a graphical way the methodology behind this method and the operations that need to be performed to apply.

The delta-scaling method put the focus on the outcome simulations of the models, of both historical and future periods, in order to calculate the biases (perturbation) between them. Afterwards, this perturbation is added to the observations to get the bias-adjusted projections. Therefore, the calculi performed are:

¹⁸ <https://cds.climate.copernicus.eu/cdsapp#!/dataset/sis-water-level-change-indicators>

- firstly, the relative change between the reference period and the future period simulations are calculated.
- secondly, the change (or delta) is applied over the historical observed time series in order to come out with the future projections.

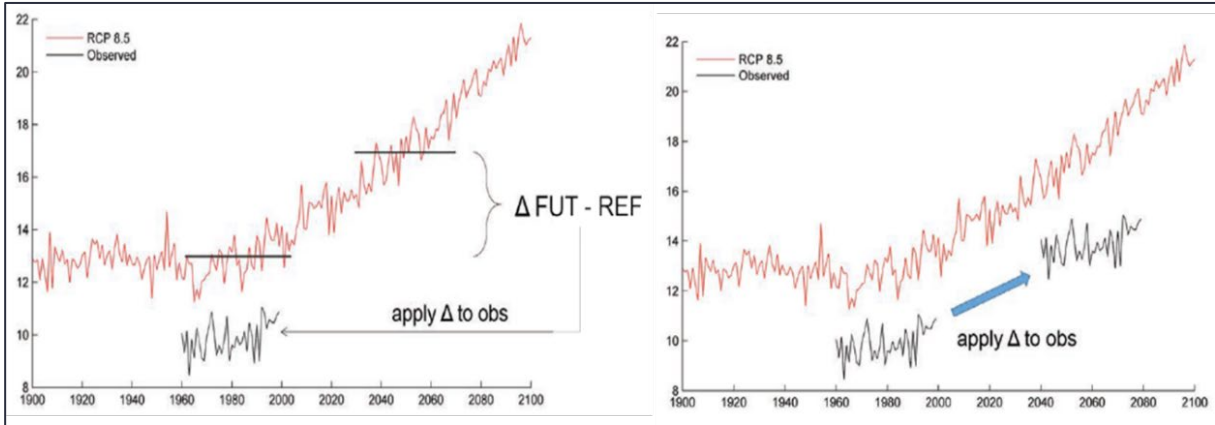


Figure 22. Graphical representation of the Delta/Scaling Method applied (Source: [28]).

For the Valencia and Bratislava cases studies, this delta method has been applied considering temperature and precipitation over CORDEX and E-OBS datasets:

- **Scenario:** There are available three scenarios RCP 2.6, 4.5 and 8.5 providing different pathways of the future climate forcing. The most adverse scenario (RCP8.5) has been selected to showcase the worst-case possible situation and the total time-frame provided (2006-2100) has been divided in three periods of 30 years. 2011-2040, 2041-2070, 2071-2100
- **Historical:** Following the same approach, the total time-frame provided (1950-2005). A fixed period from 1976 to 2005 has been selected.
- **E-OBS:** considering that the time coverage is from 1950 to present, the historical period from 1981-2010 has been selected.

Figure 23 summarises in a graphical way the operations performed to apply this delta-scaling method with the previous datasets. This methodology allows obtaining the temperature and precipitation time series for the future that will be used to calculate the derived indicators in each case study.

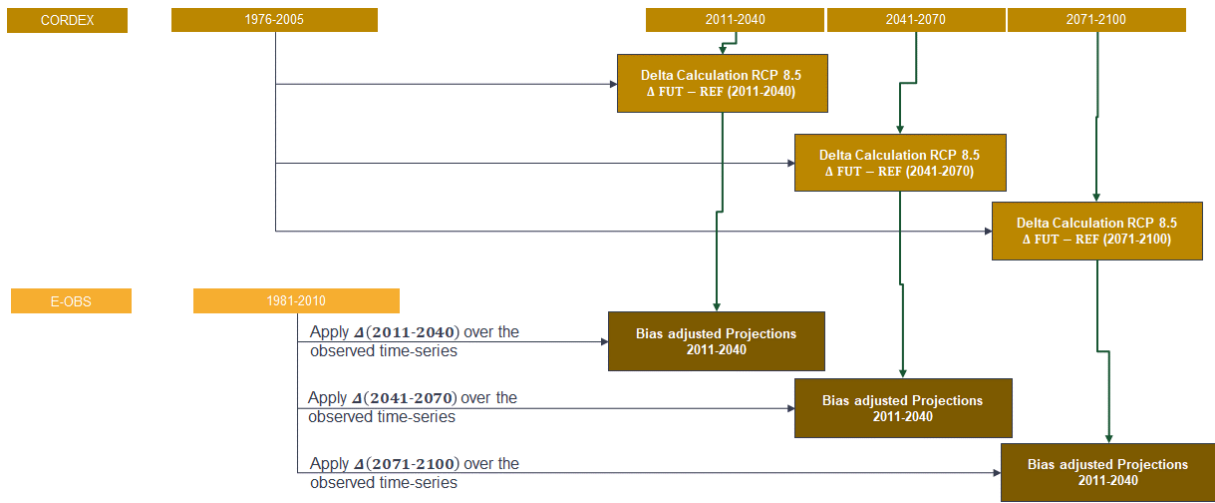


Figure 23. Delta Calculation in Valencia and Bratislava

Due to the discontinuous nature of the Water Level Change Indicators datasets, for the Hamburg cases study, this delta method has been applied considering the same approach but considering the statistics of the model for RCP 8.5 from 2041-2070 and statistics of the model for RCP4.5 from 2071-2100 with regard to the statistics for the historical model from 1977 to 2005 (Figure 24).

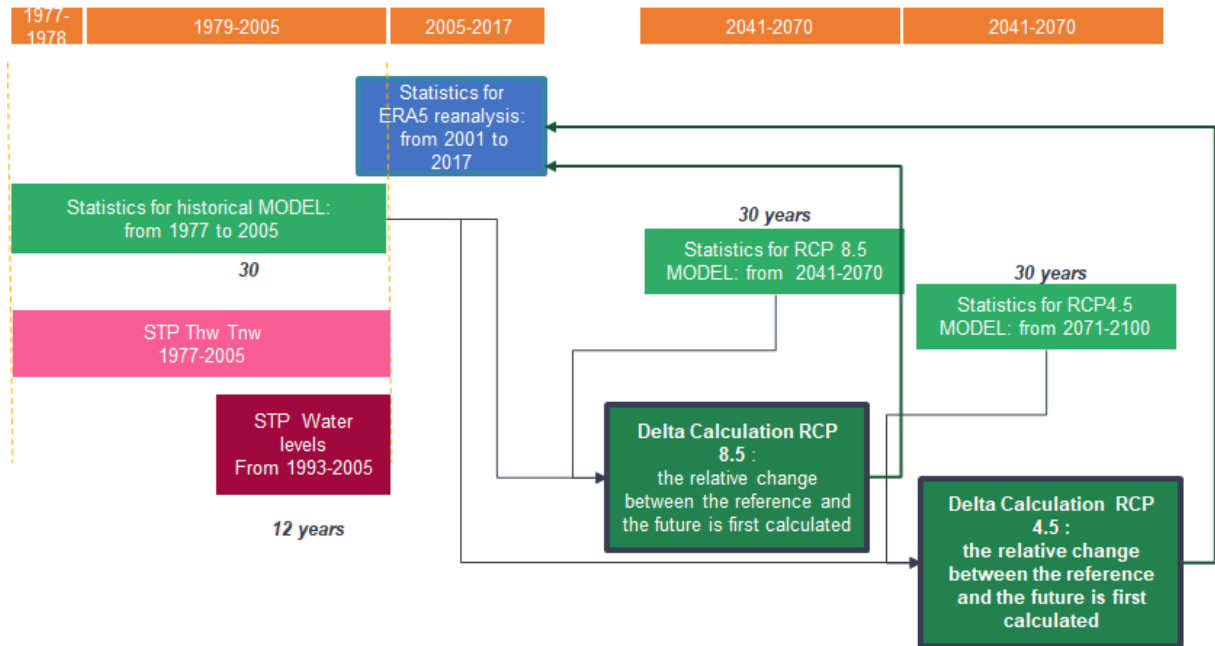


Figure 24. Delta Calculation datasets in Hamburg

6.3. Approach for EURO-CORDEX Models selection ensemble

In the context of the ARCH project, as previously mentioned, the CORDEX regional climate model data for the European domain (EURO-CORDEX) available at Copernicus Climate Data Store has been used for the development of climate services. These projections are a quality-controlled subset of the wider CORDEX dataset. The CDS subset of CORDEX data has been through a metadata quality control procedure which ensures a high standard of reliability of the data. Similar data can be found in the main CORDEX archive at the ESGF (Earth System Grid Federation), however, these data come with no quality assurance and may have metadata errors or omissions. The quality-control process performed in the CDS means that the CORDEX data is further reduced to exclude data that have metadata errors or inconsistencies.

CORDEX contains different combinations (ensembles) of Global Climate Models (GCM) and Regional Climate Models (RCM), but not all the possible combinations are available. Table 20 summarizes all possible combinations.

Table 20. List and abbreviations of climate models (GCM–RCM combinations) included at least once in the EURO-CORDEX ensemble. The asterisk (*) means that two versions of the GCM–RCM combination are available. The first row lists the GCM, while the first column lists the RCMs.

	CNRM-CERFACS-CNRM-CM5	ICHEC-EC-EARTH	IPSL-IPSL-CM5A-MR	MOHC-HadGEM2-ES	MPI-M-MPI-ESM-LR	NCC-NorESM1-M
CNRM-ALADIN53	CM5-ALAD	–	–	–	–	–
RMIB-UGent-ALARO-0	CM5-ALAR	–	–	–	–	–
CLMcom-CCLM4-8-17	CM5-CCLM	ECE-CCLM	–	Had-CCLM	MPI-CCLM	–
DMI-HIRHAM5	–	ECE-HIRH	–	–	–	Nor-HIRH
KNMI-RACMO22E	–	ECE-RACM*	–	Had-RACM	–	–
SMHI-RCA4	CM5-RCA4	ECE-RCA4	IPS-RCA4	Had-RCA4	MPI-RCA4	–
MPI-CSC-REMO2009	–	–	–	–	MPI-REMO*	–
IPSL-INERIS-WRF331F	–	–	IPS-WRF	–	–	–

Additionally, a key important issue is that RCM simulations needs lateral boundary conditions from GCMs. At the moment the CDS-CORDEX subset boundary conditions are extracted from CMIP5 global projections (CMIP6 global projections not available yet at CDS).

- **Global Climate Models** can provide reliable climate information on global, continental and large regional scales covering what could be a vastly differing landscape with greatly varying potential for floods, droughts or other extreme events. Horizontal resolution limits the possibility to address smaller scales ranging from regional to local. Table 21 shows the list of GCMs available.

Table 21. List of GCMs, abbreviations and responsible institutions

Model name	Abbreviation	Reference	Institution
CNRM-CERFACS-CNRM-CM5	CM5	Voldoire et al. (2013)	Centre National de Recherches Météorologiques
ICHEC-EC-EARTH	ECE	Hazeleger et al. (2010)	Irish Centre for High-End Computing EC-Earth Consortium, Europe
IPSL-IPSL-CM5A-MR	IPS	Dufresne et al. (2013)	Institut Pierre Simon Laplace
MOHC-HadGEM2-ES	Had	Collins et al. (2011)	Met Office Hadley Centre
MPI-M-MPI-ESM-LR	MPI	Giorgetta et al. (2013)	Max Planck Institute for Meteorology
NCC-NorESM1-M	Nor	Bentsen et al. (2013), Iversen et al. (2013)	Norwegian Earth System Model

- **Regional Climate Models** applied with higher spatial resolution over a limited area and driven by GCMs can provide more appropriate information on such smaller scales supporting more detailed impact and adaptation assessment and planning. Table 22 shows the list of RCMs available.

Table 22. List of RCMs, abbreviations and responsible institutions

Model name	Abbreviation	Reference	Institution
CNRM-ALADIN53	ALAD	Colin et al. (2010)	Météo-France/Centre National de Recherches Météorologiques
RMIB-UGent-ALARO-0	ALAR	De Troch et al. (2013)	Royal Meteorological Institute of Belgium and Ghent University
CLMcom-CCLM4-8-17	CCLM	Baldauf et al. (2011), Rockel et al. (2008)	Climate Limited-area Modelling Community (CLM-Community)
DMI-HIRHAM5	HIRH	Christensen et al. (2007)	Danish Meteorological Institute
KNMI-RACMO22E	RACM	van Meijgaard et al. (2008)	Royal Netherlands Meteorological Institute, De Bilt, the Netherlands
SMHI-RCA4	RCA4	Strandberg et al. (2014)	Swedish Meteorological and Hydrological Institute, Rosby Centre
MPI-CSC-REMO2009	REMO	Teichmann et al. (2013)	Helmholtz-Zentrum Geesthacht, Climate Service Center, Max Planck Institute for Meteorology
IPSL-INERIS-WRF331F	WRF3	–	Institut Pierre-Simon Laplace and French National Institute for Industrial Environment and Risks (Ineris)

As stated before, each of the above global and/or regional climate models present some biases and produce slightly different results for the different variables and therefore it is not possible to select just one to be provided with the «best» future scenario. Moreover, it is very difficult to test which model is the best as they all possess different strengths and weaknesses. Significantly, there is no climate model that is always able to give the best results for all variables for all seasons over all regions. Therefore, when providing climate information, the most prudent option is to consider a simulation ensemble.

Considering the above, it has been decided by the research partners involved in this task (ENEA & TECNALIA) that the best option was to consider an ensemble based on the selection of the ICHEC-EC-EARTH global climate model developed by Irish Centre for High-End Computing as it provides low temperature biases averaged over continental Europe [29] together with the RCMs available at the CDS that take the boundary conditions from this ICHEC-EC-EARTH:

- Ensemble 1: ['ichec_ec_earth', 'knmi_racmo22e']
- Ensemble 2: ['ichec_ec_earth', 'dmi_hirham5']
- Ensemble 3: ['ichec_ec_earth', 'smhi_rca4']

The final ensembles were used both for the development of the climate services (inside the Toolbox) and to download the data projections (to be integrated within THIS) from the CDS and perform operations outside the CDS.

6.4. CDS Toolbox

The CDS Toolbox¹⁹ is a free and available environment that allows to link raw data available in the Copernicus catalogue²⁰ to online computing power through a programming interface. It

¹⁹ CDS toolbox documentation: <https://cds.climate.copernicus.eu/toolbox/doc/index.html>

²⁰ <https://cds.climate.copernicus.eu/cdsapp#!/search?type=dataset>

allows to create online web applications in Python programming language and run them on the CDS computers, allowing to directly visualize data, retrieve direct data and/or make the calculations required to display the outcomes in the format that better suit the end-user needs.

These applications can be shared and freely accessible by other users, without needing any particularly powerful computer or a lot of storage, as the calculations and the data processing take place online within the CDS. The only pre-requisite to run these applications is to get a user_id in the CDS.

In the ARCH project, the toolbox interface has been utilised for different purposes:

- To develop prototypes:
 - to facilitate dialogue between Foundation Cities and climate research partners. Several prototypes were created before the workshops with cities in order to showcase to them the type of available climate information as well as possible outcomes and formats.
 - to understand better their needs and climate information gaps that may be relevant for decision-making
- To develop climate services for assisting decision-making:
 - by transforming already available information from the Copernicus Climate Change Service into relevant knowledge to be used to support decision making.
 - by creating maps and graphs that allow to visualising trends which may help to better understand and anticipate the degree of future impacts and to build robust awareness raising campaigns.
 - to download georeferenced information (datasets) to be used outside the toolbox.

6.5. Climate Services for Bratislava

A round of four meetings was held to identify the climate change services most relevant for Bratislava case study. It was concluded, aligned with the baseline report, that climate change impacts on erosion and rock displacement were the most relevant hazard to address through climate services (cf. D3.3 “City baseline report – Bratislava” and D3.2 “Local partnership and work plan for Bratislava”). Local stakeholders have already described the importance of daily and annual thermal oscillations in the rock displacement and cracks [30].

In Slovakia the majority of castle ruins are located in areas of flysch and neovolcanic uplands and core middle mountains at a height of 350–700 m.a.s.l. Based on previous studies, which considered historical records, it is known that the effect of the climatic conditions is a climatic driver for the rock displacement and more specifically the daily temperature fluctuations play a crucial role on the degradation of the rocks. This is the reason why Bratislava local stakeholders considered it important to gather high quality historical data (not part of this work) and know the projections and trends of these fluctuations in the future periods to assess the degree of worsening of this critical problem for Bratislava’s historic heritage.

Table 23 details the most relevant climate related measurable indicators to address through climate services that stakeholders in Slovakia considered relevant to characterize the climate change impacts on erosion and rock displacement.

Table 23. Indicators, metrics, reference periods and outcomes developed for Bratislava

Measurable Indicators				
	Metrics	Source	Reference period	Outcome
<ul style="list-style-type: none"> • Daily/Monthly maximum temperatures • Daily/Monthly minimum temperatures • Daily/Monthly temperatures range 	°C			<ul style="list-style-type: none"> • Bratislava Thermal Oscillations application (see section 6.5.1) • Georeferenced dataset integrated and available through the ARCH Portal/Bratislava.
<ul style="list-style-type: none"> • Monthly accumulated precipitation 	mm	C3S-CDS	1981-2010 2011-2040 2041-2070 8071-2100	<ul style="list-style-type: none"> • Bratislava Monthly Precipitation application (see section 0)
<ul style="list-style-type: none"> • RR1 • RR2 • RR10 • RR20 	Days/period			<ul style="list-style-type: none"> • Bratislava Precipitation Extreme Indexes application (see section 0) • Georeferenced dataset integrated and available in ARCH Portal/Bratislava
<ul style="list-style-type: none"> • RX1DAY • RX2DAY • RX5DAY 	Mm/period			

As the local researchers have in-situ measures of some of these indicators for a period of years, the aim of this case study was also to compare these in-situ measures with historical and future projections in order to measure the future impacts. An additional climate service was developed to select specific periods of time to download NetCDF georeferenced information for stakeholders.

6.5.1. Thermal Oscillations application in the Toolbox

A Toolbox application has been developed²¹ to allow the end-user to easily visualize and get the thermal oscillations at any location within Slovakia considering past information and future projections. The application offers four different outcomes.

Firstly, in-situ observed data from 1981-2010 is plotted for Bratislava city (Figure 25); the plot shows the temperature maximum, temperature minimum as well as the temperature oscillations per day from 1981 to 2010. This interactive plot allows searching for specific data at any year/month/day and zoom in to better visualize in a graphical way the thermal oscillations of maximum and minimum temperature.

²¹ Developed in the CDS Toolbox.

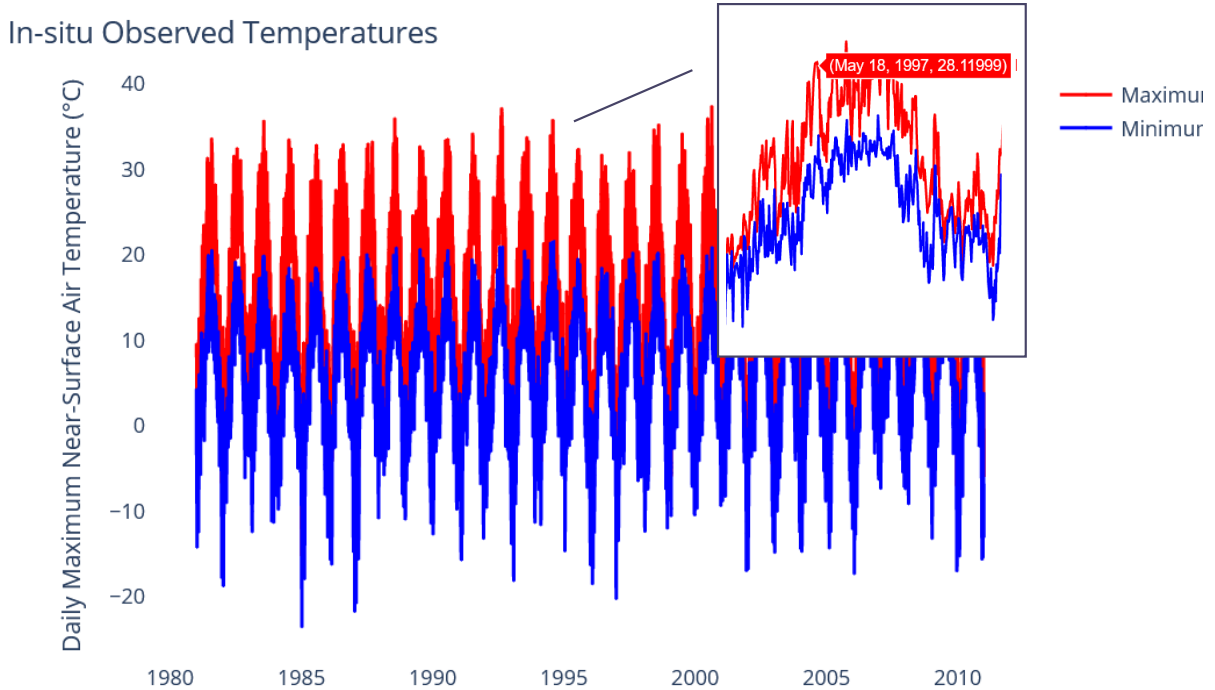


Figure 25. In-situ observed temperatures (maximum & minimum) in Bratislava city based on E-OBS dataset.

Secondly, the application provides a plot with the daily temperature oscillations (Figure 26) considering the future and reference periods predefined in Table 18. Each data period can be removed or added in order to better visualize the outcomes and trends. In addition, a zoom can be done to compare in detail the values and/or differences between the periods for specific dates.

Thirdly, the application provides a plot with the monthly temperature oscillations (Figure 27) considering the periods predefined in Table 18: historical (1981-2010), near future (2011-2040), mid-term future (2041-2070) and far future (2071-2100). Each data period can be removed or added in order to better visualize the projections outcomes. Also, a zoom can be done on the chart also to compare in specific points the values. As the future projections are based on three ensembles of CORDEX models (see section 6.3), the application allows visualising the average values as well as the standard deviations for each future period in a graphical way (Figure 27)

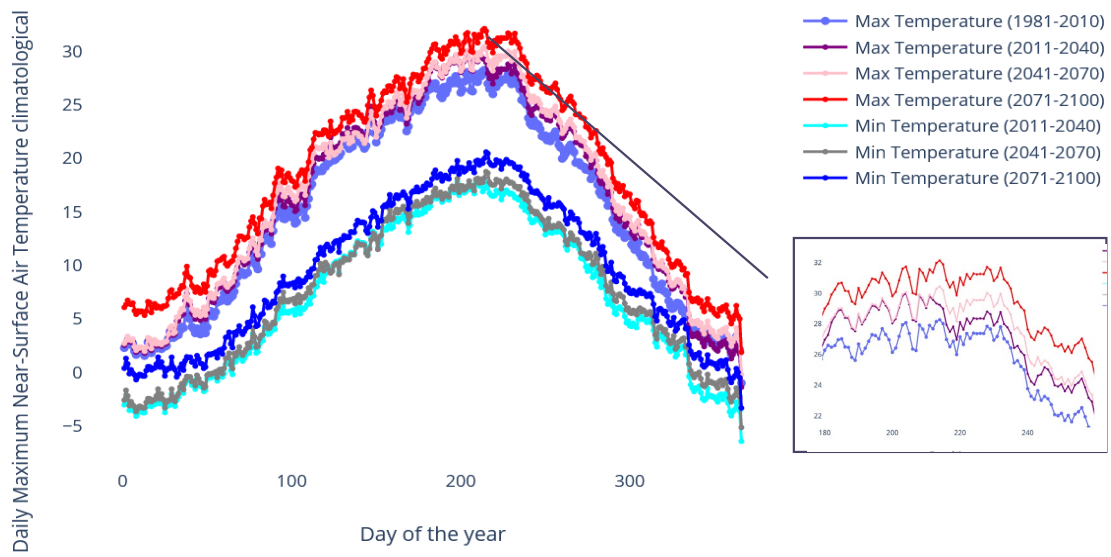


Figure 26. Daily Temperature maximum and minimum climatology in Bratislava city [latitude = 48.14816; longitude = 17.10674]

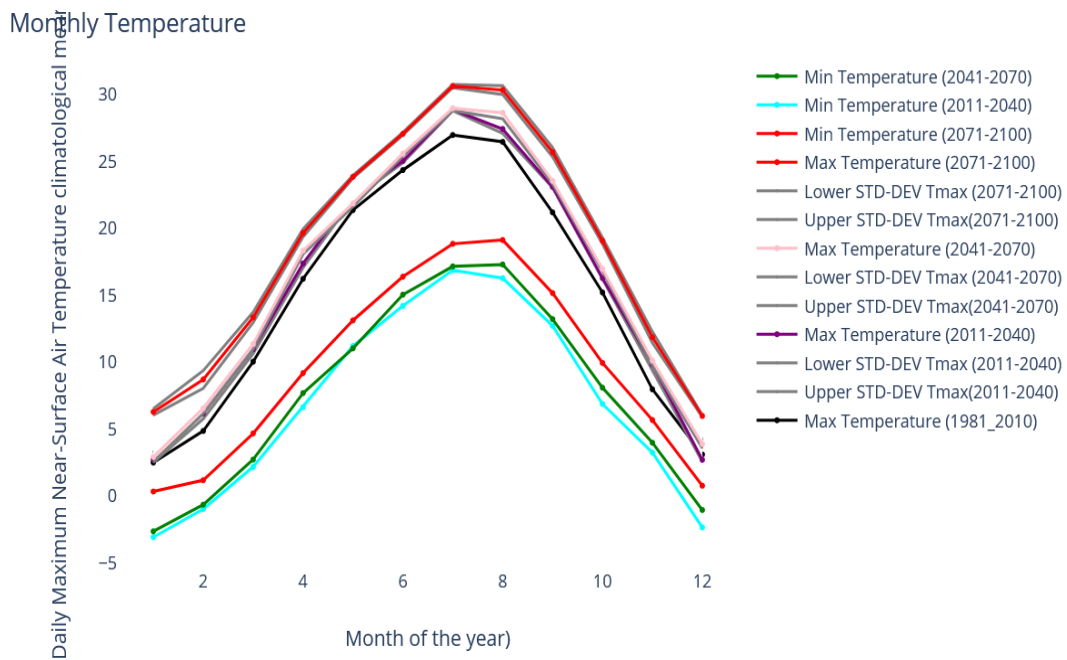
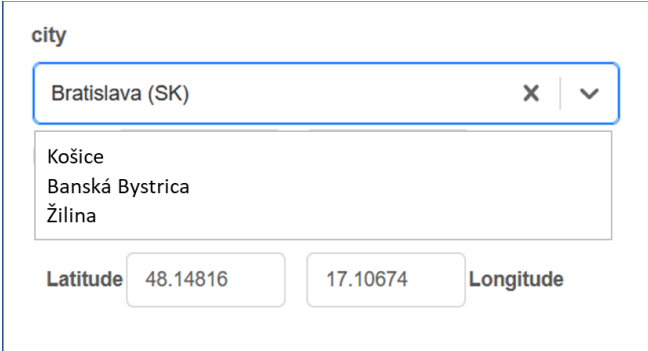


Figure 27. Monthly Temperature maximum and minimum climatology in Bratislava city [latitude = 48.14816; longitude = 17.10674]

The application also allows downloading each of the previous plotted thermal oscillations in separate specific NetCDF files, to be compared and/or processed outside of the toolbox to accommodate all user needs.

The application allows to search any other city or specific locations (based on latitude, longitude – cf. Figure 28) in order to compare outcomes for different locations, as Bratislava city centre and Devin Castle.



city

Bratislava (SK) X | v

Košice
Banská Bystrica
Žilina

Latitude 48.14816 17.10674 Longitude

Figure 28. Drop-down menu to select a city.

6.5.2. Precipitation indexes application in the Toolbox

Bratislava stakeholders also highlighted the importance of intense precipitation events over several days in relation to mass movement and other related impacts. Consequently, they showed interest in knowing the intense daily/monthly precipitation regime variation for future periods. To facilitate understanding extreme precipitation trends considering the climate change, a second Toolbox application was developed to allow end-users to get the monthly accumulated precipitation and some specific extreme indexes linked to precipitation, considering past time series and future long-projections. The application offers three different outcomes (see Figure 29 and Figure 30).

Firstly, in-situ observed data from 1981-2010 is presented for Bratislava city in Figure 29; the plot shows the accumulated daily precipitation from 1981 to 2010. This interactive plot allows searching for specific data at any year/month/day and zooming in to better visualize in a graphical way the exact date where that accumulated precipitation happened in the past.

Secondly, the application provides a plot with the monthly precipitations considering the periods predefined in Table 18: historical period (1981-2010), near future (2011-2040), mid-term future (2041-2070) and far future (2071-2100). Each data period can be excluded or included in order to better visualize the projection's outcomes.

Thirdly, considering the future projections of the three ensembles of CORDEX models (see section 6.3), the precipitation extreme indexes have been calculated per selected period (Figure 30): historical period (1981-2010), near future (2011-2040), mid-term future (2041-2070) and far future (2071-2100).

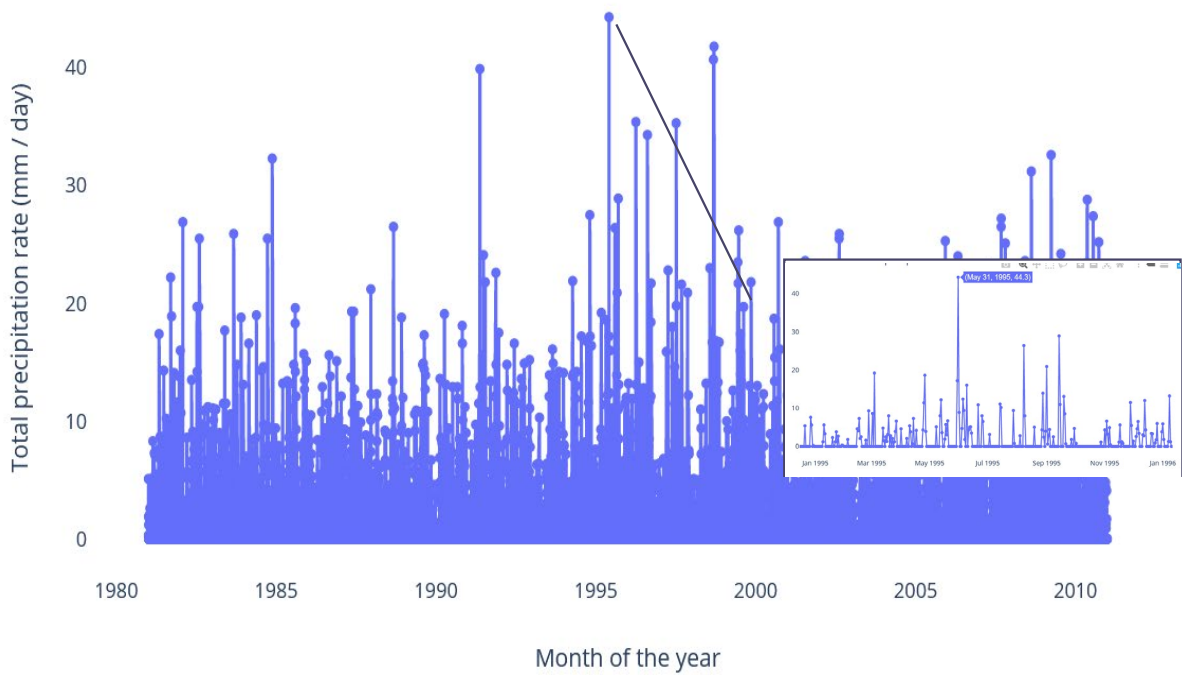


Figure 29. In-situ observed monthly accumulated precipitation in Bratislava city, based on E-OBS dataset.

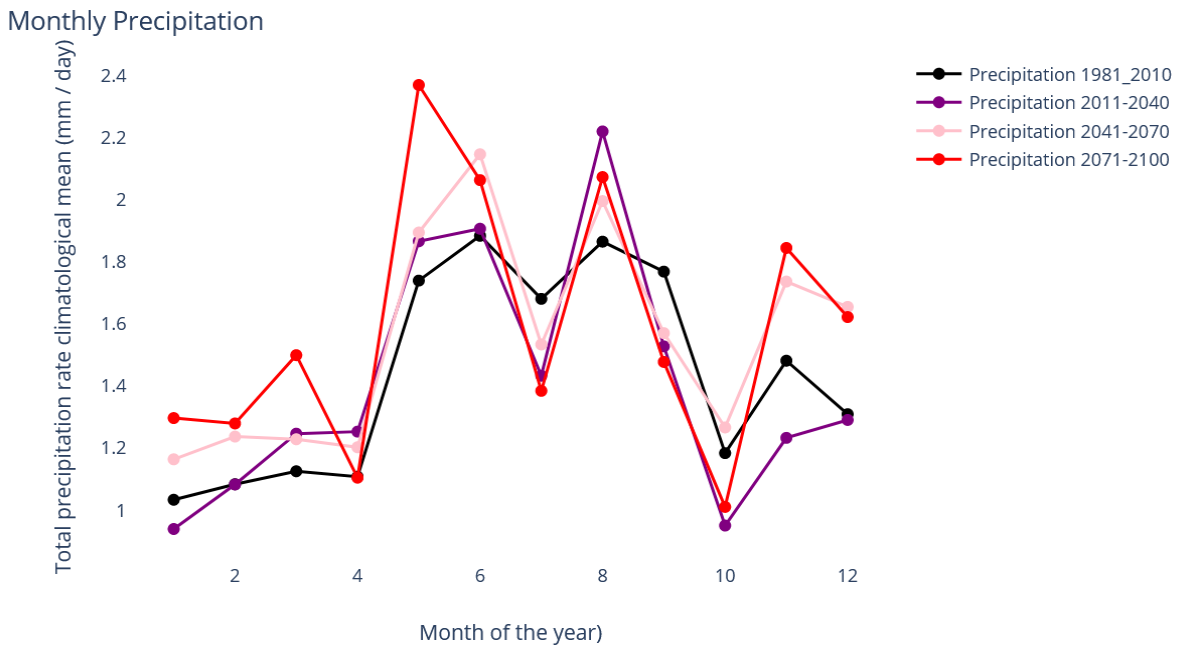


Figure 30. Monthly average accumulated precipitation in Bratislava city, based on CORDEX projections.

6.5.3. Georeferenced datasets

The previous toolbox applications have allowed maintaining a fluid and ongoing dialogue with local stakeholders along the process by sharing with them the datasets, plots and possible outcomes. It also allowed a rapid visualization of trends. However, as ARCH project aimed at the integration of all hazard related indices/information into the ARCH THIS Portal to be

accessible through a common gateway for WP5 end users, Tecnalía also developed outside the toolbox the georeferenced datasets that contain the projections and the previous indicators summarized in Table 23. The georeferenced datasets can be found through the GIS-platform for THIS, as described in the section 7.7 Climate Services.

6.6. Climate Services for Valencia

Valencia is highly interested, on the one hand, in the assessment and improvement of the resilience of the agricultural heritage sites of La Huerta and La Albufera and on the other hand in the influence and benefits of these sites in regard to heat impacts to Valencia city (cf. D3.3 “City baseline report – Valencia” and D3.2 “Local partnership and work plan for Valencia”). Following a local online consultation process, potential climate services for Valencia were identified together with the city partner (Las Naves-LNV). It was concluded that climate information to support adapted agriculture activity would be of high interest for the intermediate agriculture users within Valencia which could be used for awareness raising, acquiring knowledge of agriculture related climate indices and climate trends to support end-users and policy-making. A screening work to identify indices that could support agriculture adaptation at the appropriate spatial and temporal resolution was carried out by Tecnalía and LNV. This screening and pre-selection of indices was done based on knowledge generated by Life Agri-Adapt Project²², Tecnalía’s knowledge and Copernicus Climate Change Service. The pre-selected information was consulted in one workshop with local stakeholders, where the ARCH climate service definition was also validated.

As a result of this process, the calculation of expected changes in relevant agro-climatic indices under regional climate change scenarios was selected as one of the priority elements to build resilient in La Huerta. Likewise, the calculation of expected changes in relevant bio-climatic indices under regional climate change scenarios was selected as one of the priority elements to build resilient in La Albufera. The local stakeholders also commented the importance of climate services showing the evolution of these indicators (cf. Table 24) which influence both the crop yield loss and biodiversity loss.

Apart from the selected climate indicators identified by the local stakeholders, an extra set of climate change related data was captured and exploited as a requirement for WP5. The work was related to the characterization of a typical summer day in the context of climate change, which was a needed input for Task 5.1 “Hazard models for impact estimation” as well as the heatwaves frequency, intensity and duration.

Table 24 summarizes the selected indicators that stakeholders in Valencia consider relevant for characterize the climate change impacts on biodiversity loss and crop yield loss.

²² <https://agriadapt.eu/?lang=es>

Table 24. Indicators, metrics, reference periods and outcomes developed for Valencia

Type of Indicator	Measurable Indicators	Metrics	Source	Reference period	Outcomes
Bio-indicator	BIO1 BIO2	°C	C3S-CDS	1981-2010 2011-2040 2041-2070 8071-2100	<ul style="list-style-type: none"> • Valencia Bioclimatic Indicators application (see section 6.6.1) • Georeferenced datasets containing the bioclimatic information for the historical bioindicators (1981-2010) and the average and standard deviation for each of the selected future periods, 2011-240, 2041-2070, 2071-2100: <ul style="list-style-type: none"> - <i>BioIndicatorsValencia_1981_2010</i> - <i>BioIndicatorsValencia_2011-2040_AVERAGE.nc</i> - <i>BioIndicatorsValencia_2011-2040_STDEV.nc</i> - <i>BioIndicatorsValencia_2041-2070_AVERAGE.nc</i> - <i>BioIndicatorsValencia_2041-2070_STDEV.nc</i> - <i>BioIndicatorsValencia_2071-2100_AVERAGE.nc</i> - <i>BioIndicatorsValencia_2071-2100_STDEV.nc</i> <p>The above datasets have been integrated and available through the ARCH Portal/Valencia:</p>
	BIO3	-			
Bio-indicator	BIO4 BIO5 BIO6 BIO7 BIO8 BIO9 BIO10 BIO11	°C	C3S-CDS	1981-2010 2011-2040 2041-2070 8071-2100	<ul style="list-style-type: none"> • Georeferenced datasets containing the agroclimatic information for each quarter of the historical bioindicators (1981-2010) and the average and standard deviation for each of each quarter of the future periods, 2011-240, 2041-2070, 2071-2100: <ul style="list-style-type: none"> - <i>AgroIndicatorsValencia_1981_2010_[Q1_Q2_Q3_Q4].nc</i> - <i>AgroIndicatorsValencia_2011-2040_AVERAGE[Q1_Q2_Q3_Q4].nc</i> - <i>AgroIndicatorsValencia_2011-2040_STDEV[Q1_Q2_Q3_Q4].nc</i> - <i>AgroIndicatorsValencia_2041-2070_AVERAGE[Q1_Q2_Q3_Q4].nc</i> - <i>AgroIndicatorsValencia_2041-2070_STDEV[Q1_Q2_Q3_Q4].nc</i> - <i>AgroIndicatorsValencia_2071-2100_AVERAGE[Q1_Q2_Q3_Q4].nc</i> - <i>AgroIndicatorsValencia_2071-2100_STDEV[Q1_Q2_Q3_Q4].nc</i> <p>The above datasets have been integrated and available through the ARCH Portal/Valencia.</p>
	BIO12 BIO13 BIO14 BIO15 BIO16 BIO17 BIO18 BIO19	mm			
Agro-indicator	CSU CWD FD SD TR WSDI	days/period	C3S-CDS	1981-2010 2011-2040 2041-2070 8071-2100	<ul style="list-style-type: none"> • Georeferenced datasets containing the agroclimatic information for each quarter of the historical bioindicators (1981-2010) and the average and standard deviation for each of each quarter of the future periods, 2011-240, 2041-2070, 2071-2100: <ul style="list-style-type: none"> - <i>AgroIndicatorsValencia_1981_2010_[Q1_Q2_Q3_Q4].nc</i> - <i>AgroIndicatorsValencia_2011-2040_AVERAGE[Q1_Q2_Q3_Q4].nc</i> - <i>AgroIndicatorsValencia_2011-2040_STDEV[Q1_Q2_Q3_Q4].nc</i> - <i>AgroIndicatorsValencia_2041-2070_AVERAGE[Q1_Q2_Q3_Q4].nc</i> - <i>AgroIndicatorsValencia_2041-2070_STDEV[Q1_Q2_Q3_Q4].nc</i> - <i>AgroIndicatorsValencia_2071-2100_AVERAGE[Q1_Q2_Q3_Q4].nc</i> - <i>AgroIndicatorsValencia_2071-2100_STDEV[Q1_Q2_Q3_Q4].nc</i> <p>The above datasets have been integrated and available through the ARCH Portal/Valencia.</p>
Heat wave-indicator	Global intensity Frequency Duration	°C days number	C3S-CDS	1981-2010 2011-2040 2041-2070 8071-2100	<ul style="list-style-type: none"> • Heatwaves Valencia city-center 1981-2010.xlsx • Heatwaves Valencia La Huerta 1981-2010.xlsx • Heatwaves Valencia La Albufera 1981-2010.xlsx • HeatWaves Valencia 2071-2010.xlsx • HeatWaves Valencia 2041-2070.xlsx • HeatWaves Valencia 2071-2100.xlsx

Type of Indicator	Measurable Indicators	Metrics	Source	Reference period	Outcomes
Summer typical Dyas	Temperature maximum Temperature minimum Total number	°C °C days/year	C3S-CDS	1981-2010 2011-2040 2041-2070 8071-2100	<ul style="list-style-type: none"> • Summer days characterization in Valencia 1981-2010.xlsx • Summer days characterization in Valencia 2011-2040.xlsx • Summer days characterization in Valencia 2041-2070.xlsx • Summer days characterization in Valencia 2071-2100.xlsx

6.6.1. Bioindicators for Valencia

Bioindicators are used to assess the quality of the environment and how it changes over time. Changes in the environment are often attributed to anthropogenic disturbances (e.g., pollution, land use changes) or natural stressors (e.g., drought, late spring freeze, etc.). The bioclimatic indicators can be used in species distribution modelling, ecological modelling techniques or to monitor the impact of climate change on biodiversity loss.

Bioclimatic indicators are derived from the monthly temperature and rainfall values in order to generate more biologically meaningful variables. These variables represent annual trends (e.g., mean annual temperature, annual precipitation), seasonality (e.g., annual range in temperature and precipitation) and extreme or limiting environmental factors (e.g., temperature of the coldest and warmest month, and precipitation of the wet and dry quarters).

For Valencia case study, 19 bioclimatic variables²³ were calculated, based on the original list of bioclimatic variables offered by WorldClim²⁴. Each bioindicator was translated into Python language to generate the variables from current and future climatology (Figure 31).

The schema in figure was applied to the E-OBS dataset to calculate present climatology. As explained in the previous section, to calculate the deltas the selected CORDEX ensembles were used to calculate deltas for different future horizons with regard to the historical modelled data of the same CORDEX ensembles. Applying these deltas to the E-OBS climatology a new climatology was generated for each of the future scenarios (cf. section 6.2

Delta scaling methodology and Figure 23).

²³ The correspondence between code and bioindicator can be found in the list of indicators.

²⁴ <https://www.worldclim.org>

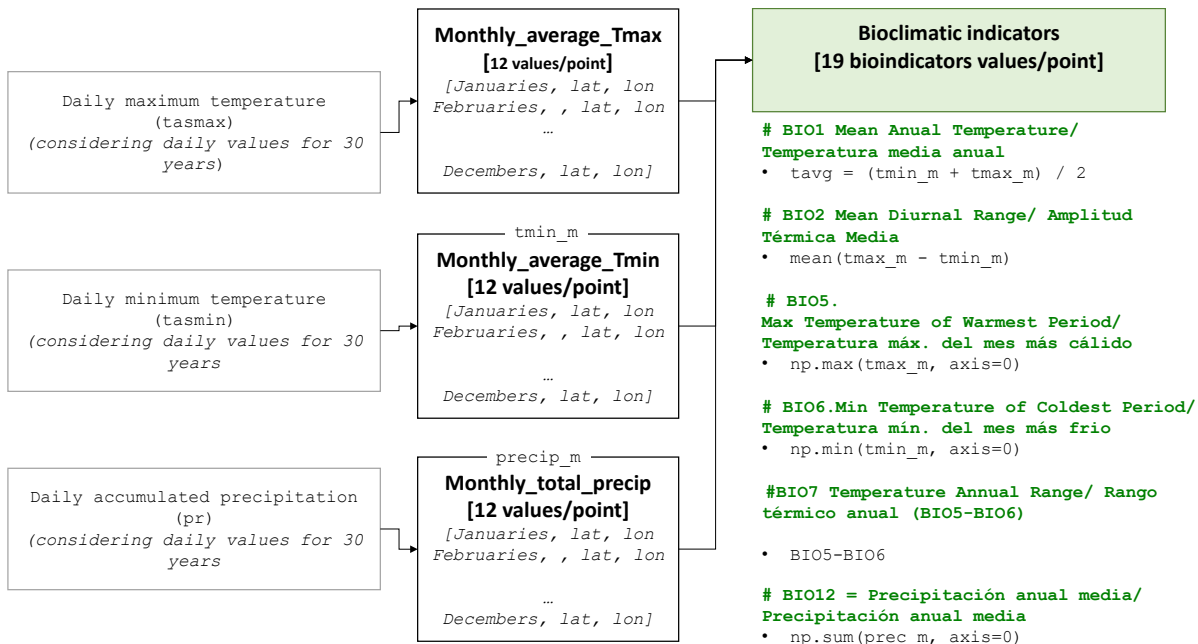


Figure 31. Schema for the development of the bioindicators.

Considering the above information and in order to facilitate a dialogue with stakeholders a prototype application was developed in the Toolbox in order to show the possible outcomes to show the trends of these indicators (Figure 32).

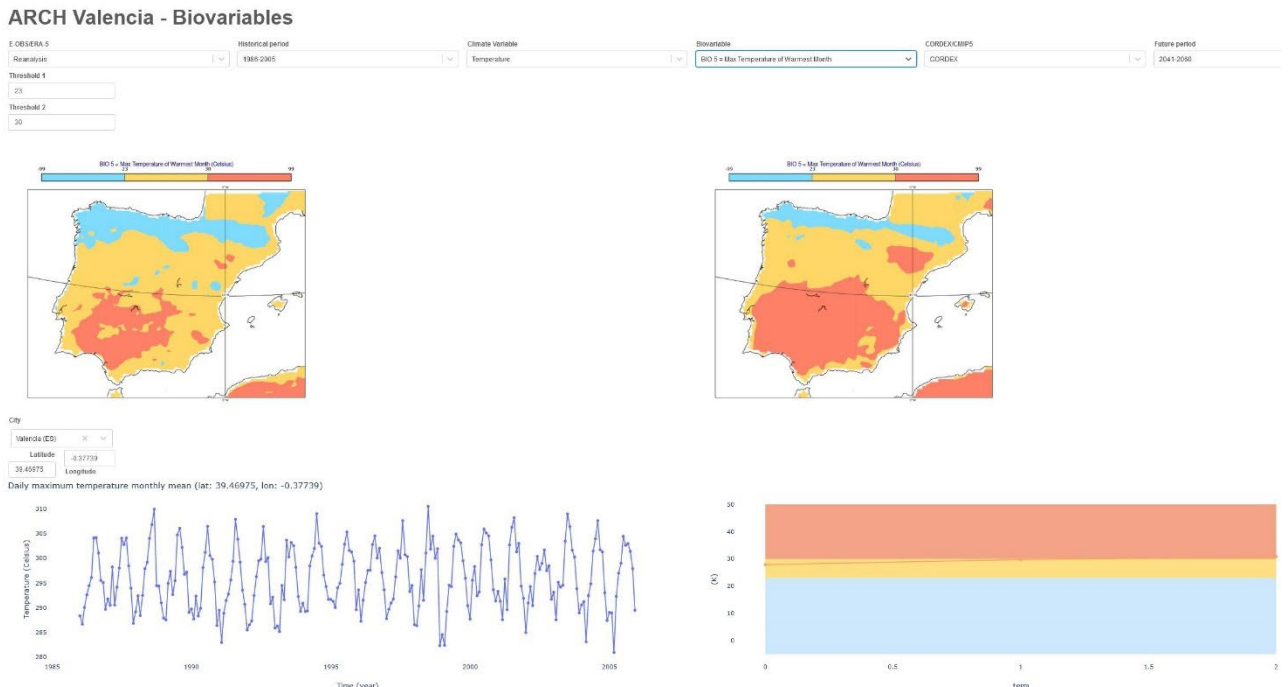


Figure 32. Prototype application developed for the workshop with Valencia stakeholders

The maps allow comparing the evolution of these indicators in Spain for the selected periods based on a minimum and maximum threshold values. The left-hand side plot allows to visualise the evolution of the indicators for each period (past, near future and long future) as well as

change the threshold values of the temperature minimum and temperature maximum based on what the colours of the map and chart are changed (Figure 33).

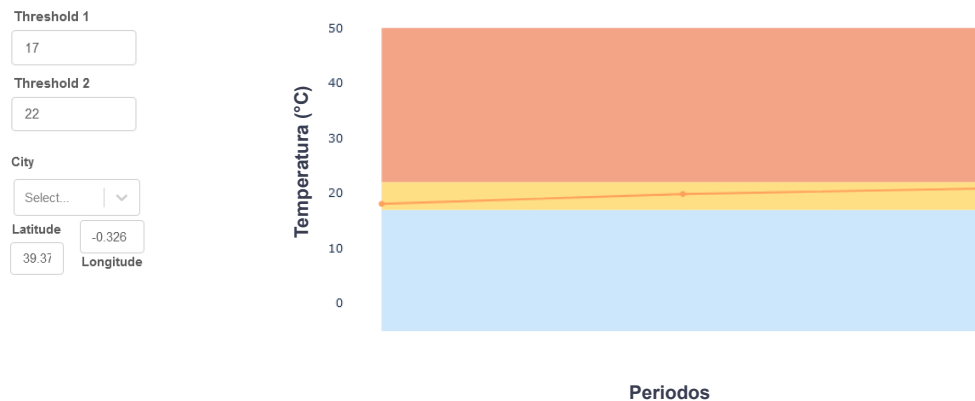


Figure 33. Evolution of BIO1 (Annual Mean Temperature) in La Albufera [latitude= 39.371, longitude=-0.326]

Although the application was interesting for the local stakeholders (consultation workshop with local stakeholders), the preferred output format (plots, maps, comparative tables, threshold evolution plots, files to be easily integrated in GIS) data analysis was a set of georeferenced datasets containing the bioclimatic information for the historical bioindicators (1981-2010) and the average and standard deviation for each of each quarter of the future periods information, to be integrated in the THIS GIS-platform or ad-hoc into a GIS application.

6.6.2. Agro-indicators for Valencia

The preferred agro-indicators to be developed within ARCH project were based on the previous research and development made in the Global Agriculture project²⁵ as part of the C3S Global Agriculture Sectoral Information Systems (SIS). However, this project developed the indices at higher spatial resolution than considered optimal by Valencia's local stakeholders. Thus, the selected indicators were adapted to the local needs.

Considering the above mentioned C3S project definition, agroclimatic indicators represent features of the climate that are used to characterize plant-climate interactions. They can be derived from daily or monthly meteorological variables (e.g. temperature and rainfall).

To calculate each indicator there are different *formulas* that measure climatic factors and conditions that may positively/negatively affect vegetation and may correlate to the main type of vegetation of an area. They are commonly used in agriculture to reconstruct climate and environmental changes such as climatically induced phases of plant growth, moisture and heat supply, drought spells, etc.

There are two main categories of indicators:

²⁵ <https://climate.copernicus.eu/global-agriculture-project>

- **Generic Agroclimatic Indicators:** these are aggregation, accumulation or occurrence indicators calculated as a function of temperature and precipitation.

- **Tailored crop-specific indicators:** These indicators require information such as sowing date, harvest date, growing range of min and max temperatures, thermal requirements, geographical distribution, etc. in order to provide outputs specific to the crops of interest.

Considering the prioritisation process done with the local stakeholders, the ARCH project focused on a small subset of generic agroclimatic indicators. The most valuable information for the local stakeholders was that they would be defined to describe seasonal evolution. Consequently, these indicators have been calculated for each annual quarter (Table 25).

Table 25. Annual quarters for agroindicators of Valencia

	1981-2010	2011-2040	2041-2070	2071-2100
Q1 (January-February-March)	X	X	X	X
Q2 (April-May-June)	X	X	X	X
Q3 (July, August-September)	X	X	X	X
Q4 (October-November-December)	X	X	X	X

Also, a prioritisation of the most relevant agro-climatic indicators was done, coming out with the list of indicators in Table 26.

Table 26. Prioritisation of the agro-indicators by stakeholders in Valencia

Agroindicator	percentage of vote
WSDI - Warm spell duration index	80%
FD - Frost days (daily minimum temperature < 0°C)	60%
CSU - Maximum number of consecutive summer days	60%
HWD - Intensity, duration, and frequency of heat waves	60%
SD - Days of summer (maximum daily temperature > 25°C)	40%
CWD - Maximum number of consecutive wet days	20%
TD - Tropical nights (minimum daily temperature > 20°C)	20%

The preferred outcome are georeferenced datasets containing the agro-climatic information for each quarter of the historical bioindicators (1981-2010) and the average and standard deviation for each future period information -- to be integrated in THIS GIS-platform or ad-hoc into a GIS application.

6.6.3. Heatwaves characterization in Valencia

Heatwaves are a specific type of extreme temperature event, and was one of the hazards selected by stakeholders in Valencia, as there are many adverse impacts of heatwaves already observed in agriculture but also on human health or tourist activity (other sectors important in Valencia).

Impacts of heatwaves may vary from thermal discomfort, lack of productivity, loss in crop yield, more energy consumption and/or health problems. These impacts will increase under enhanced global warming, where more rapid heatwave trends will likely produce more severe and possibly irreversible impacts. To reduce or at least mitigate these impacts added-value information regarding the risks of these extreme temperature events is needed to take proper decisions to prepare, protect and prevent the city and citizens.

There are multiple characteristics to heatwaves, including their intensity, frequency, duration, timing and spatial extent. But specifically, in Valencia Heat Wave Duration index (HWD) was selected as the most representative to measure the impact of climate change in agriculture.

Therefore, the analysis of heatwaves and their representation in a comprehensible and accessible way is a crucial challenge for climate services, in particular for delivering scientific support to policy makers. In order to fulfil this need, a method for analysing the heatwaves in Valencia has been defined and developed following the approach of a previous research made in France [31].

Considering the Spanish Meteorological Agency definition for heatwave, “A heatwave day is a day when both the daily minimum and maximum temperatures exceed the 95th and 90th percentile respectively for at least 3 consecutive days between the months of May and September”

The Heatwaves in ARCH have been characterized considering the following three parameters:

- **Intensity of the heatwave:**
 - Maximum temperature reached
 - Global Intensity: Average of the temperature maximum reached of all days during the heatwave event
- **Duration of the heatwave:**
 - Average Heatwave duration
- **Frequency of the heatwave:**
 - Number of Heat Waves

Apart from the intensity, frequency and duration characteristics, the spatial extent of the heatwaves has also been studied in Valencia, to do so, a statistical analysis has been done for the three representative points in Valencia (Table 27).

Table 27. Representative points in Valencia for heatwaves characterization

Representatives points	Geographical coordinates
Valencia city-centre	-0'3774, 39'4709
La Huerta	-0'384, 39,513
La Albufera	-0'326, 39'371

The next Box shows the statistical analysis performed for these three points considering the historical timeframe of 1981-2010 of the e-OBS dataset available at CDS. As mentioned before one of the key points of the heatwave definition is the establishment of the threshold values linked to the Tmax and Tmin for Valencia. In the ARCH project, the study has been done for this geographical area (see Figure 34) from which the percentiles 95 and 90 of Tmax and Tmin have been calculated:

Percentile 95 Tmax = 33.23°C
Percentile 90 Tmin = 21.41°C

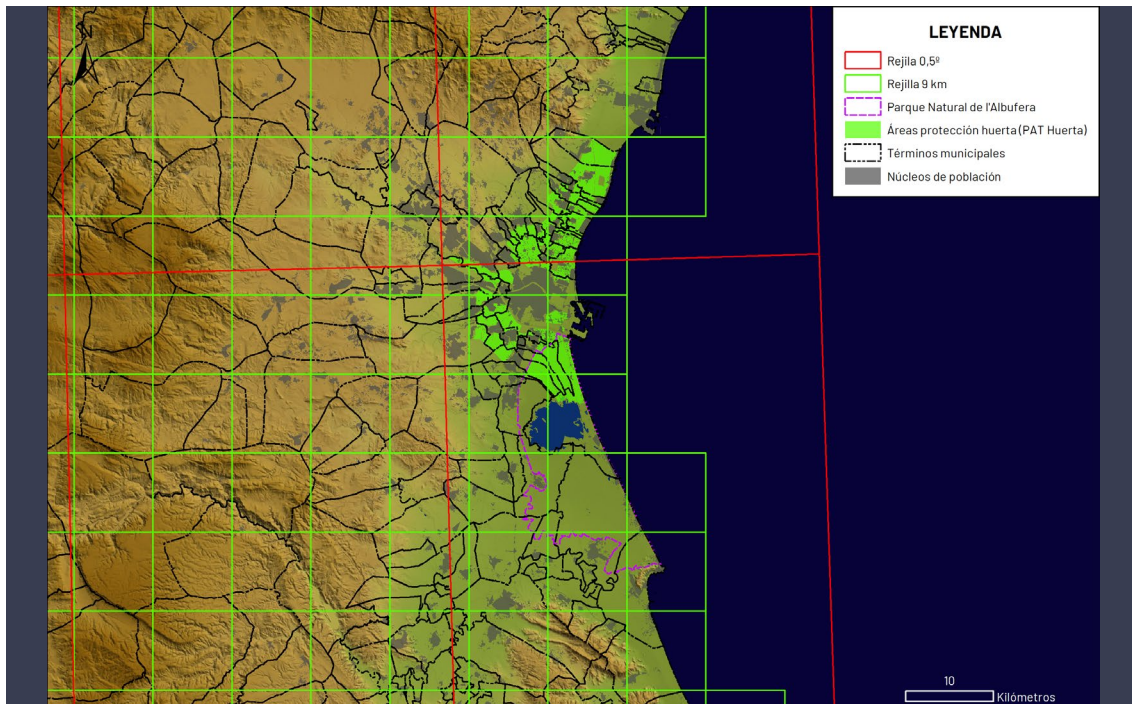


Figure 34. Geographical coordinates of the analysed area. NW: -0' 8075, 39'7187, SE: 0'1573, 39'0918 (Source: ICV, IGN, Copernicus Climate Change Service)

The next figures (Figure 35 - Figure 37) show the graphical representation of the historical heatwaves in Valencia city-centre, La Huerta and La Albufera, respectively, considering the same graphical approach of Ouzeau et al.(2016) [31].

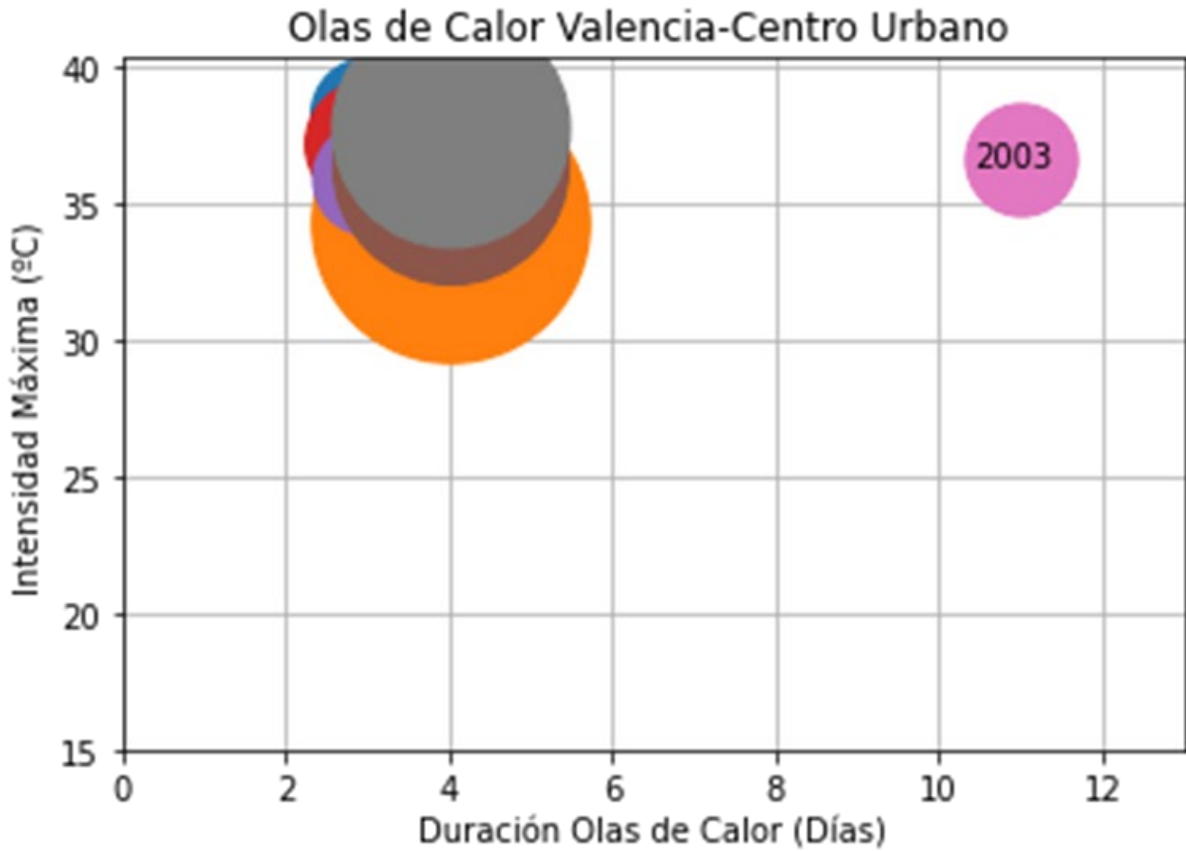


Figure 35. Graphical representation of the duration and intensity of historical (1981-2010) heatwaves in Valencia's city centre. X axis represent the heatwave duration (days) and Y axis represent the maximum intensity reached during that heatwave event (°C)

Table 28. Heatwaves statistics in Valencia city

Duration	Intensity (average)	Tmax (average)	Stats (Frequency)
3	35.39	37.16	4
4	34.69	36.18	3
11	34.67	36.64	1

Table 29. Records of heatwave events in Valencia city

Duration	Intensity	Tmax	Start date
3	36.17	38.29	1985-07-28
4	33.67	34.32	1991-08-26
3	34.95	37.18	1993-08-05
3	35.22	37.24	1994-08-09
3	35.23	35.92	2003-06-14
4	35.20	36.42	2003-06-29
11	34.67	36.64	2003-08-04
4	35.21	37.81	2004-08-17

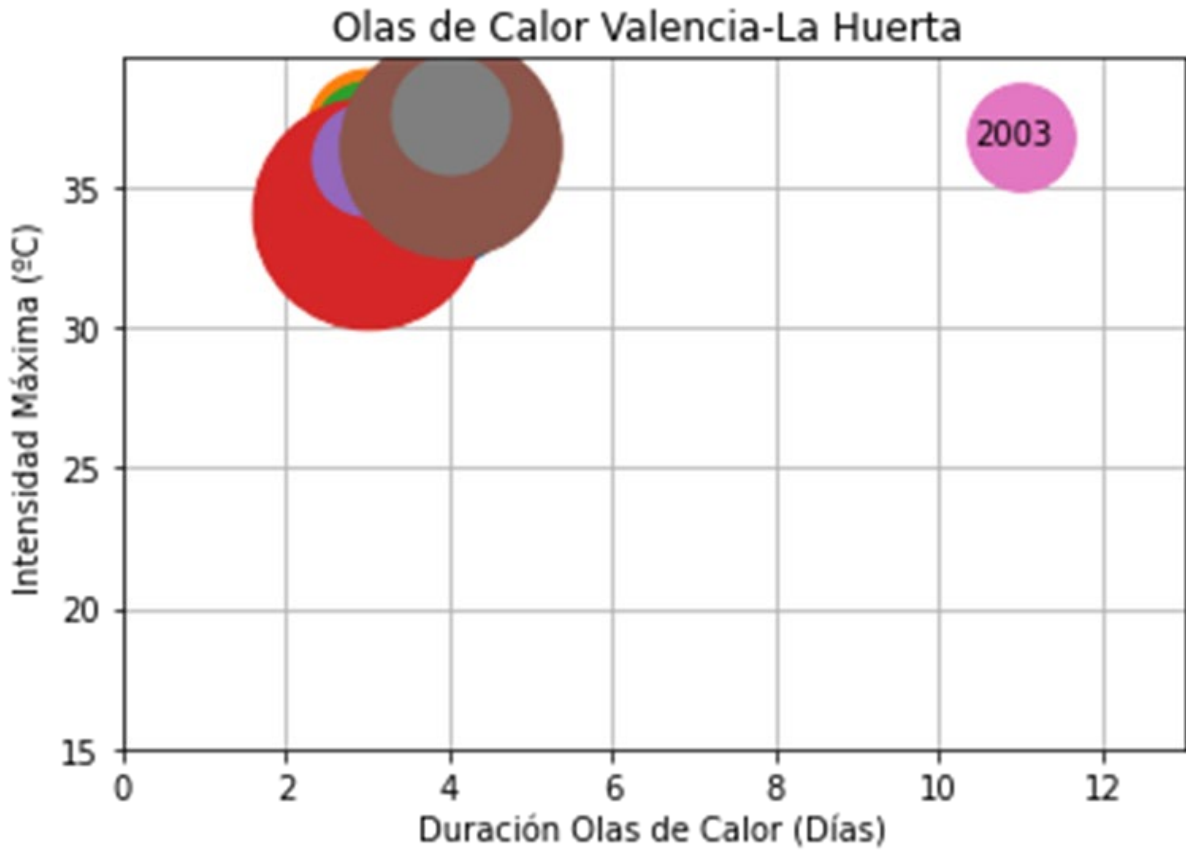


Figure 36. Graphical representation of the duration and intensity of historical (1981-2010) heatwaves in La Huerta. X axis represent the heatwave duration (days) and Y axis represent the maximum intensity reached during that heatwave event (°C)

Table 30. Heatwaves statistics in La Huerta

Duration	Intensity (average)	Tmax (average)	Stats (Frequency)
3	34.79	35.98	4
4	34.66	36.07	3
11	34.79	36.8	1

Table 31. Records of heatwave events in La Huerta

Duration	Intensity	Tmax	Start date
4	33.81	34.23	1991-08-26
3	35	37.05	1993-08-05
3	35.13	36.79	1994-08-09
3	33.70	34.08	2001-07-31
3	35.33	36	2003-06-14
4	35.05	36.41	2003-06-29
11	34.79	36.8	2003-08-04
4	35.11	37.57	2004-08-17

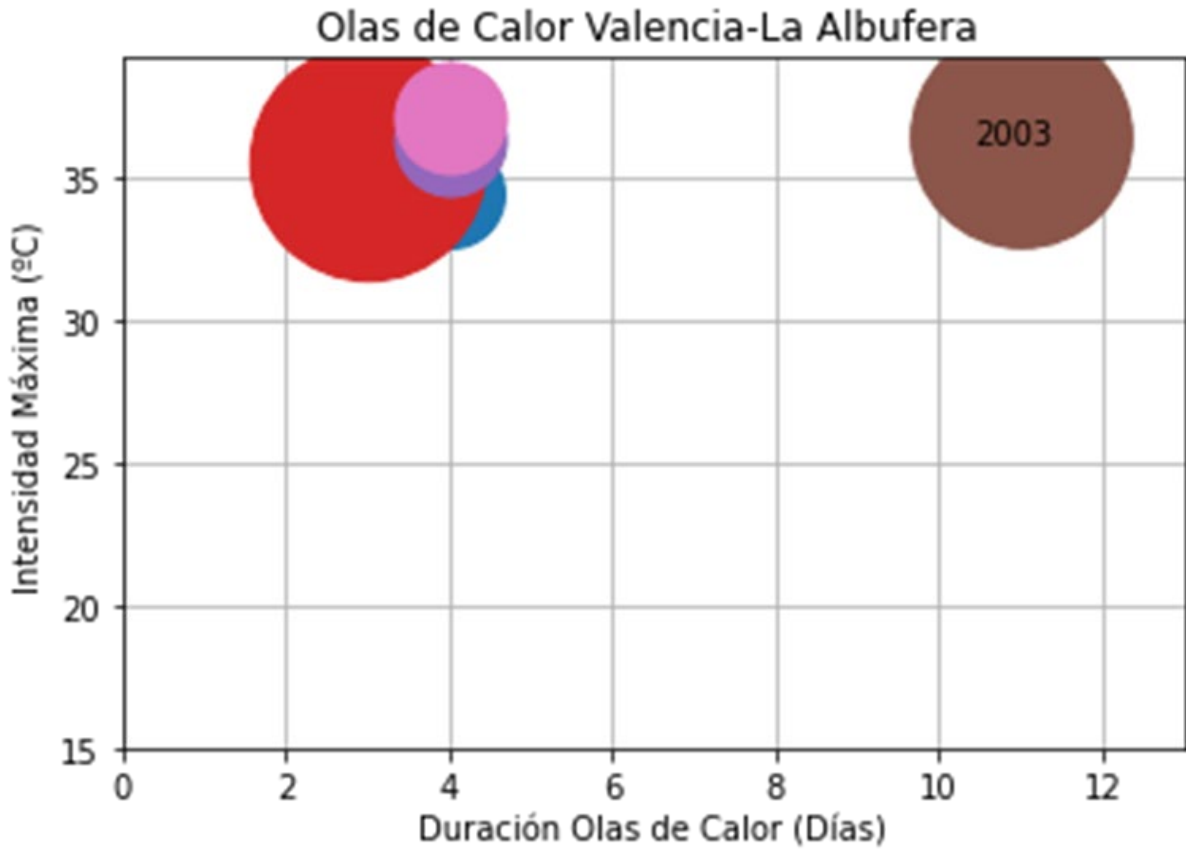


Figure 37. Graphical representation of the duration and intensity of historical (1981-2010) heatwaves in La Albufera. X axis represent the heatwave duration (days) and Y axis represent the maximum intensity reached during that heatwave event (°C)

Table 32. Heatwaves statistics in La Albufera

Duration	Intensity (average)	Tmax (average)	Stats (Frequency)
3	35.07	36.54	3
4	34.68	35.97	3
11	34.67	36.49	1

Table 33. Records of heatwave events in La Albufera

Duration	Intensity	Tmax	Start date
4	33.91	34.51	1991-08-26
3	35.22	37.2	1993-08-05
3	34.98	36.8	1994-08-09
3	35.02	35.62	2003-06-14
4	35.01	36.32	2003-06-29
11	34.67	36.49	2003-08-04
4	35.1125	37.08	2004-08-17

A similar statistical analysis has been done but considering the projections of daily temperature maximum and temperature minimum based on the selected CORDES ensembles. Next figures (Figure 38, Figure 39, Figure 40) and tables (Table 34, Table 35, Table 36) summarize the outcomes projected for Valencia city centre for the periods 2011-2040, 2041-2070 and 2071-

2100. As it can be observed the number of heatwaves increase over time together with their global intensity as well as the maximum temperature reached.

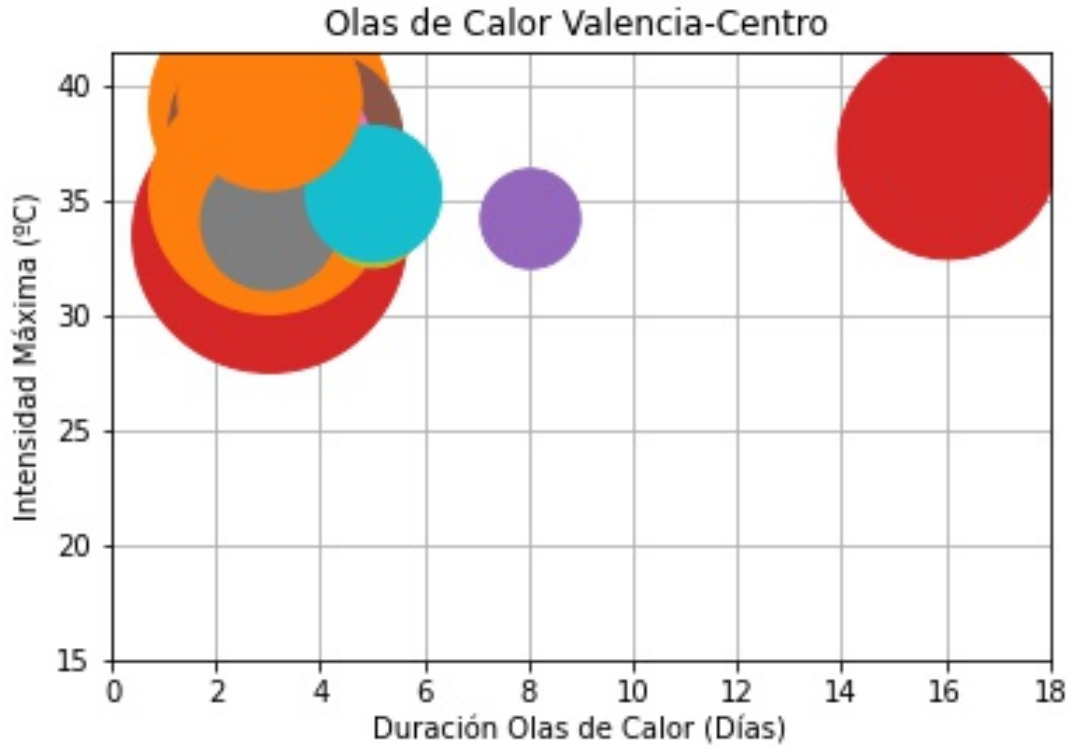


Figure 38. Heatwaves representation (duration and intensity) in Valencia city for 2011-2040 period. X axis represent the average projected heatwave duration (days) and Y axis represent the average projected maximum intensity reached during that heatwave event (°C)

Table 34. Heatwaves statistics in Valencia (2011-2040)

Duration	Intensity (average)	Tmax (average)	Stats (Frequency)
3	35.28	36.67	14.67
4	35.42	36.82	6.17
5	34.40	35.75	1.17
6	33.93	34.74	0.67
7	33.78	34.49	0.17
8	33.73	34.34	0.17
9	33.84	34.52	0.67
12	35.17	37.13	0.17
16	35.16	37.50	0.67

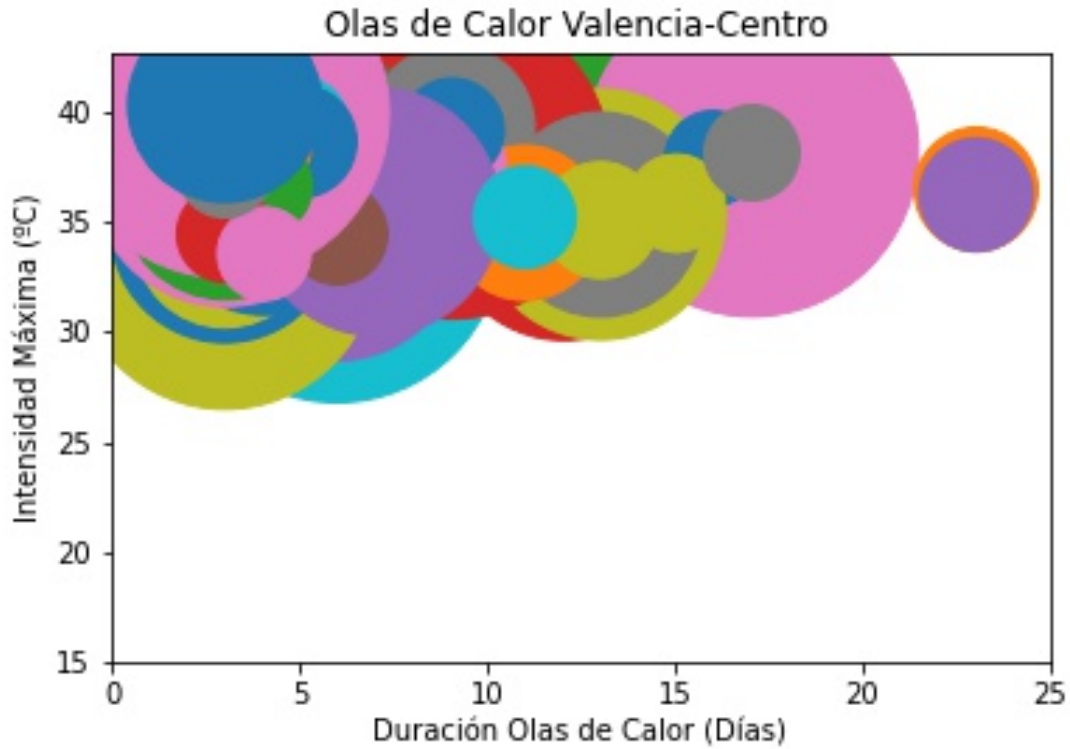


Figure 39. Heatwaves representation (duration and intensity) in Valencia city for 2041-2070 period. X axis represent the average projected heatwave duration (days) and Y axis represent the average projected maximum intensity reached during that heatwave event (°C)

Table 35. Heatwaves statistics in Valencia (2041-2070)

Duration	Intensity (average)	Tmax (average)	Stats (Frequency)
3	34.89	35.97	25.83
4	35.12	36.82	17.00
5	35.20	37.83	4.50
6	34.90	37.08	3.17
7	34.46	36.43	1.83
8	35.52	40.36	0.17
9	34.47	37.52	2.67
10	34.49	40.13	0.17
11	34.30	36.60	0.50
12	34.35	35.34	0.17
13	34.39	35.30	1.33
15	34.17	35.94	0.17
16	35.60	37.93	0.17
17	35.84	38.32	0.67
23	34.44	36.29	0.83
30	35.24	40.36	0.17

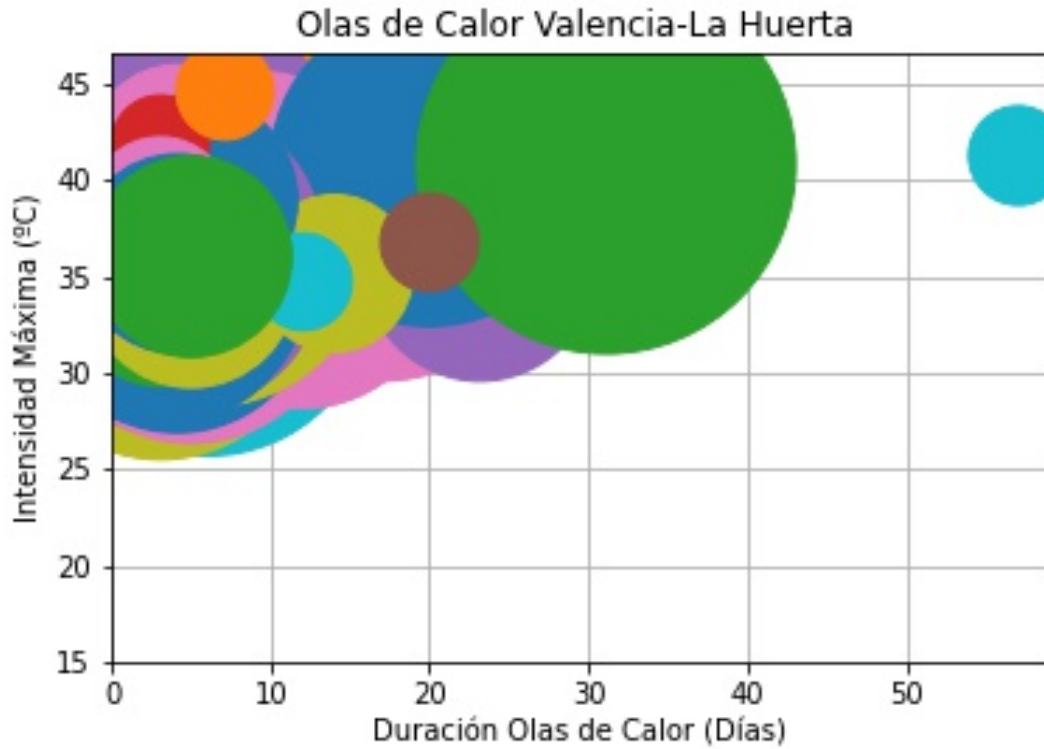


Figure 40. Heatwaves representation (duration and intensity) in Valencia city for 2071-2100 period. X axis represent the average projected heatwave duration (days) and Y axis represent the average projected maximum intensity reached during that heatwave event (°C)

Table 36. Heatwaves statistics in Valencia (2071-2100)

Duration	Intensity (average)	Tmax (average)	Stats (Frequency)
3	34.78	35.96	31.17
4	34.97	36.76	24.00
5	34.76	36.59	14.00
6	34.80	36.69	13.17
7	35.11	38.21	7.67
8	35.18	38.13	3.50
9	35.09	38.00	5.67
10	35.16	38.39	1.50
11	35.10	38.10	2.67
12	34.74	37.03	3.83
13	34.76	38.16	2.33
14	35.06	38.11	4.50
15	34.90	38.24	1.50
...			
30	35.31	37.57	0.50

6.6.4. Typical Summer Days Characterization in Valencia

Changes in the territory and its use may affect exchanges of water, energy, GHGs, thus altering the state and dynamics of the atmosphere, which, as a result, may dampen or amplify climate change at the local scale.

Thermal modelling - activity to be developed under WP5 – would require inputs on the possible land use scenarios as well as inputs regarding the climate change perspective by considering the evolution of summer hot days and heatwaves in Valencia.

Within the ARCH project it was decided to carry out the work by analysing the current and future climate in Valencia through the characterisation of a 'typical summer day' by taking into account the daily evolution of the maximum and minimum temperature. In order to do so a classification of typical summer days and their evolution in time was performed by means of a cluster analysis (K-means). For this analysis the daily maximum and minimum temperature of the summer period (June, July, August, September) was examined during the last 30 years (1981-2010) as well as for future periods 2011-2041, 2041-2070 and 2071-2100. This information was obtained from e-OBS dataset as well as CORDEX ensembles. This permitted to characterize different day classes for the summer in Valencia. The methodology followed for this classification is graphically explained in Figure 41.

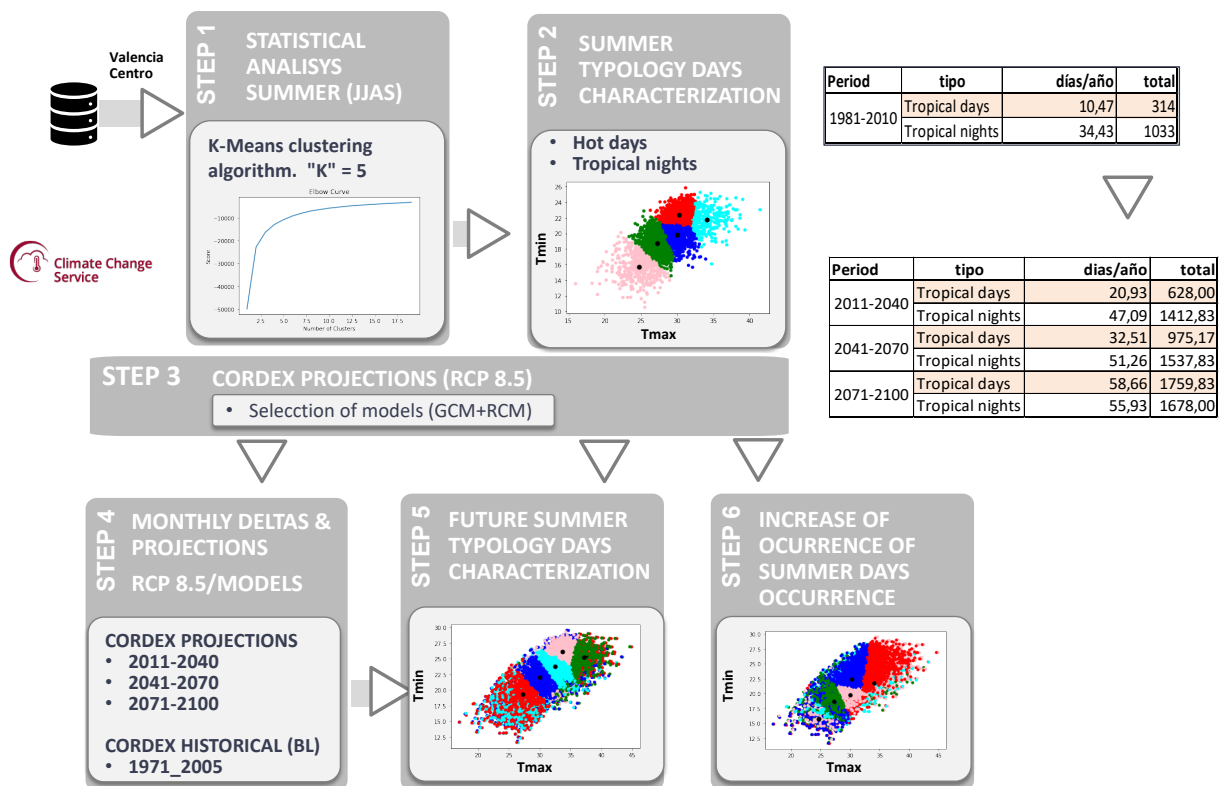


Figure 41. Methodology applied for past and future summer days characterization

The K-means Clustering algorithm is one of the most widely used algorithms for finding groups/clusters. The algorithm uses an iterative process in which the groups are adjusted to

produce the final result. To run the algorithm, the input data set, in this case study, is the daily Tmax and Tmin endowments for a specific point (Valencia city centre) during the last 30 years.

In particular, in this case study the cluster of highest interest was the one characterised by the highest daily maximum temperatures and at the same time very high minimum temperatures (extreme heat days and night). So the algorithm clusters the information in different groups attending to the characteristics of Tmax and Tmin. Figure 42 represents in a graphical way the clusters obtained. The y-axis represents the Tmax an x-axis represents the Tmin.

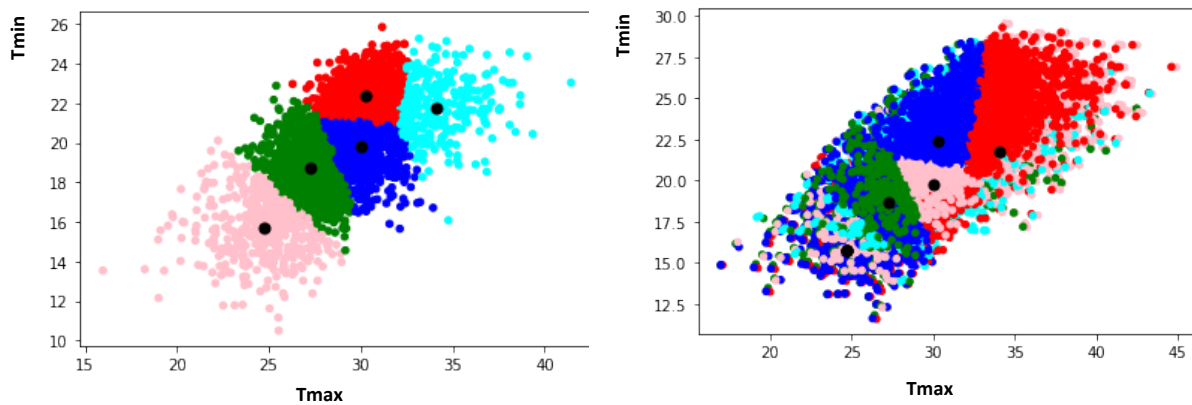


Figure 42. Clusters identified in Valencia city for past (left) and future periods (right).

As we are interested in thermal stress in Valencia, we have selected from the previous clusters the ones with highest Tmax and highest Tmin which represent typical tropical days and tropical nights. The characterisation of each of these clusters (tropical days and tropical nights) has been done considering the historical data, near future, mid future and far future data. Table 37 presents the parameters that describe each type of day for the different periods. The evolution of the frequency of these types of days considering the historical Tmax and Tmin percentiles is shown in Figure 43.

Table 37. Parameters that describe the typical day associated to the tropical day and night cluster

Periods	Type of day	Days/ year	Total days/ period	Tmax (medium)	Tmin (medium)
1981-2010	Tropical days	10.47	314	34.09	21.74
	Tropical nights	34.43	1033	30.29	22.38
2011-2040	Tropical days	20.93	628.00	33.98	22.71
	Tropical nights	47.09	1412.83	30.64	22.94
2041-2070	Tropical days	32.51	975.17	34.07	23.56
	Tropical nights	51.26	1537.83	30.79	23.28
2071-2100	Tropical days	58.66	1759.83	34.59	25.05
	Tropical nights	55.93	1678.00	30.99	23.77

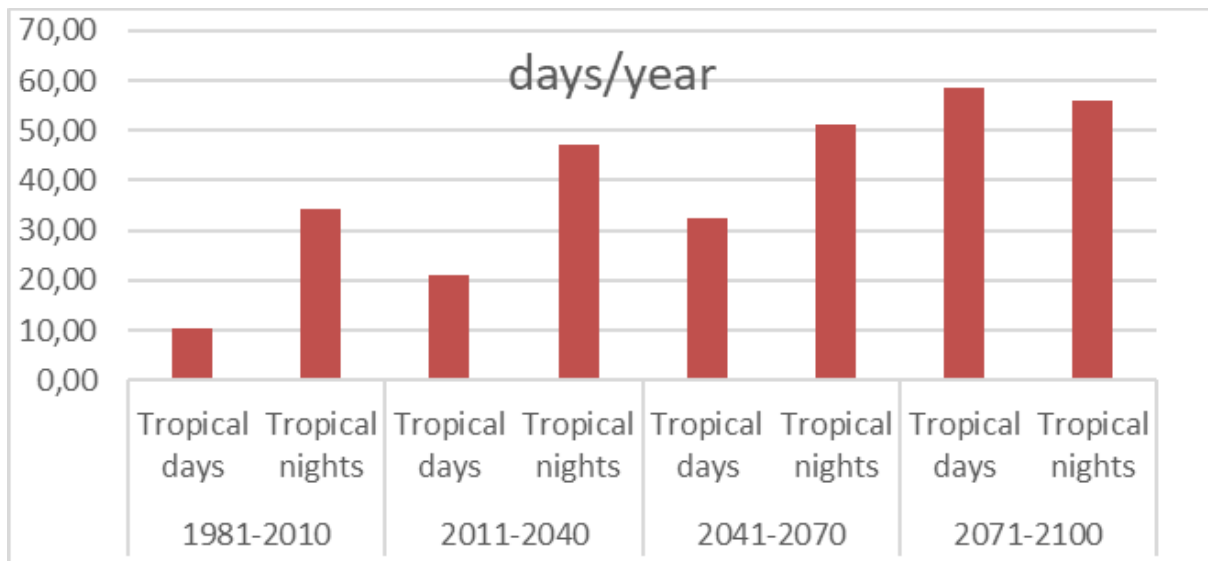


Figure 43. Graphical representation of the evolution of the tropical days and nights in Valencia. The graph represents the average number of tropical days/tropical nights per year for each of the periods studied.

6.7. Sea Level Rise and Floods in Hamburg

Hamburg city is strategically located along the powerful Elbe River. It is at a sheltered natural harbour on the southern fanning-out of the Jutland Peninsula. Several times in the past, hurricane-force winds have pushed strong storm surges up the channel, overwhelming the downstream flow of the Elbe river affecting those who live in Hamburg. It is foreseen that by the end of the century, extreme floods that once happened only every 100 years may occur annually along Europe’s northern coasts.

Therefore, the identification of extreme water level values is of relevance for flood-risk assessments (cf. D3.3 “City baseline report – Hamburg” and D3.2 “Local partnership and work plan for Hamburg”), as they not only point out the highest water-level one can expect in a specific location, but also how frequently one can expect such unusually high values. The frequency with which the extreme value can be expected is described by the return period. Therefore, the indicator can be defined as the total water level associated with a certain return period. There are two perspectives from which changes in extreme-value indicators can be viewed: an increase in the extreme value associated with a fixed return period or frequency, or an increase in the frequency (decrease of return period) of a given extreme water level value.

For this case study in Hamburg the Water level change indicators²⁶ dataset available at CDS was used (Figure 44). This dataset provides extreme-value, return period, and percentile indicators for coastal sea levels in specific locations of the European-wide domain. The indicators are computed from tidal dynamics, storm surge and sea level rise data based upon past observational data and future climate projections.

²⁶ <https://cds.climate.copernicus.eu/cdsapp#!/dataset/sis-water-level-change-indicators>



Figure 44. Location covered by the GTSM in the European Coast (Source [CDS](#))

It is important to note that to compute these indicators, the *Deltares Global Tide and Surge Model (GTSM) version 3.0* is used together with regional climate forcing and sea level rise initial conditions. The regional climate forcing employed is the HIRHAM5 model from the Danish Meteorological Institute (DMI), a member of the EURO-CORDEX climate model ensemble, which is downscaled from the global climate model EC-EARTH. In order to assess the impact of climate change, the GTSM model is run for three different climate scenarios:

- The present climate (labelled 'historical'),
- A reanalysis dataset is computed by forcing GTSM with ERA5 reanalysis. This provides recent historical water-levels that can be used to look at specific (extreme) events in the past.
- Two Representative Concentration Pathway (RCP) scenarios that correspond to an optimistic emission scenario where emissions start declining beyond 2040 (RCP4.5) and a pessimistic scenario where emissions continue to rise throughout the century often called the business-as-usual scenario (RCP8.5).

It is important to take into consideration that all projections provided by this dataset are based on a single combination of the regional and global climate models and therefore there is an inevitable underestimation of the uncertainty associated with this dataset.

The above datasets allow calculating the deltas based on the methodology explained in section 0 and graphically represented in Figure 24. Table 38 to Table 41 present the final outcomes provided by the CDS dataset for the station located at 53.84033, 8.898926, for the different future periods 2041-2070 and 2071-2100 linked to the two RCP scenarios that correspond to an optimistic emission scenario (RCP4.5) and a pessimistic scenario (RCP8.5).

Table 38. Total water level for different return periods for 2041-2070 - RCP8.5 at CDS Station.

Variable	CDS Station (53.84033, 8.898926) Deltares Global Tide and Surge Model (GTSM) statistics			
	Historical 1977-2005	Projections (2041-2070)	Delta (Absolute) RCP8.5-Historical	Delta (Relative) RCP8.5-Historical
Total water level for return period 2	468.01 cm	514.11 cm	46.1 cm	1.1
Total water level for return period 5	530.54 cm	568.42 cm	37.88 cm	1.07
Total water level for return period 10	571.94 cm	604.38 cm	32.44 cm	1.06
Total water level for return period 25	624.25 cm	649.82 cm	25.57 cm	1.04
Total water level for return period 50	663.06 cm	683.53 cm	20.47 cm	1.03
Total water level for return period 100	701.58 cm	716.98 cm	15.41 cm	1.02

Table 39. Total water level for different return periods for 2071-2100 - RCP8.5 at CDS Station.

Variable	CDS Station (53.84033, 8.898926) Deltares Global Tide and Surge Model (GTSM) statistics			
	Historical 1977- 2005	Projections (2071-2100)	Delta Absolute (Future- Historical)	Delta Relative (Future- Historical)
Total water level for return period 2	468.01 cm	504.41 cm	36.4 cm	1.08
Total water level for return period 5	530.54 cm	548.31 cm	17.78 cm	1.03
Total water level for return period 10	571.94 cm	577.38 cm	5.44 cm	1.01
Total water level for return period 25	624.25 cm	614.11 cm	-10.14 cm	0.98
Total water level for return period 50	663.06 cm	641.36 cm	-21.7 cm	0.97
Total water level for return period 100	701.58 cm	668.41 cm	-33.17 cm	0.95

Table 40. Tidal indicators for period 2041-2070 - RCP 8.5 provided at the CDS dataset station

Variable	CDS Station (53.84033, 8.898926) Deltares Global Tide and Surge Model (GTSM) statistics		
	Historical 1977-2005	Projections 2071-2100	Delta Absolute (Future - Historical)
Epoch-mean highest high water	217.18 cm	219.67 cm	2.49 cm
Epoch-mean lowest low water	-209.79 cm	-212.51 cm	-2.72 cm
Highest astronomical tide	255.18 cm	258.18 cm	3.0 cm
Lowest astronomical tide	-238.97 cm	-240.13 cm	-1.16 cm
Mean sea level	4.98 cm	24.26 cm	19.28 cm
Tidal range	426.97 cm	432.18 cm	5.21 cm

Table 41. Tidal indicators for period 2071-2100 - RCP 4.5 provided at the CDS dataset station

Variable	CDS Station (53.84033, 8.898926) Deltares Global Tide and Surge Model (GTSM) statistics		
	Historical 1977-2005	Projections 2071-2100	Delta Absolute (Future - Historical)
Epoch-mean highest high water	217.18 cm	220.44 cm	3.26 cm
Epoch-mean lowest low water	-209.79 cm	-213.43 cm	-3.64 cm
Highest astronomical tide	255.18 cm	259.44 cm	4.26 cm
Lowest astronomical tide	-238.97 cm	-240.32 cm	-1.35 cm
Mean sea level	4.98 cm	38.09 cm	33.11 cm
Tidal range	426.97 cm	433.87 cm	6.9 cm

Additionally, as pointed in Figure 44, the inland points along the Elbe River are not included and therefore it is also important to correlate the dataset outcomes with real data in other locations. This is the reason why we have also included in this case study additional historical records of the hydrographic curve of the Elbe at two different locations (see Figure 45) provided by the Hamburg Port Authority.



Figure 45. Stations along Elbe River considered in this case study

The files provided by the Port Authority contain two different information:

1. STP Thw Tnw 1977-2005.txt: Thw and Tnw peak values of the St. Pauli gauge from 1.1.1977 to 31.12.2005. In the file, the first number of each line refers to the hydrographical year, the second indicates the consecutive number of the Thw or Tnw in the respective hydrographical year. "H" stands for tidal high water (Thw), "N" for tidal low water (Tnw). This is followed by the date and time, whereby it should be noted that the time always refers to CET, i.e. summer time is not taken into account. The water level is given in cm gauge zero (PN), whereby the following applies for the entire period: PN = NN - 500 cm. The last characters in the lines describe any influences on the water level (e.g. by ice) and should not be relevant for you.
2. STP W 1993-2005.txt: This is the water level hydrograph of the St. Pauli gauge from 1.11.1992 to 31.12.2005 (10-minute values). Please also note here that the time refers to CET all year round and the water level is given in cm gauge zero (PN).

To model the distribution of the extreme values, it is used the Gumbel distribution over the annual maxima values for each epoch from which the annual maxima value for each station is computed for total water levels. This is done following the same approach done in the CDS dataset to compute the total water levels and storm surges.

These real observed values are then fitted to the Gumbel distribution to derive the parameters defining the function, which can in theory be evaluated for any given return period. See Table 42 and Table 43 with the values outcomes for each return period and scenario obtained from the CDS data and from the real observed records.

Afterwards the analysis of return periods for HAMBURG St. Pauli and CUXHAVEN has been done considering the observed measured historical records.

Table 42. ST. PAULI

Annual bases		
Return period (years)	Analytical Gumbel	Fit Gumbel
2	450.152	455.35
5	534.12	521.49
10	589.71	565.29
25	659.96	620.62
50	712.07	661.67
100	763.79	702.42

Table 43. CUXHAVEN-STEUBENHÖF

Annual bases		
Return period (years)	Analytical Gumbel	Fit Gumbel
2	194.47	333.81
5	270.16	393.99
10	320.27	433.83
25	383.59	484.17
50	430.56	521.51
100	477.19	558.58

The correlations factor between both stations has been done by trying to visualise it considering all the values from the historical records, where period 1978-1986 and 1997-2005 won't be the same, and by analysing the theoretical correlation factors considering the Gumbel distribution of each station (Figure 46 and Figure 47).

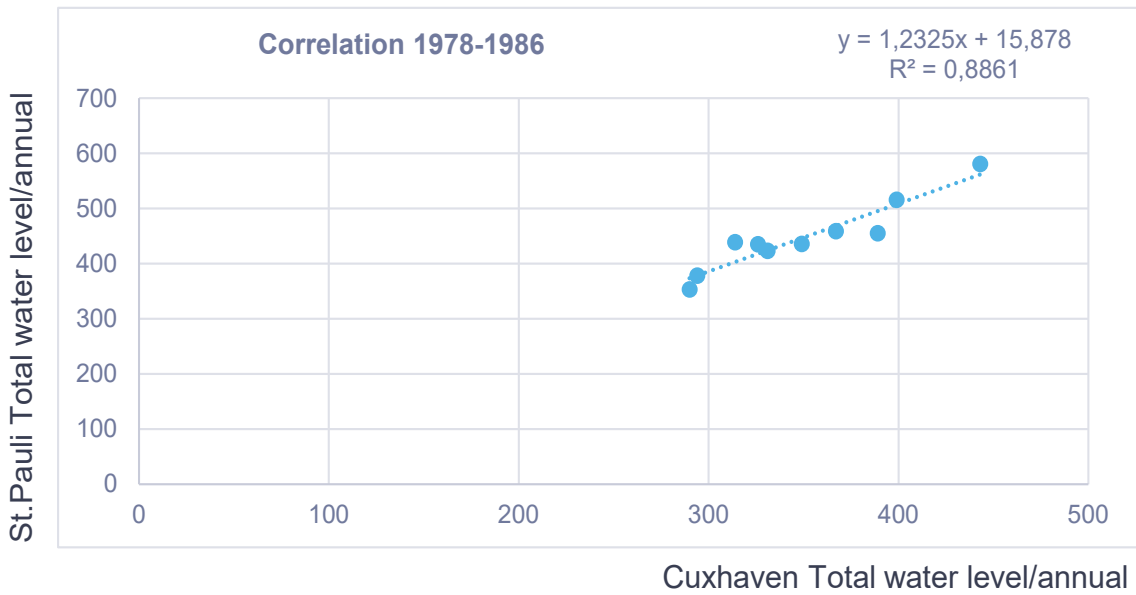


Figure 46. Average correlation factor= 1.28 (Standard deviation = 0.06)

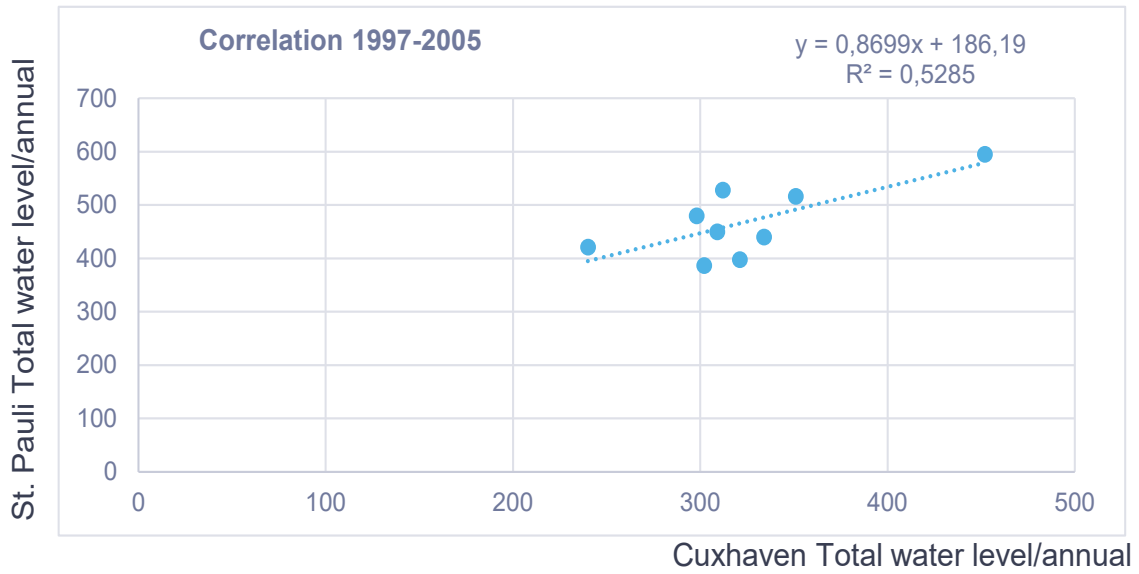


Figure 47. Average correlation factor= 1.36 (Standard deviation = 0.1)

Finally, considering Table 44, the total water levels projected for the different periods and scenarios have been calculated for Cuxhaven and St Pauli. Table 45 and Table 46 present these outcomes for Hamburg case study.

Table 44. Correlation factor between both stations considering the Gumble distribution outcomes per return period.

Return period (years)	St. Pauli station (1977 - 2005)	Cuxhaven station (1977 - 2005)	Correlation factor (St. Pauli / Cuxhaven)
2	455.35	333.81	1.36
5	521.49	393.99	1.32
10	565.29	433.83	1.3
25	620.62	484.17	1.28
50	661.67	521.51	1.27
100	702.42	558.58	1.26

Table 45. Total water levels projections for Cuxhaven

Future projections (RCP 8.5 2041-2070); Cuxhaven

Return period	ABSOLUTE DELTA	RELATIVE DELTA	Cuxhaven historical (1977 - 2005)	Cuxhaven projections (2041-2070)	Cuxhaven projections (2041-2070) (relative delta applied)
2	46,1 cm	1,1	333,81	379,92 cm	366,7 cm
5	37,88 cm	1,07	393,99	431,87 cm	422,12 cm
10	32,44 cm	1,06	433,83	466,27 cm	458,44 cm
25	25,57 cm	1,04	484,17	509,74 cm	504 cm
50	20,47 cm	1,03	521,51	541,98 cm	537,61 cm
100	15,41 cm	1,02	558,58	573,99 cm	570,85 cm

Future projections (RCP 4.5 2071-2100); Cuxhaven

Return period	ABSOLUTE DELTA	RELATIVE DELTA	Cuxhaven historical (1977 - 2005)	Cuxhaven projections (2071-2100)	Cuxhaven projections (2071-2100) (relative delta applied)
2	36,4 cm	1,08	333,81	370,22 cm	359,78 cm
5	17,78 cm	1,03	393,99	411,77 cm	407,19 cm
10	5,44 cm	1,01	433,83	439,27 cm	437,96 cm
25	-10,14 cm	0,98	484,17	474,03 cm	476,31 cm
50	-21,7 cm	0,97	521,51	499,82 cm	504,45 cm
100	-33,17 cm	0,95	558,58	525,41 cm	532,17 cm

Table 46. Total water levels projections for St. Pauli

Future projections (RCP 8.5 2041-2070); St. Pauli

Return period	ABSOLUTE DELTA	RELATIVE DELTA	Correlation factor (St. Pauli / Cuxhaven, HISTORICAL)	St. Pauli station (ABSOLUTE)	St. Pauli station (RELATIVE)
2	46,1 cm	1,1	1,36	518,23 cm	500,2 cm
5	37,88 cm	1,07	1,32	571,64 cm	558,73 cm
10	32,44 cm	1,06	1,3	607,56 cm	597,35 cm
25	25,57 cm	1,04	1,28	653,4 cm	646,04 cm
50	20,47 cm	1,03	1,27	687,64 cm	682,1 cm
100	15,41 cm	1,02	1,26	721,8 cm	717,85 cm

Future projections (RCP 4.5 2071-2100); St. Pauli

Return period	ABSOLUTE DELTA	RELATIVE DELTA	Correlation factor (St. Pauli / Cuxhaven, HISTORICAL)	St. Pauli station (ABSOLUTE)	St. Pauli station (RELATIVE DELTA)
2	36,4 cm	1,08	1,36	505 cm	490,76 cm
5	17,78 cm	1,03	1,32	545,02 cm	538,97 cm
10	5,44 cm	1,01	1,3	572,38 cm	570,67 cm
25	-10,14 cm	0,98	1,28	607,63 cm	610,55 cm
50	-21,7 cm	0,97	1,27	634,15 cm	640,02 cm
100	-33,17 cm	0,95	1,26	660,71 cm	669,21 cm

6.7.1. Elbe river- Hamburg Water level changes application in the Toolbox

Considering the above information and in order to facilitate a dialogue with stakeholders, a prototype application was developed in the Toolbox in order to show the possible outcomes to show the trends of these indicators for the station id available in the CDS dataset.

The applications²⁷ allows to select the different type of indicators (Table 47)

Table 47. Indicators available in the CDS dataset

Name	Unit	Description
Annual highest high water	m	Annual highest high tide including mean sea level and sea level rise. Storm surge caused by atmospheric forcing is not taken into account.
Annual lowest low water	m	Annual lowest low tide including mean sea level and sea level rise. Storm surge caused by atmospheric forcing is not taken into account.
Annual highest mean high water	m	Annual average of the highest high tide of each tidal day (24-hour window) including mean sea level and sea level rise. Storm surge caused by atmospheric forcing is not taken into account.
Annual lowest mean low water	m	Annual average of the lowest low tide of each tidal day (24-hour window) including mean sea level and sea level rise. Storm surge caused by atmospheric forcing is not taken into account.
Epoch-mean highest high water	m	Highest high tide of each tidal day (24-hour window), including mean sea level and sea level rise, averaged over the 30-year period simulated. Storm surge caused by atmospheric forcing is not taken into account.
Epoch-mean lowest low water	m	Lowest low tide of each tidal day (24-hour window), including mean sea level and sea level rise, averaged over the 30-year period simulated. Storm surge caused by atmospheric forcing is not taken into account.
Highest astronomical tide	m	Highest astronomical tide over the 30-year period simulated.
Lowest astronomical tide	m	Lowest astronomical tide over the 30-year period simulated.
Mean sea level	m	Mean sea level including sea level rise observed over the 30-year period simulated. Storm surge caused by atmospheric forcing is not taken into account.
Surge level for different percentiles	m	Storm surge level , defined as the difference between the pure tide and the total water level simulations , for the following percentiles: 10th, 25th, 50th, 75th and 90th.
Surge level for different return periods	m	Storm surge level , defined as the difference between the pure tide and the total water level simulations, for the following return periods: 2, 5, 10, 25, 50 and 100 years. The return period is a standard way of describing the likelihood and severity of an event. It describes the estimated time interval between events of a similar size or intensity.
Tidal range	m	Average tidal range observed over the 30-year period simulated.
Total water level for different percentiles	m	Total water level , including the pure tide and storm surge level , for the following percentiles: 10th, 25th, 50th, 75th and 90th.
Total water level for different return periods	m	Total water level, including tide, surge level and taking future sea level rise into account , for the following return periods: 2, 5, 10, 25, 50 and 100 years. The return period is a standard way of describing the likelihood and severity of an event. It describes the estimated time interval between events of a similar size or intensity.

²⁷ <https://cds.climate.copernicus.eu/toolbox-editor/2851/arch-waterlevels-elb-hamburg>

The application shows different outcomes: firstly it allows to plot the values of the indicators (Figure 48) belonging to the first category (Annual highest high water, Annual lowest low water, Annual mean highest high water, Annual mean lowest low water) for the historical, reanalysis as well as for the two future projections linked to 2041-2070 and 2071-2100. These are time-dependent indicators (with 29 values per station) also include effects of sea level rise. In this way, these series give additional temporal information, not contained in the next tidal indicators, about the evolution of the tidal levels over time.

For the rest of indicators, the applications allow to select from the drop-down menu and to compare historical values of the indicators as well as the future projections and the changes for each return period (Figure 49).

Elb river- Hamburg Water level changes

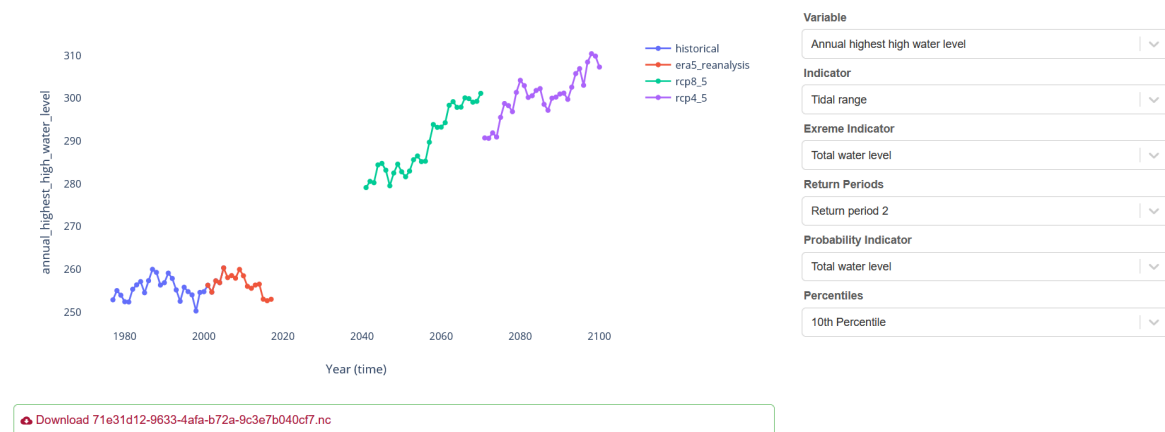


Figure 48. Toolbox application for Hamburg case study

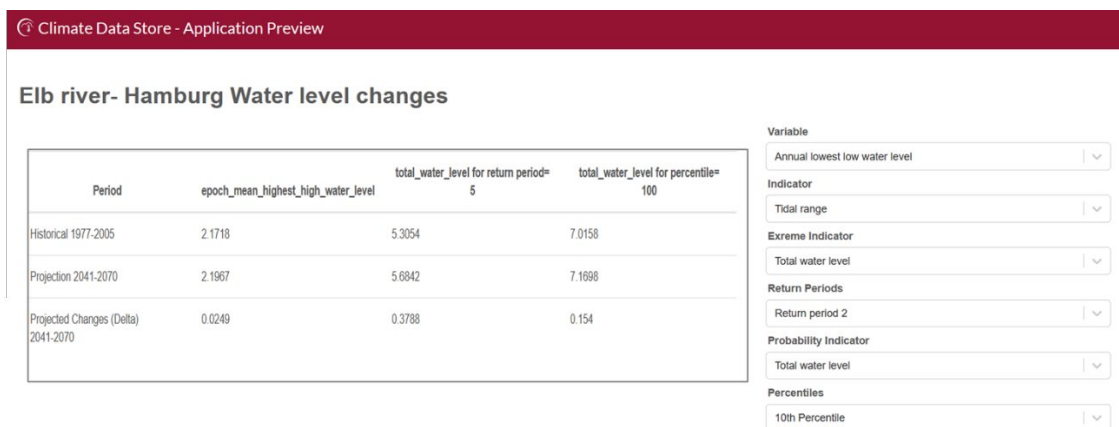


Figure 49. Toolbox application for Hamburg case study (II)

6.8. Climate services for Camerino

In order to assess effect of the climate change on the material degradation, as discussed with the partner city of Camerino (cf. D3.3 “City baseline report – Camerino” and D3.2 “Local partnership and work plan for Camerino”), specific climate services were developed.

We considered climate projection data for 7 combinations of GCM and RCM among those made available from the CORDEX²⁸. In particular, data related to the EUR-11 domain (i.e., at 0.11° grid spacing, ~ 12.5 Km) referring to the years 1986-2005 and to the Representative Concentration Pathway 8.5 (RCP8.5) scenario, which represents the future evolution of the greenhouse gas atmospheric emissions and concentrations without any mitigation policy, were downloaded from the website <https://esgf-data.dkrz.de/search/cordex-dkrz/>. Indeed, the worst-case scenario (RCP8.5) was considered the most suitable for these climate services. Other climate change scenarios (RCP4.5 and RCP2.6) representing a reduced forcing of greenhouse gases, due to the successful implementation of mitigation strategies have not been considered in the present stage because of the limited resources available.

The GCM and RCM models, included in the ensemble utilized within this work, are reported in Table 48. In particular, as suggested for climate change impact or adaptation studies, risk assessment and other analyses requiring climate projections at a regional or local scale, bias-adjusted data were used. Specifically, the RCM model data utilized are the daily bias-adjusted maximum and minimum temperature and precipitation over the European continental area.

Table 48. EURO-CORDEX Regional Climate Models considered for the climate services related to Camerino, along with the respective forcing Global Climate Models

Global Climate Model (GCM)	EURO-CORDEX Regional Climate Model (RCM)	Institution	References
MPI-M-MPI-ESM	REMO2009	Helmholtz-Zentrum Geesthacht, Climate Service Center, Max-Planck Institute for Meteorology	Jacob et al (2001) [32]
MPI-M-MPI-ESM ICHEC-EC-EARTH	RCA4	Swedish Meteorological and Hydrological Institute	Samuelsson et al (2011) [33]
MPI-M-MPI-ESM	CCLM4-8-17	Climate Limited-area Modelling Community	Rockel et al (2008) [34]
ICHEC-EC-EARTH	HIRHAM5	Danish Meteorological Institute Koninklijk Nederlands	Christensen et al (2007) [35]
ICHEC-EC-EARTH	RACMO22	Koninklijk Nederlands Meteorologisch Instituut	Van Meijgaard et al (2008) [36]
CNRM-CERFACS	CNRM-ARPEGE5.1	Center National de Recherches Meteorologiques, France	Deque M. (2010) [37]

²⁸ Coordinated Regional Climate Downscaling Experiment: <https://cordex.org/>

6.8.1. Multi-model ensemble building

To perform a robust assessment of the projected changes of the precipitation and temperature a EURO-CORDEX multi-model ensemble (MME) was built as follow. In order to assess the performance of the different RCMs a qualitative and quantitative evaluation of temperature and precipitation resulting from the EURO-CORDEX RCMs was performed by comparing these data against the “quasi-observational data” provided by the ERA5 Reanalysis. To this aim, for the 3 variables of interest, namely the daily maximum, minimum Temperature (TX, TN) and total precipitation (RR) the annual mean and standard deviation of single RCM and MME as well as ERA5 observational data were computed for each grid point. These data were then compared using a set of statistical metrics, such as bias, spatial correlation, and the Pearson correlation. A good correlation between EURO-CORDEX model data and the quasi-observational ERA5 data was observed. Also, such a comparison showed that the EURO-CORDEX MME outperforms most of the individual RCMs, giving confidence to us to perform the climate change hazard assessment in this study using the MME (Table 49). Therefore, the TX, TN and RR MME of future climate projections (2031-2100) are expected to provide a robust long-term scenario for climate change hazards evaluation.

Table 49. Correlation between 1986-2005 means and standard deviations of daily precipitation (RR) and maximum temperature (TX) data of single models and MME and ERA5 reanalysis data

	CORDEX MME	RCA4	CCLM4	HIRLAM5	RACMO22	REMO2015
RR-mean	0.96	0.95	0.93	0.96	0.87	0.94
RR-std	0.87	0.81	0.86	0.71	0.87	0.75
TX-mean	0.99	0.97	0.98	0.98	0.98	0.98
TX-std	0.96	0.95	0.93	0.96	0.96	0.94

6.8.2. Indices of climate change

The World Meteorological Organization (WMO) implemented the Global Framework for Climate Services (GFCS), with the intent to “enable better management of the risks of climate variability and change and adaptation to climate change, through the development and incorporation of science-based climate information and prediction into planning, policy and practice on the global, regional and national scale”. The WMO Commission for Climatology (CCI) established an Expert Team on Sector-specific Climate Indices (ET-SCI), to contribute to this goal. The ET-SCI has developed a number of climate indices for use in sector applications. The *ClimPACT* software was developed to calculate 27 indices based on daily maximum and minimum temperature and daily precipitation²⁹.

The ARCH project goals require indices focusing on climate extremes related to possible risks for cultural heritage. The *ClimPACT* indices herein utilized measures the *annual maxima or minima of daily temperature or maximum amount of daily precipitation*. These types of

²⁹ The definition of the indices is available at: https://github.com/ARCCSS-extremes/climpact/blob/master/www/user_guide/Climpact_user_guide.md#appendixa.

extremes indices have been widely used in engineering applications to infer design values for engineering structures. Another type of index involves the calculation of the number of days in a year exceeding specific thresholds that have fixed values or thresholds that are relative to a base period climate. Some other indices are defined to measure periods of dryness, wetness, heat or cold, or periods of mildness as in the case of growing season length periods.

We calculated series of annual indices for the 70 years spanning from 2031 to 2100 and then analysed them according to a linear regression model. The linear regression model provides an estimate of the trend (slope of the linear regression line) and the statistical confidence of the trend (p-value). The two parameters are assumed as indicators of change for following impact and risk analysis.

In addition, to *ClimPACT* Indices the Freeze-Thaw Cycle Index was also implemented to address the specific hazard of this process on Cultural Heritage.

6.8.2.1. Freeze-Thaw cycles

This indicator is related to the deterioration of the outdoor cultural heritage due to the following deterioration processes. During freezing, water held in porous materials increases in volume, causing internal stress [38]. Although the freezing–thawing mechanism is projected to occur less frequently under climate change for most of Europe ([38]-[44]), it could increase in some regions. In the far North of Europe, a warmer climate would allow temperatures to oscillate above and below the freezing point, endangering porous materials in archaeological sites and historical buildings ([38],[41],[45],[46]). As a result of the increasing of minimum temperature in Camerino as well as in the entire European continent the number of Frost-Thaw cycles shows a decline. The hazard as well as the associated impact and risks should therefore be significantly reduced (Figure 50)

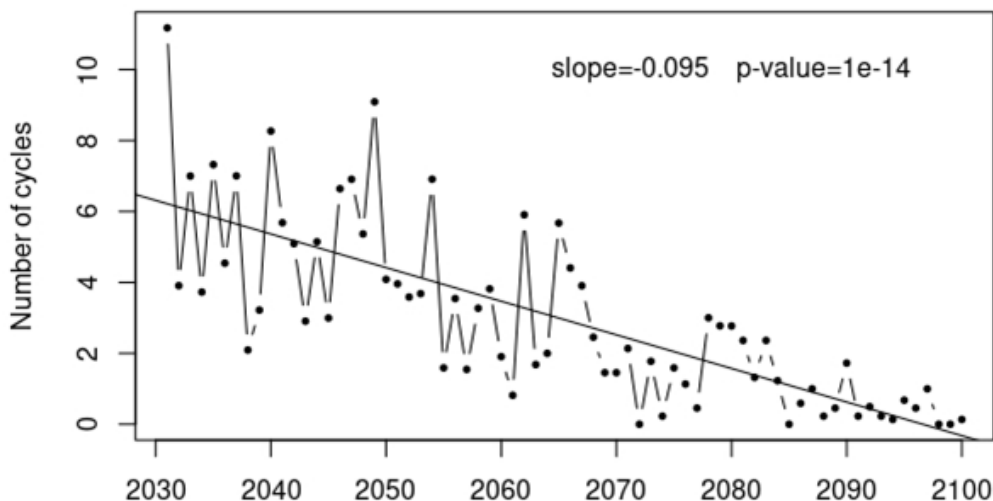


Figure 50. Trend of yearly number of Freeze Thaw cycles in Camerino (2031-2100).

6.8.2.2. Thermoclastism

Another process associated to changing temperature which can negatively affect cultural heritage materials is thermoclastism. Thermoclastism results from expansion and contraction of surface mineral grains due to thermal variations caused by seasonal variations and diurnal

changes in air temperature and direct insolation [47], and can lead to micro-cracking and exfoliation of stones as well as erosion of building material surfaces [38]. The proxy hazard indicator associated to thermoclastism is the daily temperature range (TX-TN) which is projected to increase in Camerino as well as in all the Mediterranean region. As shown in the Figure 61 and Figure 52, the trends of the yearly mean and the extreme daily temperature ranges are both statistically significant and therefore the impact of thermoclastism is expected to increase in the worst-case scenario RCP8.5.

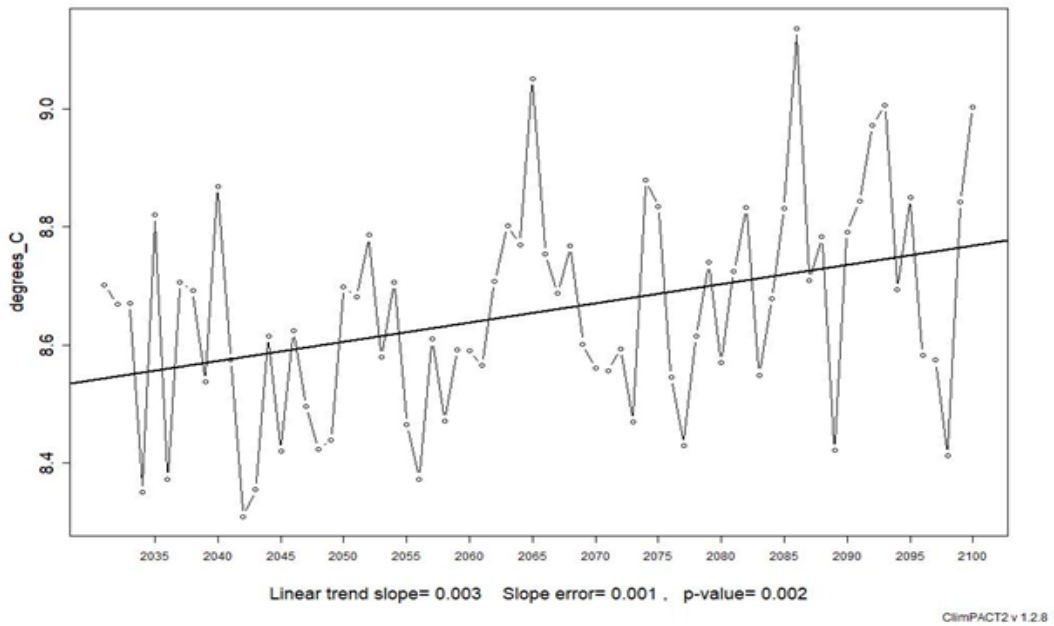


Figure 51. Trend of mean annual daily temperature range (2031-2100)

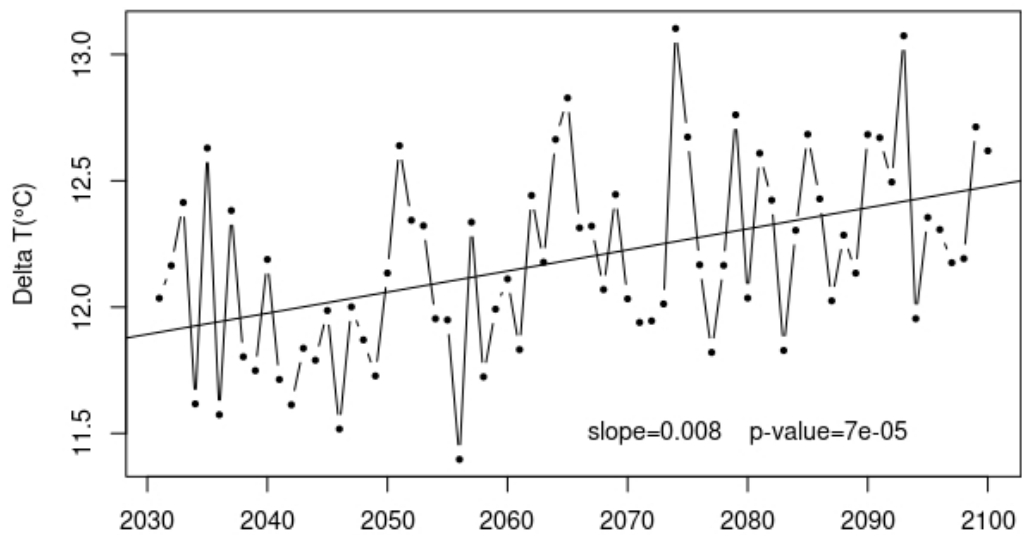


Figure 52. Trend of extreme (95° percentile) daily temperature range for Camerino (2031-2100)

6.8.2.3. Precipitation-related indicators

Water is the most important decay factor for all buildings and especially the historic environment [45]. An increase in precipitation under climate change could lead to saturation of

soils and overloading of gutters and downpipes, and hence a higher risk of damp penetration in historical materials, including masonry walls [48]. The penetration of water into porous materials can also result from condensation as well as from capillary action in the presence of soil moisture. Water ingress promotes material degradation through corrosion, biological activity, and sub florescence due to salt crystallization ([38], [45],[49]). Precipitation change projections are uncertain as also verified by the validation of model simulation against observations. This validation, made assuming ERA5 reanalysis as observational truth and not shown in this report, confirms a lower capability of models to simulate precipitation. Considering the limitation of model projections, three indicators were selected:

- total annual precipitation (RR);
- percent of extreme precipitations (R99pTOT);
- number of events of precipitation above the threshold of 20 mm (RR20).

The trends of the indicators are not statistically significant (Figure 53 - Figure 55) therefore no inference can be made at this stage regarding the change of precipitation-related climate hazard in Camerino.

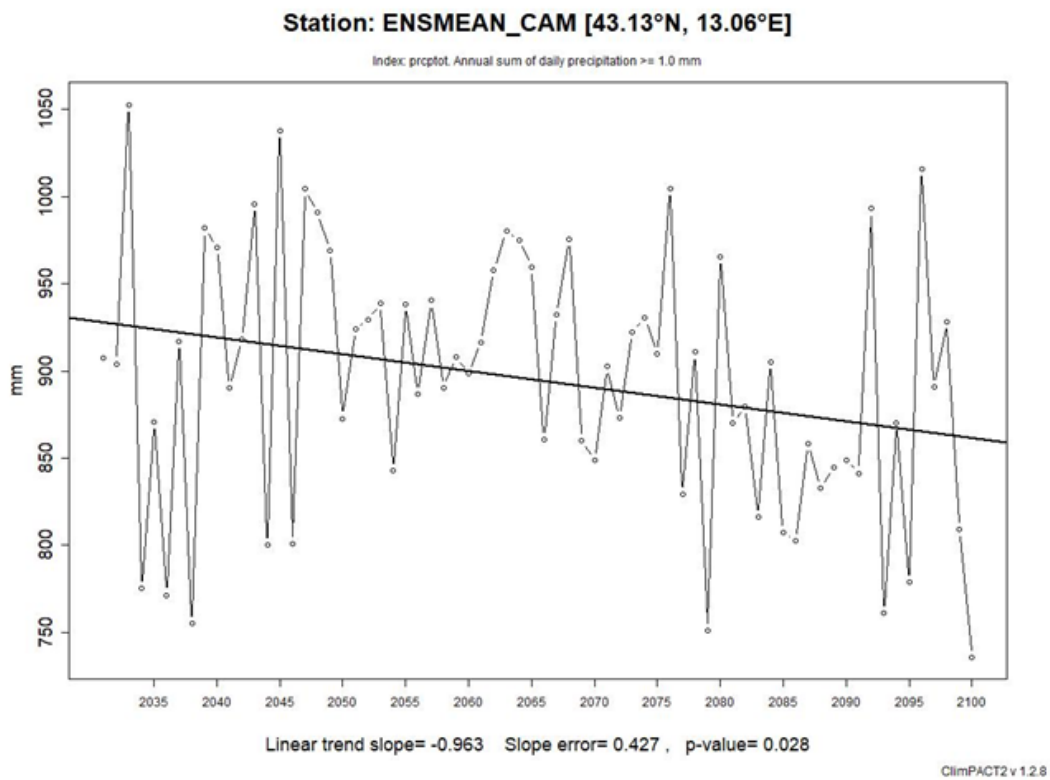


Figure 53. Trend of total annual precipitation (2031-2100)

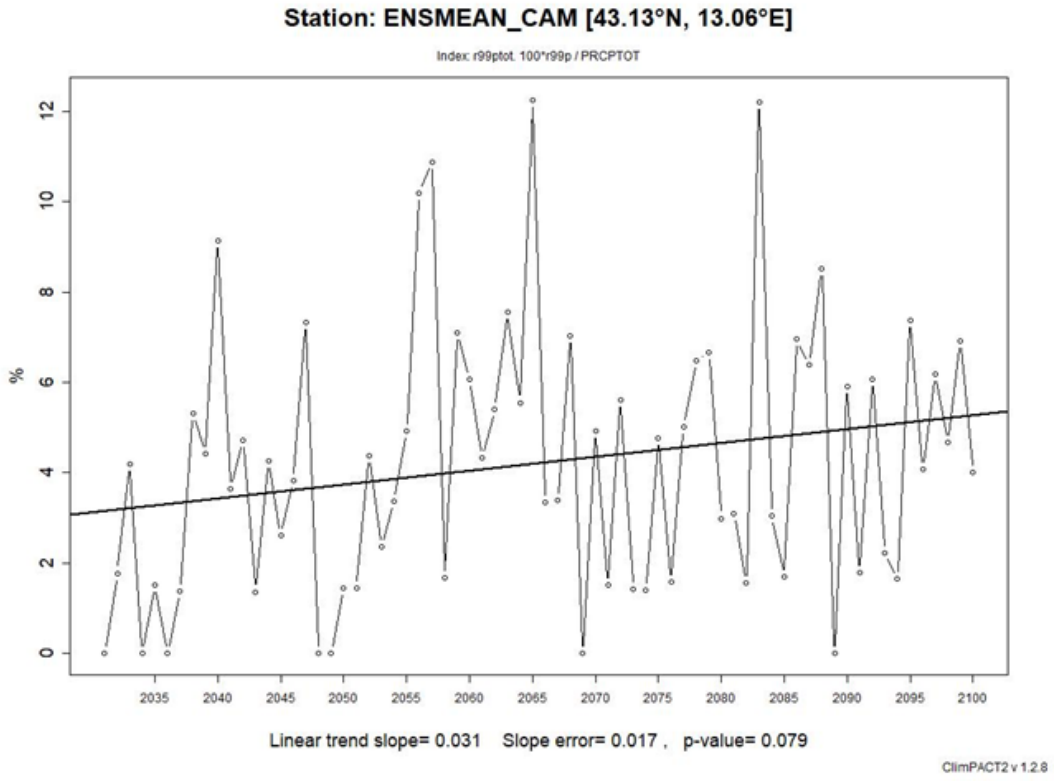


Figure 54. Trend of the percentage of total annual precipitation due to extreme precipitation (99th percentile of annual daily precipitation) (2031-2100). Trend statistically non-significant.

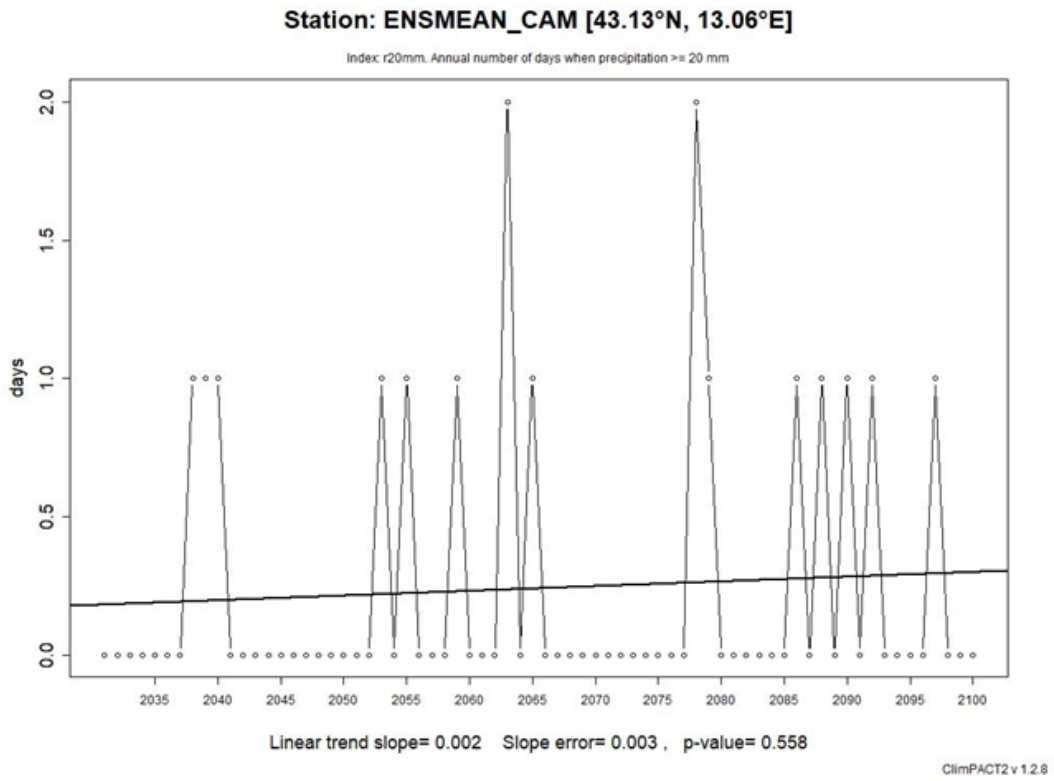


Figure 55. Trend of the yearly number of precipitation events exceeding the threshold of 20 mm.

6.8.2.4. Droughts and extreme heat

Droughts together with extreme heat can increase the risk of ignition of fires and their propagation ([38], [45]). In Europe, Sabbioni et al. (2010) [38] predicted an increase in cultural heritage exposure to fire for the Iberian Peninsula. According to the European Forest Fire Information System, the climate across almost all of Europe is projected to change toward conditions more favourable toward the occurrence of fire.

Fire causes material loss and deformation of cultural heritage assets, and may also increase the probability of cracking or splitting in built structures [50]. Under extreme heat, stones can face both macro (e.g., cracking of stones, soot accumulation, colour change in stone containing iron) and micro (e.g., mineralogical and textural changes) degradation processes, leading to potential structural instability. The long-term impacts include weakened stones and increased susceptibility to other deterioration processes such as salt weathering and temperature cycling. Furthermore, drought conditions will lead to desiccation of soil as well as structural implications for the foundations of historical buildings and archaeological sites [51].

Drought, as represented by the Standardized Precipitation Evaporation Index (Figure 56), and daily maximum temperature (Figure 57 and Figure 58) projections in Camerino indicate an increase of the above-mentioned risks.

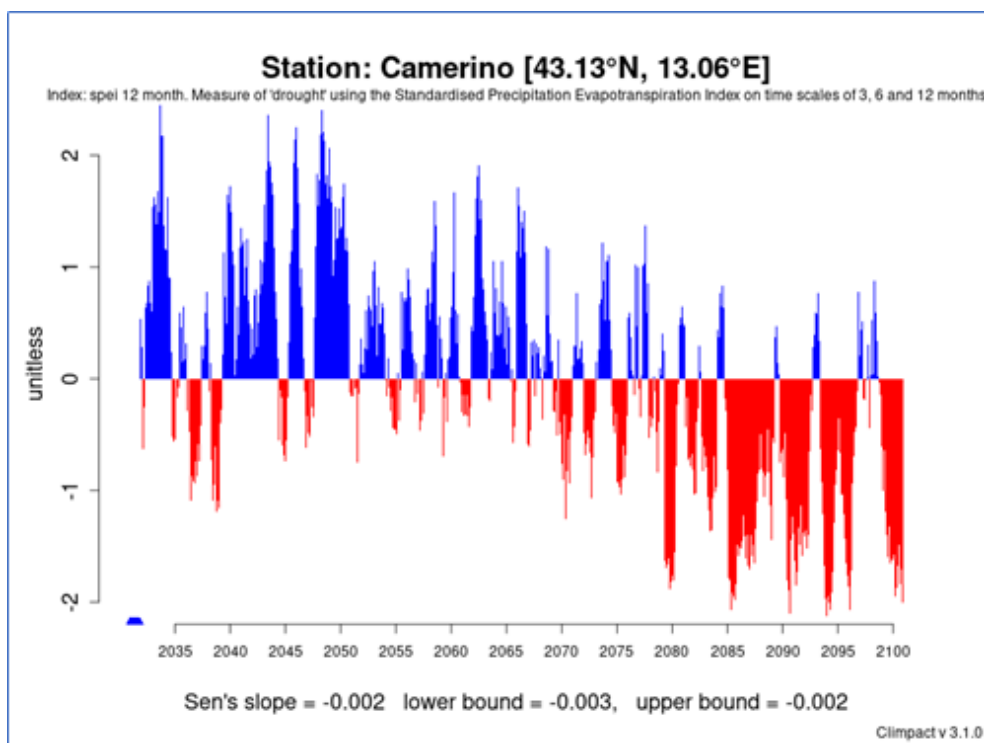


Figure 56. Standardized Precipitation Evaporation Index for Camerino.

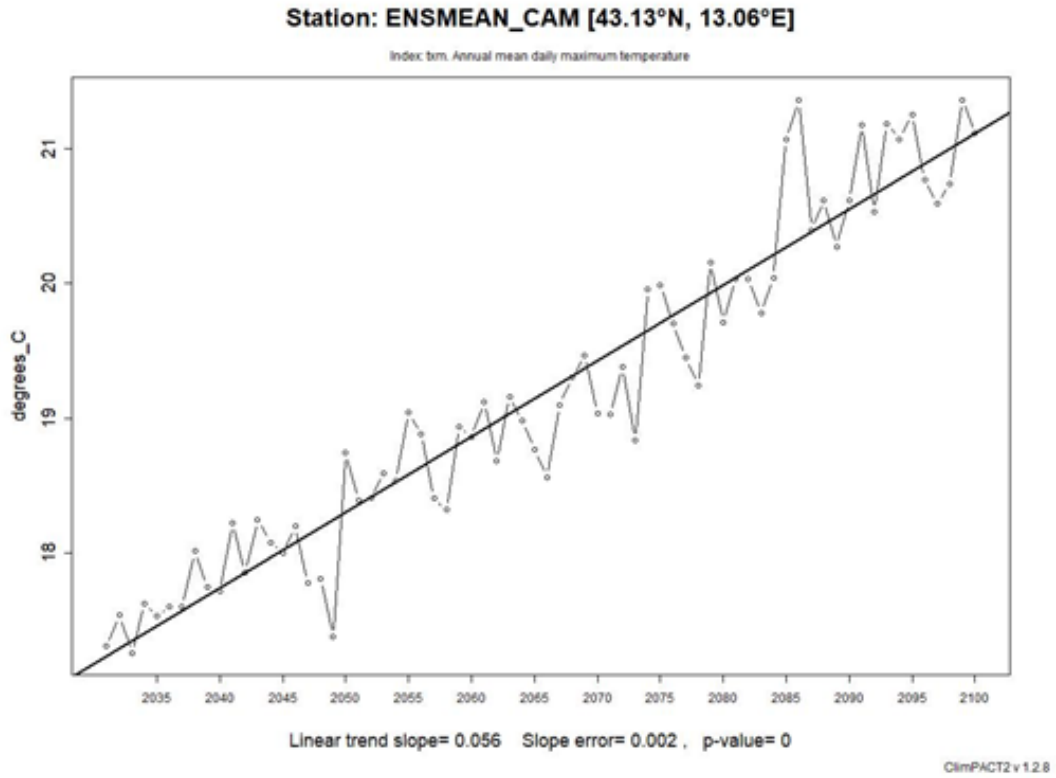


Figure 57. Trend of annual mean of daily maximum temperature. Trend statistically significant.

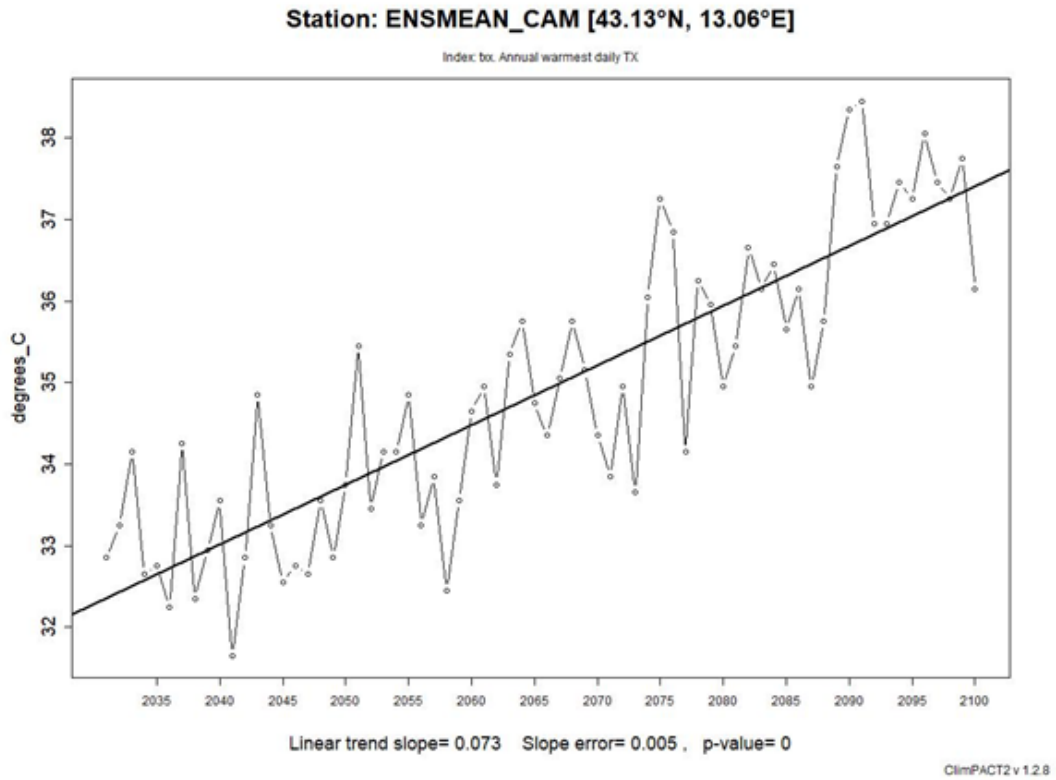


Figure 58. Trend of annual maximum daily maximum temperature. Trend statistically significant.

7. Web-dashboards and operational guide in THIS

To make the data and information accessible to the user, specific web-tools were designed by INGV. In particular, as already described in previous ARCH deliverables (e.g. D4.2 [3] and D7.5 [4]) and graphically reported in Figure 2, three tools have been developed:

- **GIS Dashboards** enable users to obtain information by location-based analytics, using intuitive and interactive data and maps to be viewed on a single screen.
- **Building/Object Sheets** to query and visualise structured data included in the databases, for example providing information about assets and objects in the historic areas; these web-sheets will be used also for editing and data entry performed by authorised users.
- **3D model viewer** to visualise the three-dimensional models of assets and objects, also enabling users to extract a subset of three-dimensional data.

The web tools are integrated into the same platform to show data in both HARIS and THIS. In particular, GIS dashboards have been developed to access the main datasets described in this document, and others included in the ARCH database and repository (eg satellite products) and already described in D4.1 [2].

The overall design of the dashboards for THIS followed the criteria, already introduced in D4.2 [1] for HARIS, i.e. easy-to-use by non-expert users (and users not familiar with GIS applications) and easy understanding of the data representation, also providing links for further information where necessary.

7.1. How to access information systems

In this section, the dashboards developed for THIS (version v1.2021) are presented and a quick user manual is illustrated. Currently, the landing page of the information systems (Figure 59) can be reached at the web link <http://www.cs.ingv.it/ARCHPortal/>.

The access way to the web-platform, as reported in this document, is the same as that already described in D4.2 [3].

After clicking on the button at the top right in the landing page, the user can login (Figure 60), if registered, otherwise she\he can request the registration of a new account (Figure 61), that will be managed by INGV before granting it. This control process is necessary as the authorised user has access to all functionalities; with the possibility also of modifying information concerning the assets of her\his own historic area. However, the unregistered user can have access in consultation mode to all public information contained in the systems.

Currently, all information in THIS is available without registration.

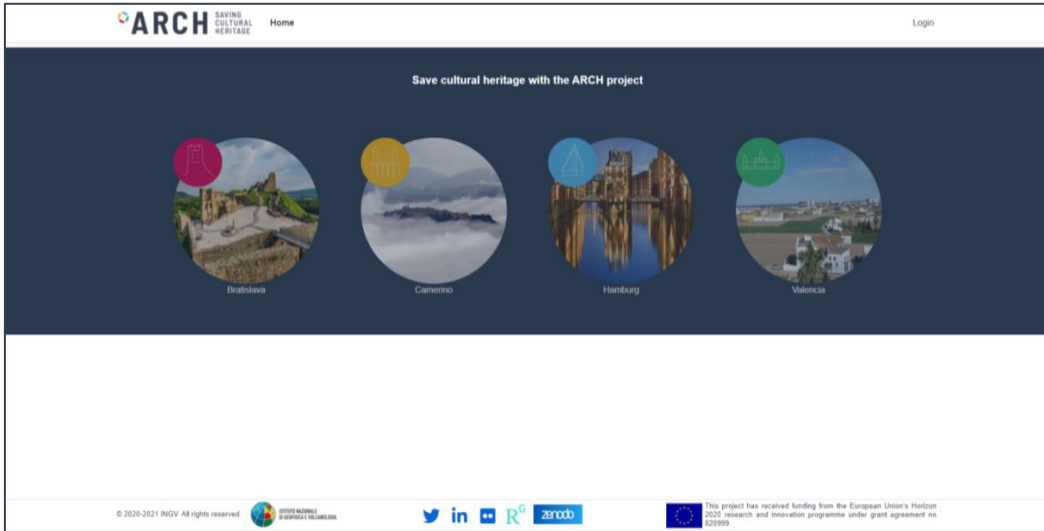


Figure 59. Landing page of the Information System platform

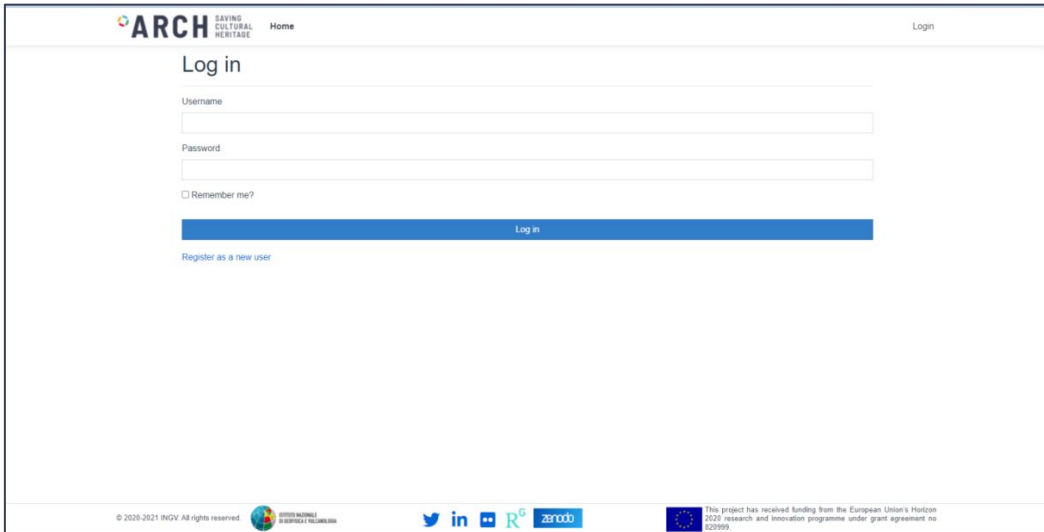


Figure 60. Login to the information systems



Figure 61. Registration of new account

In the landing page, the image of the city lights up when the mouse pointer is positioned over it and, at this point, the corresponding GIS dashboard (Figure 62) is loaded with a simple click. Once this new page has been loaded, a menu in the header (1 in Figure 62) allows accessing to the tools of the information platform, always remaining available so that the user can easily change her\his choice. This menu reports the follow link:

- “Home” to return to the landing page and choose another city;
- “GIS dashboard” to obtain the tool to query the cartographic layers both in HARIS (cf. section 4.2 in D4.2 [1]) and THIS (cf. Sections 7.2 - 7.7 below);
- “Construction\Object Sheet” to consult the information on the assets (cf. section 4.3 in D4.2 [1]);
- “Geocatalog” to browse and search metadata and link related to GIS web-services and datasets in HARIS and THIS. This functionality is being developing in Task 4.4 and will be described in D4.4 “Knowledge information management system for decision support”, including how services and data can be reached by other systems.

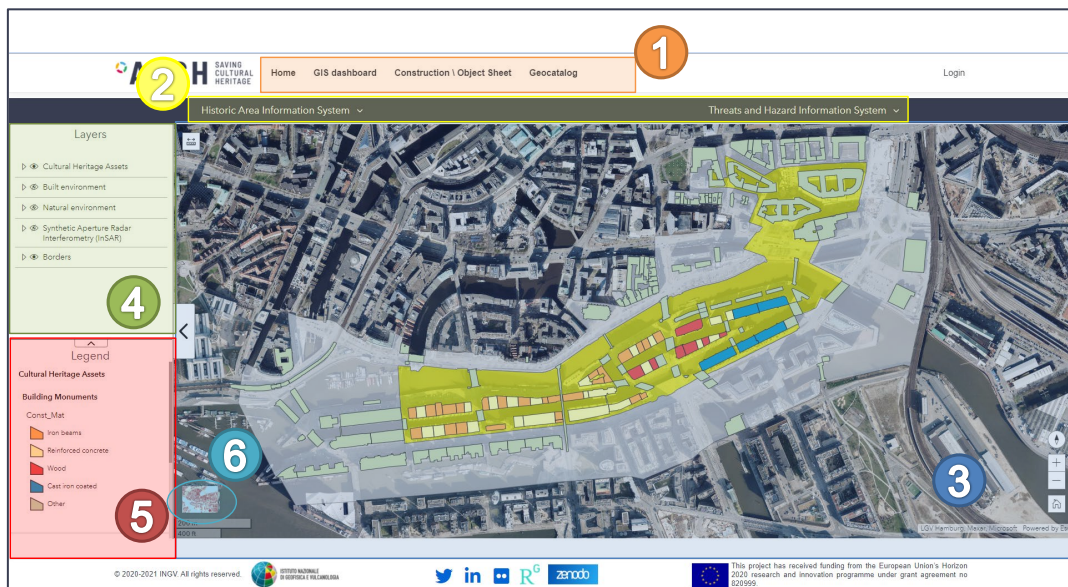


Figure 62. GIS dashboard of HARIS (example for the case of Hamburg) by D4.2 that appears when the city is selected by the landing page. From this page the THIS dashboards can be reached by clicking on Threats and Hazard Information System in menu 2

The two drop-down menus (2 in Figure 62) can be used to choose the different products related to HARIS and THIS. In particular, by clicking on Threats and Hazard Information System some links are available (depending on the selected city) to reach the following dashboards:

- **Earthquake monitoring service** (only for Camerino)
- **Air quality**
- **Historical climate**
- **Environmental parameters**
- **Climate services** (for Bratislava, Valencia and Hamburg)
- **Satellite products - SAR** (for Hamburg and Valencia) and thermal maps (for Bratislava and Valencia)

7.2. Earthquake monitoring service

Figure 63 shows the dashboard related to the earthquake monitoring service that can be used to query the information related to the earthquake monitoring (cf. Section 3.1).

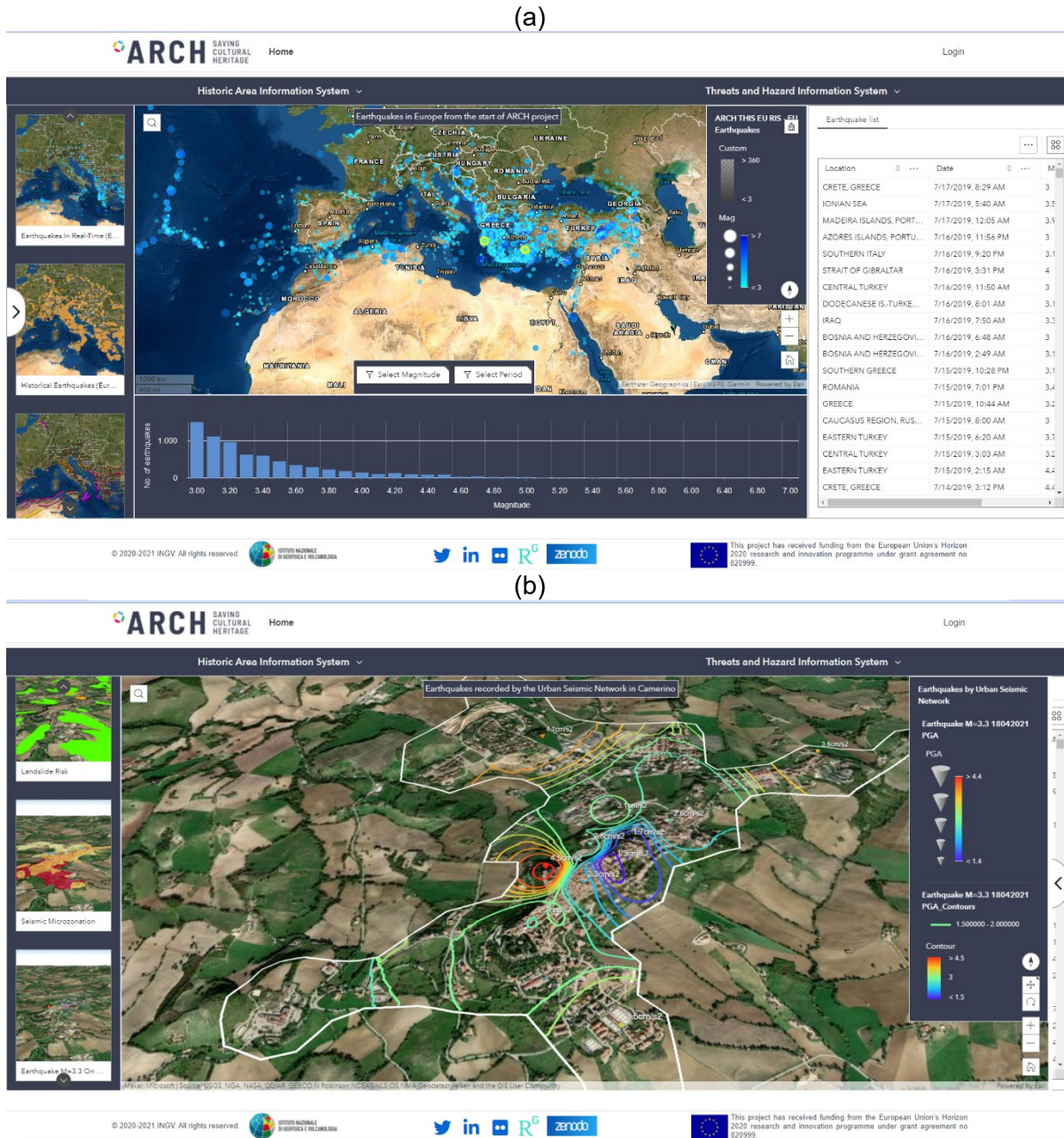


Figure 63. Seismic service dashboard: earthquakes occurred in near real-time, historical earthquakes and seismogenic sources (a); ground motion parameters related to the earthquakes that occurred near Camerino (b).

In the main page of the dashboard (Figure 63.a) the current situation in Europe is available by means of:

- a map where epicenters are plotted, and clicking on a specific earthquake details and external link can be obtained through the pop-up;

- a chart below that summarizes the number of earthquakes on the map grouped by magnitude;
- a table on the right side with the list of the earthquakes for a specific selection, with a menu that allows to show/clear selection, show/hide columns, export the selected element directly in CSV, JSON or GeoJSON format and highlight the selected earthquakes on the map.

In addition, two buttons in the map allow defining a specific period and a magnitude range to filter the entire dataset. Instead, the information about historical earthquakes, seismogenic sources and seismic hazard can be plotted using the scrolling menu on the left side of the dashboard.

The information provided by the recordings of the RUSN (cf. Section 3.1) and local information on the Camerino historic area can be obtained through the arrow button on the left side. The new map frame allows to display:

- the location of the RUSN stations;
- the local geological setting (modified by [52]);
- the landslide risk³⁰;
- the seismic microzonation [52];
- the recorded parameters of the ground motion (cf. Section 3.1).

All the local information can be easily viewed using the scrolling menu on the left side. In particular, Figure 63.b shows the PGA values and the contours obtained by processing the time-histories recorded during the low-energy earthquake, that occurred near Camerino on 18th April 2021 (cf. Section 3.2) about two months after the installation of the RUSN.

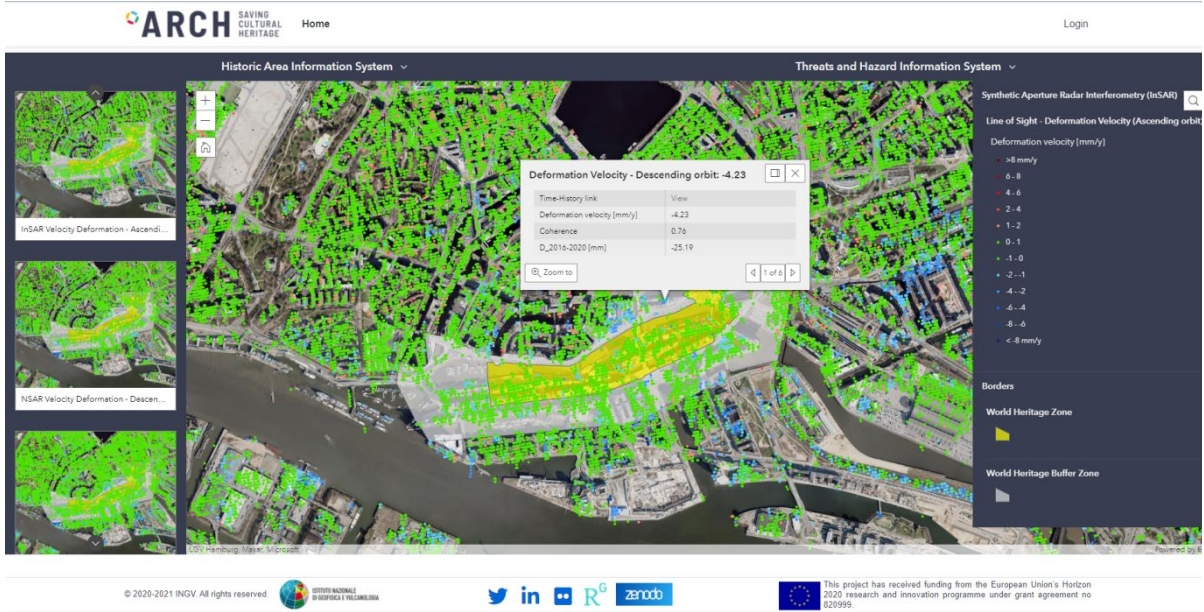
7.3. Satellite products

Figure 64 shows the dashboard related to the satellite products that were obtained by the processing of the satellite datasets as described in the Section 5.1 and 5.2 of the D4.1[2]. In particular, deformation velocities obtained by InSAR technique and temperatures from thermal images, as well as the potential UHIs, are made available to the users.

The scrolling menu on the left allows selecting the available results for the city: deformation velocity (Figure 64.a) and/or thermal map (Figure 64.b). On the right, the legend explains the information relating to the layers drawn in the map. Furthermore, clicking on a measurement point in the InSAR map the pop-up opens with the summary values and the Time-History link. The latter allows to reach the time-history of the relative displacement between the satellite sensor and the measurement point along the Line Of Sight (LOS), in fact the chart opens in a new window (Figure 65).

(a)

³⁰ Available at: <https://www.regione.marche.it/Regione-Utile/Paesaggio-Territorio-Urbanistica-Genio-Civile/Piano-assetto-idrogeologico>



(b)



Figure 64. Satellite products dashboard to show the InSAR deformation velocity map (a) and thermal map (a), as provided by processing described in D4.1 [10].

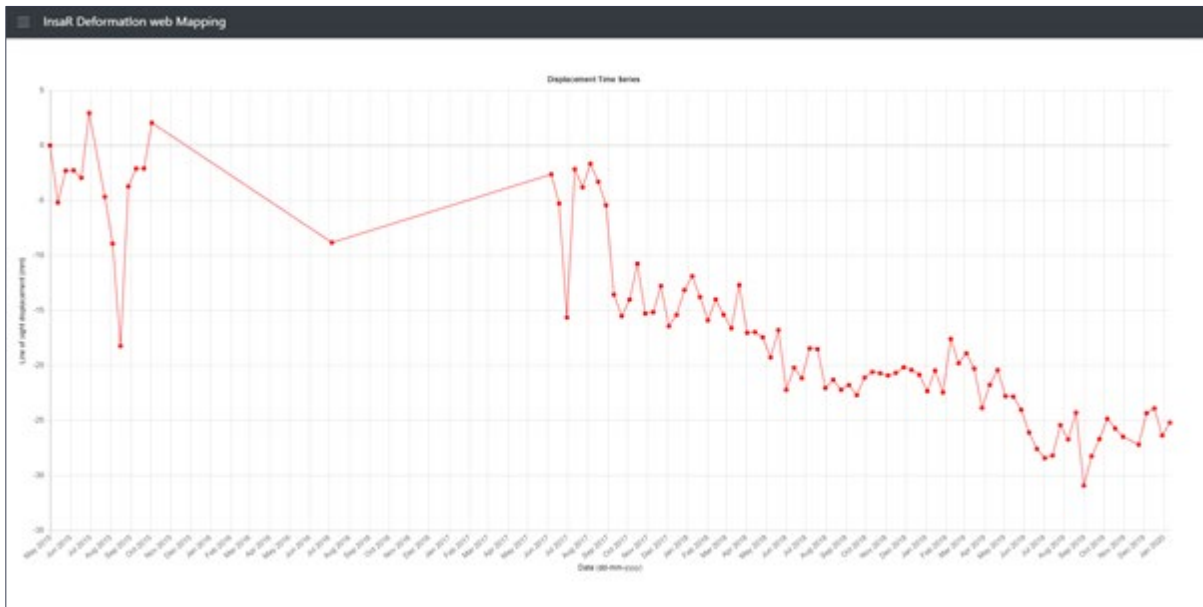


Figure 65. Displacement time-history by InSAR technique calculated along the LOS.

7.4. Air quality

Figure 66 shows the dashboard designed in the information system GIS platform in order to provide information in near-real time on the air quality in or close the HAs. Information on the data structure, ARCH services and data providers can be found in Section 4.1 of this document and in Section 2.3 of D4.1 [2].



Figure 66. Air quality dashboard to show the measures related to the pollutants in (and around) the historic areas, with values updated during the day and the trend of the last few days.

The information displayed on the dashboard can be managed by means of the drop-down menu on the left side, where the user can select:

- One or more recording station(s) shown on the map
- The pollutant measured by EEA local monitoring, that will be shown in the chart “EEA ground sensors” on the bottom side
- The pollutant measured by CAMS satellite monitoring, that will be shown in the chart “CAMS satellite sensors” on the bottom side
- The links to reach the official site of the data providers

A quick guide is also provided directly in the dashboard to inform the user.

The choices made through the previous menu have the effects on:

- the central map, with a zoom on the positions of the selected stations;
- the chart below, in fact trend(s) in the last days is displayed both for “Trend by EEA ground sensors” and “CAMS satellite sensors”;
- the indicators on the right, which indicate the maximum values of PM₁₀, NO₂, O₃ and SO₂ on the last 24-hours

Finally, on the map panel the user can choice:

- the map with the location of the official recording stations and the measurement points provided by the open platforms based on the crowd-sensing (cf. Section 2.3 of D4.1 [2]);
- the map with the current situation on the European zone provided by CAMS services, in this case the pollutant can be selected directly from layer tool on the map.

The user can enlarge the time scale simply by interacting with the bar on the chart. Moreover, each panel in the dashboard can be resized or open in full screen directly by the user.

7.5. Real-Time Environment parameters

Figure 67 shows the environmental parameters dashboard that allows visualising the parameters on the last hour available in ARCH database: temperature, relative humidity, pressure, rain, wind and gust. The measures can be plotted on the map through the scrolling menu on the left side. Instead, on the right side the measures on the last 7 days are available in a table, with the possibility to filter dataset for a specific period range and a rectangular area by defining longitude and latitude ranges. In the same table, the menu allows to show/clear selection, show/hide columns and export the selected element directly in CSV, JSON or GeoJSON format.

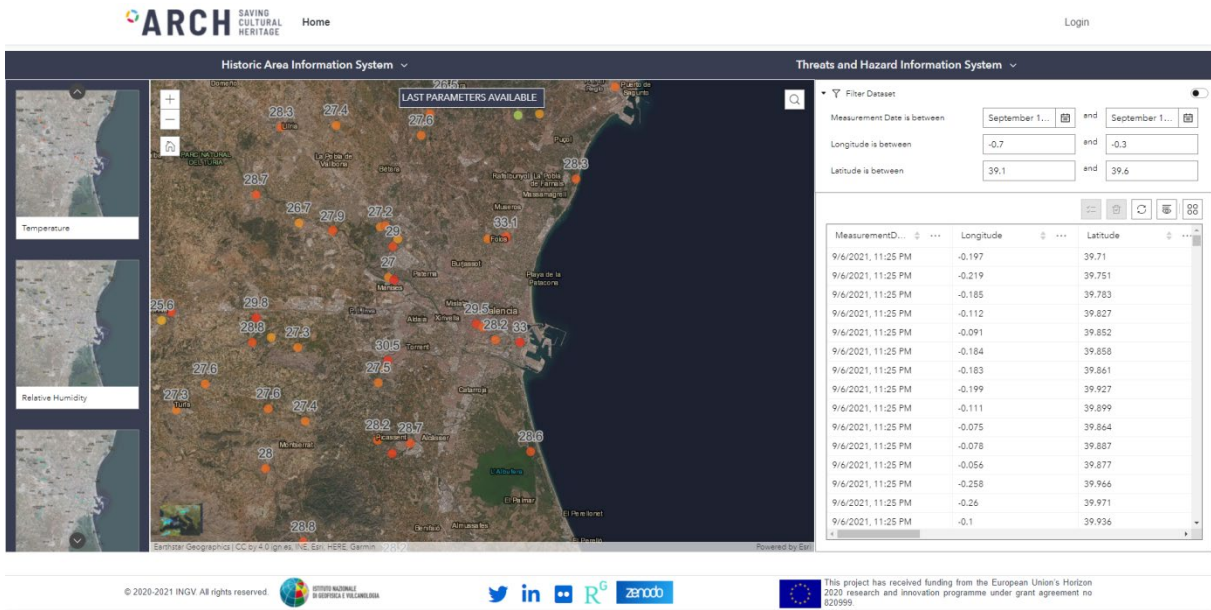


Figure 67. Dashboard for the environmental parameters: the last parameters plotted on the map (on the left side) and table to view and download data on the last 7 days (on the right side).

7.6. Historical climate

Figure 68 shows the dashboard to query the indicators of the historical climate. Information on the data structure, ARCH services and data providers can be found in Section 5.

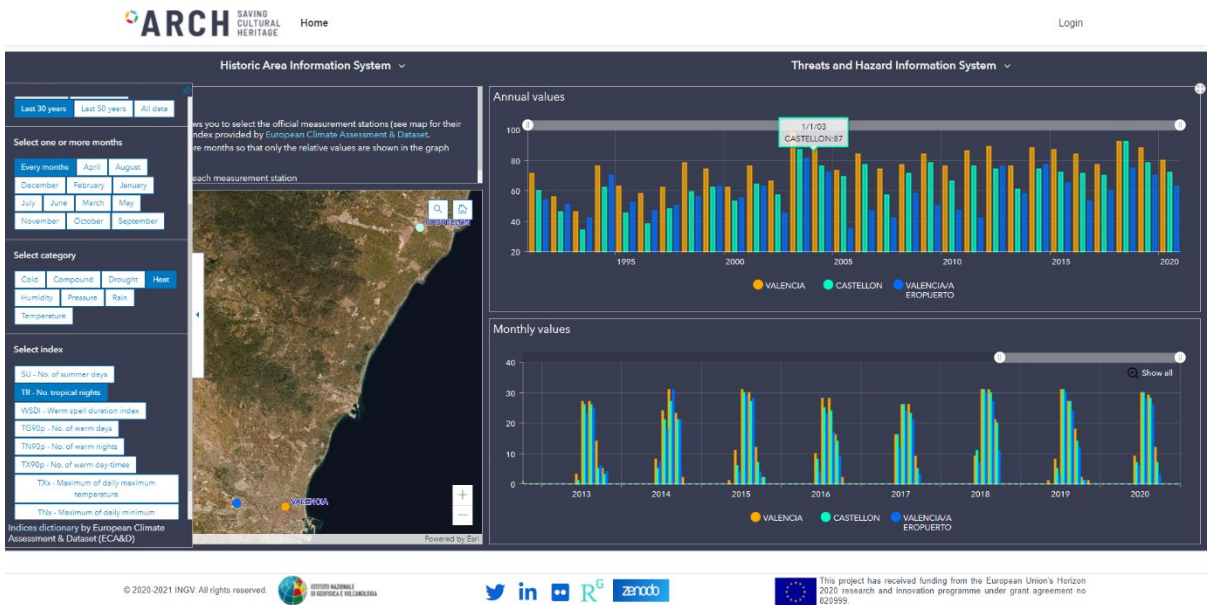


Figure 68. Historic climate dashboard to show indices related to the climate change, as provided by ECA&D [27]. Both annual and monthly values are displayed following the request of the user.

The information displayed on the dashboard can be managed by means of the drop-down menu on the left side, where the user can select:

- One or more recording station(s) showed on the map

- The period on that the indicators are graphed
- The months to be displayed in the monthly chart
- The category and, then, one of the related indices

A quick guide is also provided directly in the dashboard to inform the user.

The choices made through the previous menu have the effects on:

- the central map with a zoom on the positions of the selected stations;
- the annual values of the index are showed on the chart above;
- the monthly values of the index are showed on the chart above for the chosen months and over the observation period;

The user can enlarge the time scale simply interacting with the bars on the charts. Moreover, each panel in the dashboard can be resized or open in full screen directly by the user.

7.7. Climate Services

Figure 69 shows the climate services dashboards that are developed to structure and display the main results obtained by the data processing described in the previous Section 6. In particular, the datasets of the indicators have been gridded by starting from the NetCDF files to be included in the THIS GIS platform.

The dashboard is composed by two maps, in order to display the main indicators:

- on the left map panel can be displayed the historic (1981-2010) and near future (2011-2040) datasets;
- on the right map panel, the mid-term (2041-2070) and far future (2071-2100) datasets.

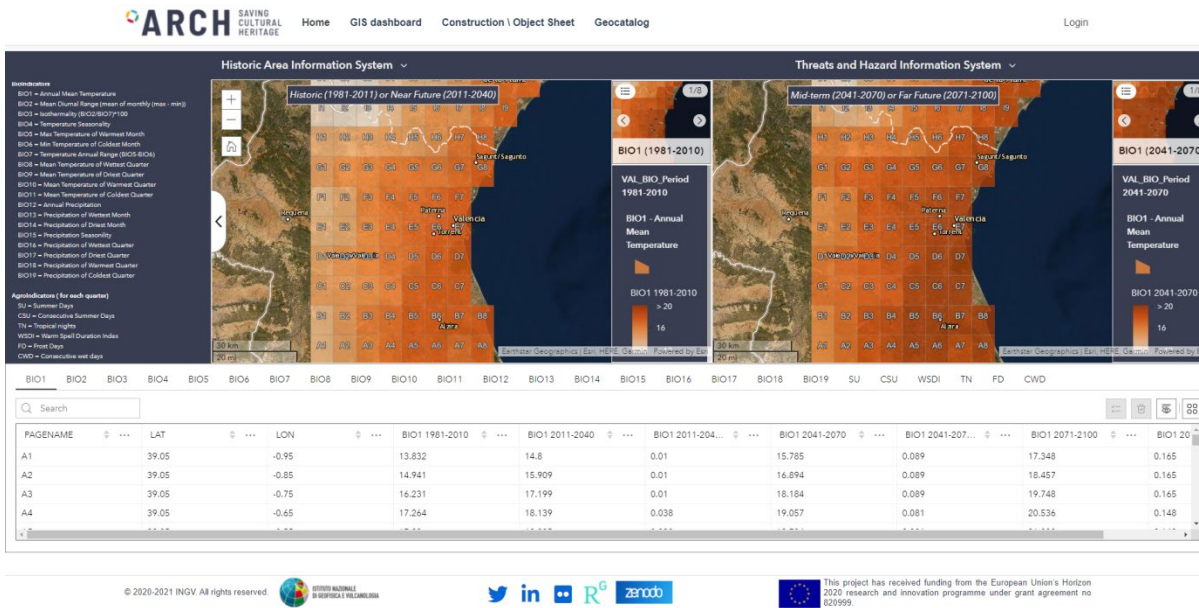
The indicator map can be selected by means of the menu-box on at the top right of the panel. Instead, on the right bottom the legend is displayed with reference to the choice.

Furthermore, on the left side of the dashboard, an arrow button allows you to open the list of indicators in which the abbreviations are explained (Figure 69.a).

The lower part of the dashboard houses the table that provides the values on the different reference periods, as well as the standard deviations, when a specific indicator is selected (see the list in the upper part of the table). In the same table are also available:

- on the left, a search box to select a specific cell of the grid on the map;
- on the right, a menu that allows to show/clear selection, show/hide columns and export the selected element directly in CSV, JSON or GeoJSON format (Figure 69.b).

(a)



(b)

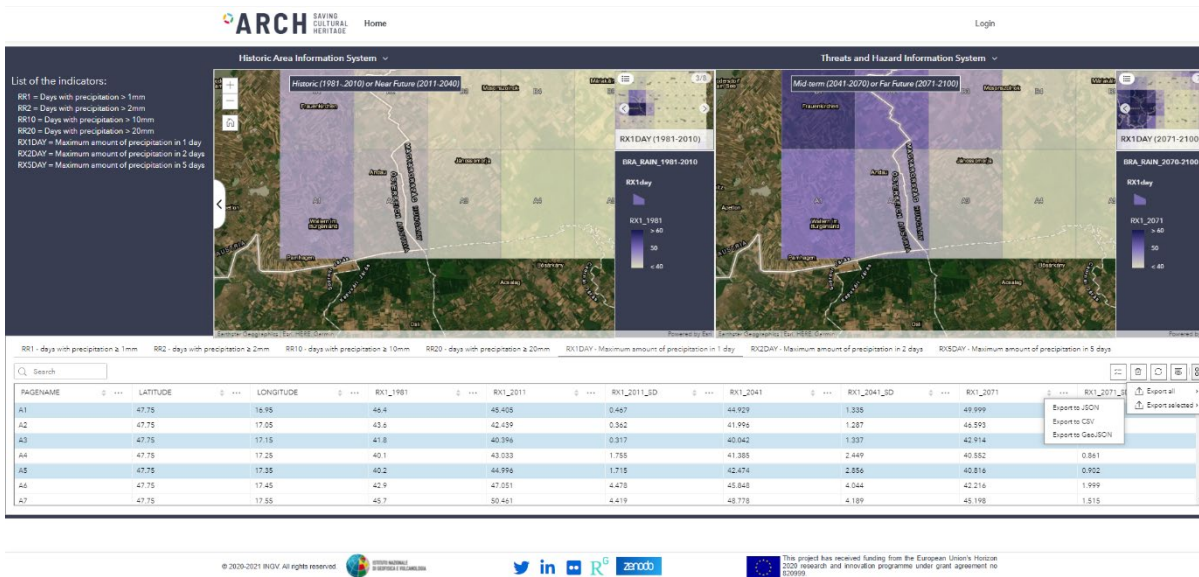


Figure 69. Climate services dashboards: datasets for Valencia (a) and Bratislava (b)

8. Conclusions

By considering that the historic areas of the ARCH cities are exposed to different threats, specific analysis, services and tools were required for each case study, and only some datasets were collected in the same way for all cities. In this framework, the match-making online meetings and co-creation processes (led by ICLEI in the WP3), involving cities, stakeholders and technical partners, allowed identifying the main environmental threats and hazards, as well as measurable indicators for their characterisation for each historic area. Thus, sub-systems, services and database were developed to manage historical datasets, measures in real-time from monitoring systems and projections for the future. The indicators, obtained from data processing and structuring of information, are provided to support the risk analysis and impact scenarios, which will be outlined in the WP5, as well as to inform cities and their stakeholders.

Task 4.3 covered the following activities:

- INGV has developed a seismic monitoring service that notifies new earthquakes in near real-time via THIS and allows triggering the processing of the recordings obtained by the RUSN, if an acceleration threshold is reached;
- INGV and RFSAT have implemented the system to structure the measurements from crowd-sensing and official sensor networks in order to characterise the current climatic conditions and air quality;
- RFSAT has developed the sub-system for mapping the environmental contaminations with their spatial and temporal evolution at large scale;
- INGV has included (and updates) in THIS the available indices relating to weather and climate extremes recorded in the past, that are provided through the infrastructure of a previous European project;
- TECNALIA and ENEA have developed *ad-hoc* climate services, by processing of datasets available from existing services, to elaborate local projections of the most relevant indicators characterising the threats and the potential effects related to the climate-change.

Finally, the main information and datasets were made accessible through user-friendly GIS dashboards in the Threats and Hazard Information System (THIS), which was developed by INGV and integrated into the web-platform of the ARCH information systems. It is worth underlining that the interfaces of these tools could be updated according to the suggestions from the partner cities and the interested stakeholders who will use them. Furthermore, other feedbacks will be collected during the training meetings provided in Task 3.4.2 and the activities will be reported in D3.4 "Report on the co-creation of the information system".

9. References

- [1] Rebollo, V., Rangil-Escribano, T., Chapman, E. (2019) ARCH-D7.1 – Report 5: Gender aspects in conservation and regulation of historic areas, disaster risk management, emergency protocols, post-disaster response techniques, and techniques for building back better - Deliverable of the H2020 ARCH project, GA no. 820999, 2019
- [2] Krukowski, A., Vogiatzaki, E., Costanzo, A., Buongiorno, F., Bignami, C., D'Alessandro, A., Falcone, S., Musacchio, M., Silvestri, M., Vitale, G., Morici, M., Dall'Asta, A., Zona, A., Giovinazzi, S., (2021) ARCH-D4.1 - Sensing and Repositories. Deliverable of the H2020 ARCH project, GA no. 820999, 2019.
- [3] Krukowski, A., Costanzo, A., Falcone, S., Giovinazzi, S., Morici, M., (2021) ARCH-D4.2 - Historic Area Information System. Deliverable of the H2020 ARCH project, GA no. 820999, 2019
- [4] Nickel, K., Milde, K., Lückcrath, D, Rome, E., Giovinazzi, S., Costanzo, A., Krukowski, A., Zorita, S., Mendizabal, M. (2020) ARCH-D7.4 – Requirements description - Deliverable of the H2020 ARCH project, GA no. 820999, 2019
- [5] Nickel, K., Milde, K., Lückcrath, D., Costanzo, A., Di Pietro, A., Giovinazzi, S., Krukowski, A., Zorita, S. (2021) ARCH-D7.5 – Interface specification and system architecture - Deliverable of the H2020 ARCH project, GA no. 820999, 2019
- [6] Stucchi, M., Rovida, A., Gomez Capera, A.A. et al. (2013) The SHARE European Earthquake Catalogue (SHEEC) 1000–1899. *J Seismol* 17, 523–544. <https://doi.org/10.1007/s10950-012-9335-2>
- [7] Grünthal, G., Wahlström, R. & Stromeyer, D. (2013) The SHARE European Earthquake Catalogue (SHEEC) for the time period 1900–2006 and its comparison to the European-Mediterranean Earthquake Catalogue (EMEC). *J Seismol* 17, 1339–1344. <https://doi.org/10.1007/s10950-013-9379-y>.
- [8] Guidoboni E., Ferrari G., Mariotti D., Comastri A., Tarabusi G., Sgattoni G., Valensise G. (2018) - CFTI5Med, Catalogo dei Forti Terremoti in Italia (461 a.C.-1997) e nell'area Mediterranea (760 a.C.-1500). Istituto Nazionale di Geofisica e Vulcanologia (INGV). <https://doi.org/10.6092/ingv.it-cfti5>
- [9] Guidoboni, E., Ferrari, G., Tarabusi, G., Sgattoni, G., Comastri, A., Mariotti, D., Ciuccarelli, C., Bianchi, M.G., Valensise, G. (2019), CFTI5Med, the new release of the catalogue of strong earthquakes in Italy and in the Mediterranean area, *Scientific Data* 6: 80. <https://doi.org/10.1038/s41597-019-0091-9>
- [10] Basili, R., Kastelic, V., Demircioglu, M. B., Garcia Moreno, D., Nemser, E. S., Petricca, P., Sboras, S. P., Besana-Ostman, G. M., Cabral, J., Camelbeeck, T., Caputo, R., Danciu, L., Domac, H., Fonseca, J., García-Mayordomo, J., Giardini, D., Glavatovic, B., Gulen, L., Ince, Y., Pavlides, S., Sesetyan, K., Tarabusi, G., Tiberti, M. M., Utkucu, M., Valensise, G., Vanneste, K., Vilanova, S., Wössner, J. (2013). The European Database of Seismogenic Faults (EDSF) compiled in the framework of the Project SHARE. <http://diss.rm.ingv.it/share-edsf/> . <https://doi.org/10.6092/INGV.IT-SHARE-EDSF>.
- [11] DISS Working Group (2018). Database of Individual Seismogenic Sources (DISS), Version 3.2.1: A compilation of potential sources for earthquakes larger than M 5.5 in Italy and surrounding areas. <http://diss.rm.ingv.it/diss/>, Istituto Nazionale di Geofisica e Vulcanologia; DOI:10.6092/INGV.IT-DISS3.2.1.
- [12] Giardini, D., Woessner, J., Danciu, L., (2014) Mapping Europe's Seismic Hazard. *EOS*, 95(29): 261-262. <https://doi.org/10.1002/2014EO290001>
- [13] Stucchi, M., Meletti, C., Montaldo, V., Akinci, A., Faccioli, E., Gasperini, P., Malagnini, L., Valensise, G. (2004). Pericolosità sismica di riferimento per il territorio nazionale MPS04 [Data set]. Istituto Nazionale di Geofisica e Vulcanologia (INGV). <https://doi.org/10.13127/sh/mps04/ag>

- [14] EMSC Seismic Portal. Available online: <https://www.emsc-csem.org/Project/#seismic> (accessed on 30 September 2021).
- [15] Beyreuther, M.; Barsch, R.; Krischer, L.; Megies, T.; Behr, Y.; Wassermann, J. (2010) ObsPy: A Python Toolbox for Seismology. *Seismol. Res. Lett.*, 81, 530–533. <https://doi.org/10.1785/gssrl.81.3.530>
- [16] Megies, T.; Beyreuther, M.; Barsch, R.; Krischer, L.; Wassermann, J. (2011) ObsPy—What can it do for data centers and observatories?, *Ann. Geophys.*, 54, 47–58. <https://doi.org/10.4401/ag-4838>
- [17] Rupakhety, R., Sigbjörnsson, R. (2014) Rotation-invariant formulation of strong ground-motion parameters. In *Proceedings of the second European conference on earthquake engineering and seismology, Istanbul, 25–29 Aug 2014*.
- [18] Arias, A. A Measure of Earthquake Intensity. In *Seismic Design for Nuclear Power Plants*; Hansen, R.J., Ed.; MIT Press: Cambridge, MA, USA, 1970; Volume 1, pp. 438–469. ISBN 978-0262080415.
- [19] Electrical Power Research Institute (EPRI). *Standardization of the Cumulative Absolute Velocity*; EPRI TR-100082-T2; EPRI: Palo Alto, CA, USA, 1991.
- [20] Costanzo, A. (2018) Shaking Maps Based on Cumulative Absolute Velocity and Arias Intensity: The Cases of the Two Strongest Earthquakes of the 2016–2017 Central Italy Seismic Sequence. *ISPRS Int. J. Geo-Inf.*, 7, 244. <https://doi.org/10.3390/ijgi7070244>
- [21] Shepard, D. A two-dimensional interpolation function for irregularly-spaced data. In *Proceedings of the 1968 23rd ACM national conference (ACM '68)*. Association for Computing Machinery, New York, NY, USA, 1968, 517–524. <https://doi.org/10.1145/800186.810616>
- [22] ArcGIS Pro Python reference. ArcPy module, function, and class provided with ArcGIS Pro. Available online: <https://pro.arcgis.com/en/pro-app/latest/arcpy/main/arcgis-pro-arcpy-reference.htm> (accessed on 30 September 2021).
- [23] Lanzo, G.; Silvestri, F.; Costanzo, A.; D'Onofrio, A.; Martelli, L.; Pagliaroli, A.; Sica, S.; Simonelli, A. (2011) Site response studies and seismic microzoning in the Middle Aterno valley (L'aquila, Central Italy). *Bull. Earthq. Eng.*, 9, 1417–1442. <https://doi.org/10.1007/s10518-011-9278-y>.
- [24] Costanzo, A., Caserta, A. (2019) Seismic response across the Tronto Valley (at Acquasanta Terme, AP, Marche) based on the geophysical monitoring of the 2016 Central Italy seismic sequence. *Bull Eng Geol Environ* 78, 5599–5616. <https://doi.org/10.1007/s10064-019-01514-1>
- [25] Costanzo, A., d'Onofrio, A. & Silvestri, F. (2019) Seismic response of a geological, historical and architectural site: the Gerace cliff (southern Italy). *Bull Eng Geol Environ* 78, 5617–5633. <https://doi.org/10.1007/s10064-019-01515-0>
- [26] Kucera, V., et al. (2007) UN/ECE ICP Materials Dose-response Functions for the Multi-pollutant Situation. In: Brimblecombe P., Hara H., Houle D., Novak M. (eds) *Acid Rain - Deposition to Recovery*. Springer, Dordrecht. https://doi.org/10.1007/978-1-4020-5885-1_27
- [27] Klein Tank, A.M.G. et al. (2002) Daily dataset of 20th-century surface air temperature and precipitation series for the European Climate Assessment. *Int. J. of Climatol.*, 22, 1441–1453.
- [28] Charron, I. (2016). *A Guidebook on Climate Scenarios: Using Climate Information to Guide Adaptation Research and Decisions*, Ouranos, 94p. ISBN (Impression): 978-2-923292-19-9 ISBN (PDF online): 978-2-923292-21-2
- [29] Cattiaux, J., Douville, H., Peings, Y. (2013) European temperatures in CMIP5: origins of present-day biases and future uncertainties. *Clim Dyn* 41, 2889–2907. <https://doi.org/10.1007/s00382-013-1731-y>
- [30] Vlcko, J., Greif, V., Grof, V., et al. (2009) Rock displacement and thermal expansion study at historic heritage sites in Slovakia. *Environ Geol* 58, 1727–1740. <https://doi.org/10.1007/s00254-008-1672-7>
- [31] Ouzeau, G., Soubeyroux, J.M., Schneider, M., Vautard, R., Planton, S. (2016) Heat waves analysis over France in present and future climate: Application of a new method on the EURO-CORDEX ensemble. *Climate Services* 4, 1–12. <https://doi.org/10.1016/j.cliser.2016.09.002>

- [32] Jacob, D., et al (2001). A comprehensive model inter-comparison study investigating the water budget during the BALTEX-PIDCAP period *Meteorol. Atmos. Phys.* 77 19–43
- [33] Samuelsson, P., Jones, C. G., Willén, U., Ullerstig, A., Gollvik, S., Hansson, U., Jansson, C., Kjellström, E., Nikulin, G. Wyser, K., (2011). The Rossby Centre regional climate model RCA3: model description and performance *Tellus Ser. A Dyn. Meteorol. Oceanogr.* 63 4–23
- [34] Rockel, B., Will, A., Hense, A. (2008). The regional climate model COSMO-CLM (CCLM) *Meteorol. Zeitschrift* 17 347–8
- [35] Christensen, O.B., Drews, M., Christensen, J.H., Dethloff, K., Ketelsen, K., Hebestadt, I. Rinke, A. (2007). The HIRHAM regional climate model version 5 (beta) DMI Technical Report 06–17 (Copenhagen: DMI)
- [36] Van Meijgaard, E., Van Uift, L. H., Van De Berg, W. J., Bosveld, F. C., Van Den Hurk, B. J. J. M., Lenderink, G., Siebesma, A, P, (2008) .The KNMI regional atmospheric climate model RACMO version 2.1 Technical Report 302 (De Bilt: KNMI)
- [37] Deque, M., 2010. Regional climate simulation with a mosaic of RCMs. *Meteorol. Z.* 19: 259–266.
- [38] Sabbioni, C., Cassar, M., Brimblecombe, P. (2010). The Atlas of climate change impact on European Cultural Heritage. Scientific Analysis and Management Strategies. ANTHEM PRESS
- [39] Viles, H. A., (2002). Implications of future climate change for stone deterioration. *Geological Society, London, Special Publications*, 205(1), 407–418. <https://doi.org/10.1144/gsl.Sp.2002.205.01.29>
- [40] Brimblecombe, P., & Grossi, C. M. (2007). Damage to buildings from future climate and pollution. *APT Bulletin: The Journal of Preservation Technology*, 38(2/3), 13–18. Retrieved from www.jstor.org/stable/40004714
- [41] Grossi, C.M, Brimblecombe, P., Harris, I. (2007) Predicting long term freeze–thaw risks on Europe built heritage and archaeological sites in a changing climate. *Science of the Total Environment* 377, 273–281.
- [42] Nijland, T. G., Adan, O. C. G., Van Hees, R. P. J., Van Etten, B. D. (2009). Evaluation of the effects of expected climate change on the durability of building materials with suggestions for adaptation. *HERON*, 54(1), 37–48.
- [43] Brimblecombe, P., Grossi, C. M., & Harris, I. (2011). Climate change critical to cultural heritage. In H. Gökçekus, U. Türker, & J. W. LaMoreaux (Eds.), *Survival and sustainability: environmental concerns in the 21st century* (pp. 195–205). Springer.
- [44] Camuffo, D. (2019). Climate change, human factor, and risk assessment. In D. Camuffo (Ed.), *Microclimate for cultural heritage* (pp. 303–340). Elsevier
- [45] Sabbioni C., Cassar M., Brimblecombe P., Lefevre R.A., 2008. VULNERABILITY OF CULTURAL HERITAGE TO CLIMATE CHANGE, Report of the European and Mediterranean Major Hazards Agreement (EUROPA)
- [46] Haugen, A., Mattsson, J. (2011) Preparations for climate change’s influences on cultural heritage. *International Journal of Climate Change Strategies and Management*, 3:4, 386-401. <https://doi.org/10.1108/17568691111175678>.
- [47] Yaldiz, E. (2010, 25–29 May). Climate effects on monumental buildings. Paper presented at the Balwois, Ohrid, Republic of Macedonia. Available online: https://www.researchgate.net/publication/266494356_Climate_Effects_on_Monumental_Buildings (accessed on 30 September 2021)
- [48] Sabbioni, C., Cassar, M., & Brimblecombe, P. (2009). Vulnerability of cultural heritage to climate change. *Pollution Atmospherique*, 203, 285–298.
- [49] Curtis, R. (2016). Water management for traditional buildings: Adaptation for a changing climate. *APT Bulletin: The Journal of Preservation Technology*, 47(1), 8–14. Retrieved from www.jstor.org/stable/43799258
- [50] ICOMOS Climate Change and Heritage Working Group. (2019). The future of our pasts: Engaging cultural heritage in climate action. *Outline of Climate Change and Cultural Heritage*.

Available online: at <https://indd.adobe.com/view/a9a551e3-3b23-4127-99fd-a7a80d91a29e> (accessed on 30 September 2021)

- [51] Gomez-Heras, M., McCabe, S., Smith, B. J., & Fort, R. (2009). Impacts of fire on stone-built heritage. *Journal of Architectural Conservation*, 15(2), 47–58. <https://doi.org/10.1080/13556207.2009.10785047>
- [52] Maccari ,M., Onorati, A., Pesaresi, A., Geological-technical map in the 3th level of the Seismic Microzonation of Camerino. Available online: http://www.comune.camerino.mc.it/wp-content/blogs.dir/11/files/Carta_geologico_tecnica-10000.pdf. (accessed on 30 September 2021)